NTNU

Norwegian University of
Science and Technology

Thermally Sprayed Aluminum (TSA) with Cathodic Protection as Corrosion Protection for Steel in Natural Seawater

Characterization of Properties on TSA and Calcareous Deposit

Solveig Egtvedt

Materials Science and Engineering
Submission date: July 2011
Supervisor: Kemal Nisancioglu, IMTE
Co-supervisor: Roy Johnsen, IMP, NTNU

Norwegian University of Science and Technology
Department of Materials Science and Engineering

Preface

I hereby declare that this work has been carried out independently and in compliance with the examination regulations of the Norwegian University of Science and Technology, NTNU. The thesis is submitted as the final work for the degree Master of Science in Material Science and Engineering at the Institute of Material Science. The experimental work has been performed at SINTEF SEALAB, Brattøra and at SINTEF Materials and Chemistry's laboratory facility at Perleporten, NTNU.

I would like to thank my supervisors Professor Kemal Nisancioglu and Professor Roy Johnsen for help and guidance during this project. I would also like to thank Sven Morten Hesjevik and Stein Olsen at Statoil for helpful input and discussions. Further on, I wish to thank Kjell Røkke for finding and cutting the aluminum plates used in the experiments.

Last, but not least, I wish to thank my fellow student for all the great times and my family for all the encouragement.

_____

Solveig Egtvedt
Trondheim, July 2011

Abstract

Cathodic protection is an effective corrosion protection for structures submerged in seawater. In addition to applying the current need to lower the metal below the protection potential, a resulting increase in interfacial pH leads to precipitation of calcareous deposit. This deposited layer act as a barrier against oxygen diffusion on the surface, hence lowering the current demand of the structure. However, this layer will also hinder the thermal conductivity, and is therefore unwanted at the surface of heat exchangers.

There are several factors influencing the precipitation of calcareous deposit. This includes potential, current, pH, seawater chemistry, flow rate etc. These factors have been thoroughly investigated for many years, but mostly with steel as substrate material.

Specimens of steel coated with thermal sprayed aluminum (AlMg5) and aluminum plates of alloys AA5082, AA1050 and Al99.99 were exposed to seawater for 5-6 weeks, polarized to -1050 mV vs Ag/AgCl. The current demand was constantly recorded using KorrosjonsLogger©. Results from introductory experiments are also included.

The unsealed TSA specimens had the highest current demand, but were also exposed to a higher seawater temperature than the other specimens, which has influenced the results. The sealed TSA specimens had a current demand around 10 mA/m^2 after 6 weeks, which is 10 times lower than usually found on steel specimens. For the aluminum plates the trend showed that the higher alloying elements, the higher current density.

The explanation for the low current demand compared to steel is that the cathodic area for aluminum is the intermetallic particles that are cathodic to the matrix, while for steel the whole surface act as a cathodic site. In addition, mechanisms during cathodic protection of aluminum lead to an isolation of the cathodic particle, hence continuously lowering the current demand.

After exposure, the specimens were investigated in SEM and the composition on the surface was found using EDS. The SEM images showed a furry surface on the TSA specimen, but no familiar structure of calcareous deposit, which has been seen on steel specimens. For the aluminum plates, the intermetallic particles had been “dug out”, showing a pit between the particle and matrix. A typical structure of calcareous deposit was not seen here either.

However, the EDS analysis showed an increase in both Mg and Ca content. The Mg/Ca ratio varied over the surface, with the highest ratio and content for the intermetallic particles for the aluminum plates and at the peaks of the surface at the TSA specimens. The Mg/Ca ratios found were much higher than found on steel.

Both the SEM images and EDS analysis confirms the theory that there will precipitate less calcareous deposit on TSA surfaces compared to steel. Further studies will show whether the small content found will have an influence on the thermal conductivity.

Table of contents

1 Introduction

There is an increasing interest, within oil and gas production, in placing most of the production on the seabed. In that connection there will, amongst other, be need for subsea heat exchangers. Normally, materials being used subsea are steel protected with cathodic protection. Steel is a relatively cheap material, and in addition to lowering the potential to an immune state, use of cathodic protection leads to precipitation of calcareous deposit, due to increased interfacial pH. This layer will function as a barrier against the corrosive environment, leading to a decrease in current demand.

However, the calcareous deposit will also hinder thermal conductivity, which is unwanted in connection to a heat exchanger. There is therefore an interest in finding a solution where calcareous deposit does not precipitate on the surface. As the heat exchanger is connected to other parts of a structure protected by sacrificial anodes, the heat exchanger will also be influenced. A suggestion to use thermally sprayed aluminum on steel has been made and results from introductory experiments indicated that calcareous deposit would precipitate on aluminum in a lesser degree than steel. The introductory experiments showed that the main element of the calcareous deposits was Mg. Studies have shown that Mg hinders the precipitation and growth of $CaCO_3$, giving reason to believe that there will be less calcareous deposit on Mg containing alloys.

The aim of this thesis is therefore to investigate further the use of thermally sprayed aluminum together with cathodic protection. In addition to study TSA specimens, aluminum plates of various alloys will be investigated to better understand the mechanisms happening on the aluminum surface. As the TSA is an AlMg5 alloy, plates of the AlMg5 alloy AA5082 is also investigated. This is to see what influence the intermetallic particles, which are easier to see on an extruded plate, have on the deposition of calcareous deposit. Also, plates of Al99.99, which should not contain any intermetallic particles, will be investigated to see whether the intermetallic particles have an influence on the precipitation of calcareous deposit. To see what influence Mg content has on the calcareous deposit, alloy AA1050, which also is a common TSA alloy with very low Mg content, is investigated.

2 Theory

2.1 Corrosion of aluminum

Corrosion is dissolution of material by chemical reactions. It does not include mechanisms such as erosion or wear, which are mechanical mechanisms. Aqueous corrosion is dissolution of a metal in water, where the water acts as an ion conducting electrolyte. When a metal surface is immersed in an electrolyte, i.e. water, metal ions detach from the metal, flow into the electrolyte, leaving electrons behind on the metal. The dissolution of metal ions will continue until the metal reaches its equilibrium potential and the system contains a certain concentration of dissolved ions to be in equilibrium. Stirring the electrolyte, continuously replacing the water, will result in the metal losing more and more ions, and not reaching equilibrium. Hence, the metal will corrode continuously.

Aluminum is known to be quite corrosion resistant, at least at neutral pH. This is due to the presence of a very stable oxide on the surface. The dissolution of aluminum occurs according to equation (2.1). A scratch in the oxide is immediately followed by oxidizing of the surface according to the equation (2.2). As opposed to steel, which needs dissolved oxygen in the solution to form an oxide, aluminum oxide will deposit by splitting the water molecules [1].The electrons released will be consumed by the reduction reactions in equations (2.3) and (2.4). The anode and cathode can be situated on the same piece of metal; hence there is no need for an external electrode to be present for the process to occur.

$$Al \rightarrow Al^{3+} + 3e^{-} \quad (2.1)$$

$$2Al^{3+} + 3H_2O \rightarrow Al_2O_3 + 6H^{+} \quad (2.2)$$

$$O_2 + 4H^{+} + 4e^{-} \rightarrow 2H_2O \quad (2.3)$$

$$2H^{+} + 2e^{-} \rightarrow H_2 \quad (2.4)$$

The aluminum oxide is amphoteric; i.e. it is unstable in both acidic and alkaline environment. This can be seen in the Pourbaix diagram for pure aluminum in seawater in Figure 2.1, where the equilibrium potential (E_e) between a metal and its various oxidized species is plotted as a function of pH. The Nernst equation (2.5) is used to construct the Pourbaix diagram.

$$E_e = E^0 - \frac{RT}{zF} \ln \frac{[reduced]}{[oxidised]} \qquad (2.5)$$

Here R is the universal gas constant (8,2145J/Kmol), T is the absolute temperature (K), z is the number of moles of electrons involved in the reaction and F is the Faraday constant (96 485 C/mole electrons). The notations [reduced] and [oxidized] is the product of the concentrations of all the species that appear on respectively the reduced side and the oxidized side of the electrode reaction, raised to the power of their stoichiometric coefficients.

As mentioned above, a cathodic reaction must take place to balance the anodic reaction of metal dissolving. The cathodic reaction's equilibrium potential, calculated by the Nernst equation will become a straight line in the Pourbaix diagram. As there is two possible cathodic reactions in water, (2.3) and (2.4), there will be two straight lines in the Pourbaix diagram, with decreasing potential as the pH increases, as seen in Figure 2.1 and the lines labeled a) and b). For each stable oxidation product the metal holds, a vertical line is drawn according to their equilibrium potential. This requires a given concentration, e.g. 10^{-6} mol/dm^3.

Based on this diagram it is possible to see whether the metal will be active, passive or immune. The Pourbaix diagram in Figure 2.1 shows that aluminum is passive

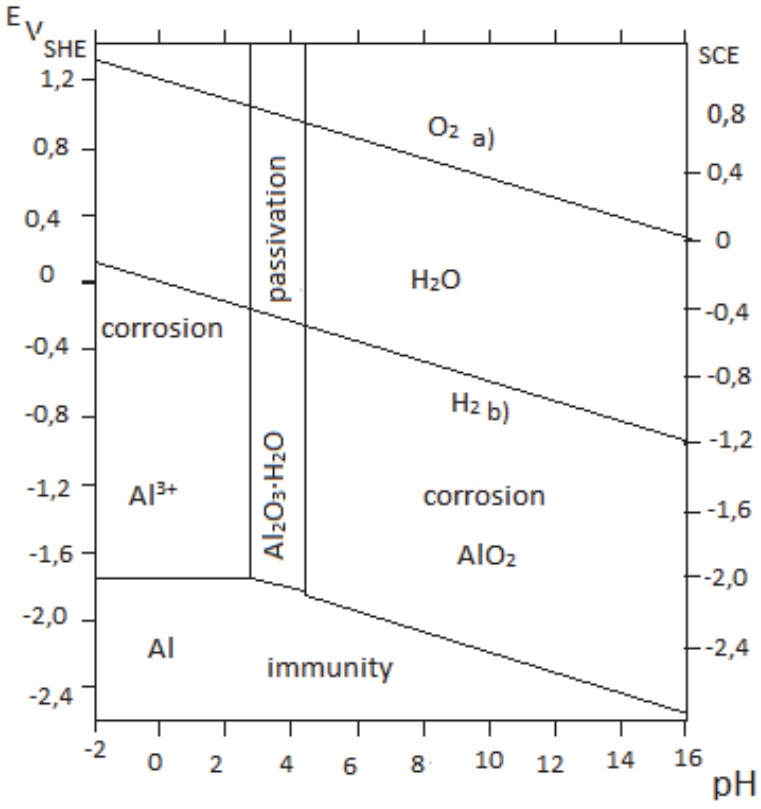

Figure 2.1: Pourbaix-diagram for pure aluminum in seawater [2]. The line labeled a) is the oxygen reduction, while line b) is hydrogen evolution.

between pH 3 and 5, at potentials higher than -1.7 mV SHE. According to the diagram, the metal is not immune until the potential is below -1.7 V SHE in sour environment and at even lower potentials when increasing pH according to the diagram. However, studies have shown that aluminum practically does not have an immune zone, due to formation of aluminum hydrides that makes the oxide unstable [1].

Considering that the pH in seawater is between 7.5 and 8.3 [3], aluminum looks unfavorable for use in seawater according to the Pourbaix diagram in Figure 2.1. However, some aluminum alloys are known as seawater resistant due to the alloying elements. An experimental potential – pH diagram for the aluminum- magnesium alloy 5086 in chloride solution is shown in Figure 2.2. Alloy 5086 contains wt% 0.1 Si, 0.3 Fe, 0.4 Mn, 4.3 Mg, 0.1 Cr [2]. The diagram shows that the passive area for the alloy is increased compared to the Pourbaix diagram for pure aluminum in Figure 2.1. Figure 2.2 shows that the aluminum alloy is passive between over the whole pH range at certain potentials and at pH 8.3 between -0.85 and -1.2 mV SCE. The reason for the increase in passive area is the passivating alloying elements Mg and Mn, which has an increasingly passive oxide with increasing pH. More about the influence of alloying elements on corrosion protection is found in the next chapter.

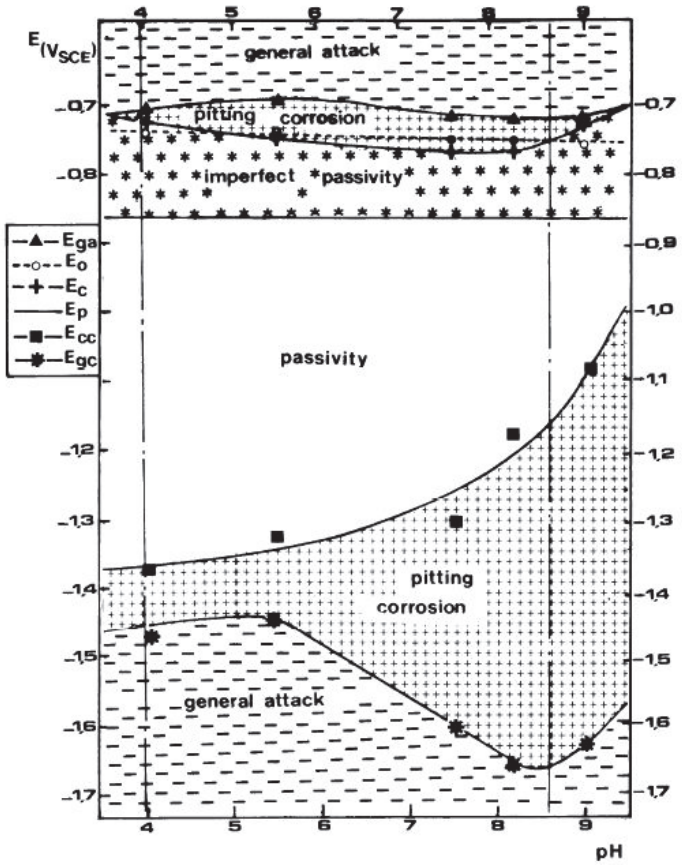

Figure 2.2: Experimental pH-potential diagram for aluminum alloy AA5086 in NaCl solution [2].

As the corrosion resistance of Al to a great extent depends on the surface oxide, any factor that reduces the effectiveness of the film may drastically reduce the corrosion resistance. One factor that weakens the oxide is the pH of the environment. As mentioned above, alloying elements make the oxide more passive in slightly alkaline environments, but at higher pH the oxide will be broken down. As will be showed later, cathodic protection will increase the pH of the environment, making the oxide unstable. If the rate of the cathodic reaction on the surface becomes too high, the surface becomes alkaline and the protective oxide may become destabilized [2].

Corrosion of aluminum can take several different forms but is in most cases localized, either as pitting, intergranular, exfoliation, stress, filiform or general corrosion [4]. Pitting is the most common corrosion form in seawater, as pitting occurs in the presence of chloride ions in the solution. The aluminum oxide will become unstable in the presence of chloride ions if the potential of the metal is raised above a critical pitting potential, E_c. Well over the pitting potential, E_c, the corrosion becomes more uniform, giving the appearance of etching [1]. The boundary between pitting and general attack can be seen in Figure 2.2 and is around -0.7 V SCE.

Aluminum can undergo both localized and general corrosion without aggressive species present, if the aluminum specimen is made a cathode, as is the case for cathodic protection. This is due to the reduction reactions in equation (2.3) and (2.4) causing an alkaline diffusion layer adjacent to the surface. As mentioned above, an alkaline environment dissolves the protective aluminum oxide leading to corrosion attack. This alkaline layer may not easily be swept away by stirring the solution of the bulk [1].

2.1.1 Effect of temperature on corrosion of aluminum

As a general rule, the corrosion reaction rates in seawater increase as the temperature increases [3]. For aluminum and its alloys increased temperature leads to a shift in the passive zone in the Pourbaix diagram towards lower pH. This means that in alkaline and neutral environments aluminum will be less resistant to corrosion with increasing temperature, while becoming more resistant in acid environments, purely based on thermodynamic considerations [1]. The temperature does not affect the pitting potential, E_c, significantly up to about 30 °C. Above 40 °C, however, E_c becomes more negative with increasing temperature [1].

2.1.2 Effect of flow on corrosion of aluminum

Increasing flow rate in seawater reduces the possibility of pitting on the cost of increased uniform corrosion. The flow rate transition depends on the alloy and hydrodynamic conditions [2]. In the pitting range of the flow rate, a decrease in corrosion rate is observed with time, whereas in the uniform corrosion range, the corrosion rate is nearly constant as a function of time [2].

2.1.3 Effect of alloying elements on corrosion of aluminum

The grade of corrosion is affected by the purity of the metal. High purity metal is more resistant to corrosion than alloyed metal and generally the more alloying elements, the less corrosion resistant [4, 5]. The most common alloying elements in aluminum is silicon, manganese, magnesium, copper and zinc [6]. These alloying elements can contribute to strength, formability, corrosion resistance of the metal and more.

The alloying elements contribute to corrosion protection depending whether the elements are more noble or active than aluminum. Fe containing intermetallic particles are electrochemically more noble than the surrounding aluminum matrix [1]. The potential difference between Fe as $FeAl_3$ and the aluminum matrix is of the order of 1.2 V [4]. Because of this potential difference, they act as sites for the reduction reactions described by equation (2.3) and (2.4). The rate of the reduction reaction is dependent on the ratio of the area of exposed intermetallic particles relative to the area of the matrix alloy. At high enough reduction reaction rates these cathodes are capable of increasing the potential of the surrounding aluminum matrix in the positive direction. Depending on the corrosivity of the environment, the oxide film breaks down at weak spots and a microgalvanic cell action is established between the cathodic and anodic area [1]. Addition of manganese, increases the resistance of pitting by preventing the formation of Fe_3Al-particles [4].Instead, $(FeMn)Al_6$, which has a negligible potential difference relative to the Al matrix, is formed. In addition, manganese is passive over a wider pH range than aluminum. An enrichment of manganese on the aluminum surface will therefore contribute to passivity; both the oxidation and reduction reaction rates will decrease.

Also alloying elements with certain solubility in aluminum, such as Cu, contribute to the corrosion behavior depending on whether these elements are more noble or active than aluminum. Cu, which is more noble then Al, will increase the rate of corrosion of the active aluminum matrix (selective dissolution). The surface will be enriched with the noble component, and will behave more according to the electrochemical properties of Cu [1]. Enrichment of the surface with Cu is known to increase the pitting resistance [2].

For alloying elements less noble than aluminum, only Mg is used commercially today [1]. Although Al can contain up to 15 % Mg in solid solution, aluminum-magnesium alloys usually contain between 1-5% Mg. This is due to the unwanted β-phase Mg_5Al_8. If the magnesium concentration is too high the β-particles will precipitate on the grain boundaries, which leads to brittleness and grain boundary corrosion due to different potential between the grain boundaries and the matrix [6]. However, in the right amounts, Mg does not only make the oxide less soluble in alkaline environments, it will corrode at a faster rate than aluminum, causing the surface to be purer in aluminum, which is more resistant to corrosion than an AlMg alloy. Dissolved Mg will act as a sacrificial anode for the aluminum surface. AlMg alloys are resistant to pitting corrosion in chloride environments [1]. These alloys are therefore used in marine environments, in such as masts, small boats and superstructures on ships.

The AlMg alloy also normally contains other alloying elements. Silicon increases the corrosion resistance of the aluminum in alkaline environment, because the silicon particles resist both most acids and salts. Aluminum alloys containing silicon is therefore commonly used in marine environments [4]. Si containing particles will be cathodic to the matrix.

What kind of compounds the alloying elements form depends on the amount of the different alloying elements and working procedure. In this thesis, three different aluminum alloys are investigated; AA5082 (ISO designation AlMg5), AA1050 (ISO designation Al99.5) and Al99.99 [7]. For the thermally sprayed aluminum AlMg5 is used. According to Mondolfo [4] the following intermetallic compounds are possible in AA5082 with the composition described in Table 3.1: Mg_5Al_8, Mg_2Si, $FeAl_3$, $(FeCr)Al_7$, $(FeMn)Al_6$. Particles containing Fe and Si will be cathodic to the aluminum matrix, while particles containing Mg will be anodic.

2.2 Corrosion protection

2.2.1 Cathodic protection

There are several ways to protect a metal from corroding. Applying a coating is one method, anodic and cathodic protections are other common methods used in seawater or other electrolytes.

To protect a metal cathodic or anodic, there are two methods; sacrificial anodes and impressed current cathodic protection (ICCP). When protecting a metal with sacrificial anodes, the two metals must be immersed in the same electrolyte and be electrically connected, hence forming an electrochemical circuit. The sacrificial anode will corrode as it is made from a metal with lower electrode potential than the metal being protected. As it corrodes it will supply electrons to the metal being protected, preventing an anode reaction at the metal. ICCP is obtained from a direct current source connected between an auxiliary anode and the metal to be protected. The current makes electrons flow to the metal, causing the metal to be cathodic, while the auxiliary anode corrodes.

While cathodic protection is lowering the potential to the immune area of the Pourbaix diagram, anodic protection means increasing the potential of the metal to the passive area. The protection potential for steel, i.e. the potential at which the steel is in the immune area, is -800mV vs Ag/AgCl [8]. Aluminum does not have a specified protection potential, instead, protection is achieved by maintaining the *passivity* of the surface. Hence, the protection can be considered anodic rather than cathodic. The potential should be sufficiently more negative than the critical pitting potential at -0.85 V SCE [9].

2.2.2 Cathodic protection of aluminum

Gundersen and Nisancioglu described the mechanisms bound to cathodic protection of aluminum in seawater as following [10]:

When submerging aluminum in seawater, oxygen reduction and hydrogen evolution occurs preferentially at the cathodic intermetallic particles, e.g. iron-rich particles. This creates an alkaline diffusion layer around the particles, as schetced in Figure 2.3a). Applying a cathodic potential accelerates the alkalinization process, as described earlier. This alkaline environment will break the protective oxide on the matrix around the particle, making the matrix unprotected. As a result, the matrix corrodes, exposing an increased area of the particle, Figure 2.3b).

In contact with the alkaline solution, the iron-rich particles leach out their more active aluminum component, resulting in iron enrichment on the particle, catalyzing the cathodic reaction. This, in turn, increases the alkalinity of the adjacent diffusion layer and the rate of anodic process on the adjoining matrix. Eventually, corrosion of the matrix around the particle may cause detachment of the particle from the matrix, but without exposing fresh particles from underneath. The crevice around the particle becomes filled with corrosion products, $Al(OH)_3$ and possible calcareous deposits, electrically isolating the particle from the metal matrix, as shown in Figure 2.3c). As a result, both the cathodic and anodic processes abate, and alkalinity of the site drops, favoring the formation of a protective oxide layer on the matrix surface adjacent to the detached particle [10].

The resulting current-time curve for this mechanism is schematically represented in Figure 2.4. The current density is increasing at the beginning of the exposure due to the dissolution of the protective oxide film and resulting corrosion of the matrix around the intermetallic particles. After reaching a maximum value, the current decreases exponentially, as a result of passivation of the cathodic sites [10].

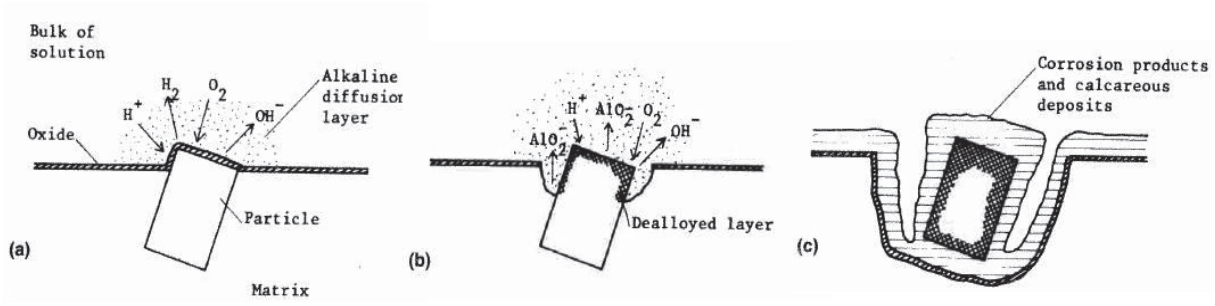

Figure 2.3: Schematic description of the mechanism of cathodic protection of aluminum alloys in seawater. (a) development of alkaline diffusion layer, (b) crevising of the matrix around the particle, (c) repassivation of the surface after detachment of particle. [10].

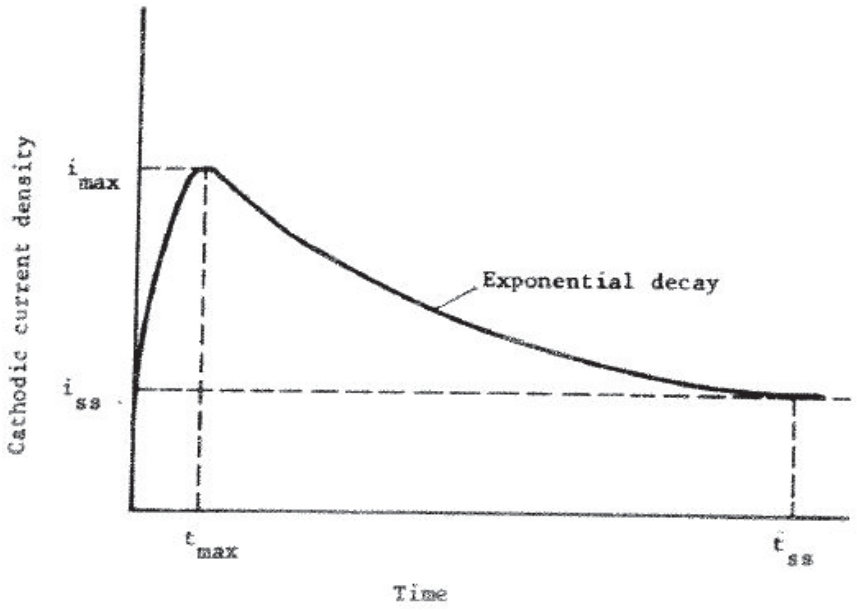

Figure 2.4: Schematic potentiostatic polarization curve for an aluminum alloy during cathodic protection [10].

Steel has almost 10 times higher current demand than aluminum and aluminum alloys [11]. In addition to aluminum's stable oxide, the main reason is, as described over, that corrosion of aluminum is primarily dependent on the properties of the intermetallic particles, whereas corrosion of steel is dependent on the properties of the matrix. The small area of the intermetallic particles, i.e. the cathodic sites, on the aluminum, together with the isolation of the cathodic sites over time, leads to a very low cathodic current demand compared to steel. In the case of steel, the entire surface will be a cathodic site. As the number, or more correctly; the size, of cathodic sites decreases on the Al surface, so does the current demand. Eventually the whole aluminum surface is covered by a stable oxide.

2.2.3 Thermally sprayed coating – application and function

To protect metals against corrosive environment coatings can be applied. Both organic and metallic coatings are being used, having different properties and range of use. Common for the two groups are that they isolate the metal from the corrosive media. The main difference is that metallic coatings are conductive, while the organic coatings are not.

Thermally sprayed coatings provide a functional surface to protect or modify the behavior of a substrate material [12]. There are several different methods for spraying, all based on the same principal. Coating material, wire or powder, is fed into the spraying gun, heated to molten or semi molten condition and accelerated by gas or air towards the component being protected. The metal hits the component like

splats and cools down. The bonding mechanism is primarily mechanical, and in some cases metallurgical. Each layer bonds to the previous, making a lamellar structure, unfortunately with some occurrence of inclusions, oxides and pores. The process used on the TSA specimen in this thesis, is the arc spraying process. Two metal wires meet in an atomizing gas and the electric potential difference causes the wire to atomize or melt and be deposited on the part. The adhesion strength is 6 000 - 8 000 psi and the coating contains 3 – 8 % porosity [13].

The advantages of thermally sprayed coatings are that they are easy to apply, inexpensive to operate, and for some of the methods, e.g. the wire arc process, the equipment is transportable and the spraying can be performed on site. The lifetime of thermal sprayed aluminum is superior to the organic coatings, with a predicted lifetime of over 30 years in the splash zone with a 200 µm TSA coating applied according to today's standards [14].

Thermally sprayed coatings have several areas of application; wear resistance, salvage and repairing and corrosion resistance. For corrosion control, the coatings fall into three groups: anodic, cathodic and neutral coatings. General for all of the coatings is that they hinder corrosive environment to the surface of the substrate to be protected. The anodic coating, where the coating is anodic relative to the component, functions as a sacrificial anode in case of a damage or leak in the coating. They are nearly solely made of zinc and aluminum. Aluminum has been found to be the most effective metal for protection of steel in offshore structures [12]. Cathodic coatings, such as coatings made from stainless steel or nickel alloys, are cathodic to the substrate. They give excellent corrosion protection, but will in case of damage be protected by the component, dramatically accelerating the corrosion on the component being protected. In the case of cathodic coatings, it is important to have a dense, thicker coating, preferably sealed.

Neutral coatings provide excellent corrosion resistance to most corrosive environments by acting as a hinder for the corrosive media. It will not accelerate nor decelerate the corrosion of the substrate in case of damage of the coating. Corrosion at the substrate-coating interface should be avoided to prevent coating separation. Thick, dense coatings are also important for neutral coatings. Examples of material used in neutral coatings are alumina and chromium oxide ceramics [12].

2.2.4 Sealing of TSA

According to NORSOK standard M-501 metal coatings shall be sealed or overcoated as specified. The sealer shall fill the metal pores and be applied until absorption is complete. There should not be a measurable overlay of sealer on the metallic coating after application [15].

Sealing of the coating is important to ensure that the coating is dense and that the component being protected is separated from the corrosive media. The purpose of a

sealant is to penetrate the coating and fill the pores, whereas the purpose of a painting, to comparison, is to be an overlaying protective coating. The sealant should be of low viscosity to penetrate into the pores and seal them of, without necessarily adding thickness to the protective system. The sealer should be sprayed on the aluminum coating as soon as possible to smooth the surface texture and hinder contamination [16]. An unsealed coating will also be sealed to some extent with corrosion products filling the pores, but this process may take some time.

It has been showed that sealing of TSA lowers the free corrosion rate, typically 30-50% lower than unsealed specimens after 11 months exposure at free corrosion potential or lower. Whereas at higher potentials the sealer has almost no effect in reducing the corrosion of the coating [17].

The use of TSA on the tethers and risers on the Hutton tension leg platform (TLP) has been studied by Fischer et al [14]. Both the tethers and risers had a flame sprayed Al99.5 coating applied. The vinyl sealer used on the coating of the tethers showed blistering after 4 years in operation, whereas no blisters where found on the risers which had a silicon sealer applied over the coating. Despite the blisters, the TSA coating was in excellent condition with no measurable reduction in coating thickness or evidence of corrosion damage to the substrate [14].

2.2.5 TSA in combination with cathodic protection

Even though TSA gives an excellent corrosion protection in itself, the aim of this thesis is to find out how it combines with cathodic protection as there are occasions were the TSA surface is electrically connected to parts of a structure which is being cathodically protected, hence influencing the TSA as well.

Gartland and Eggen have performed several experiments regarding this subject [16-18]. Gartland suggested in [16] that the protection potential for all TSA alloys should be -900 mV vs Ag/AgCl at ambient temperatures and then lowered 1 mV for each degree above 10 °C. The design current density for a 100% Al-coating, sealed, was set to 11 mA/m^2 at temperatures between 5-15 °C and 17 mA/m^2 at 40 °C [16]. This is a quite conservative assumption, as Gartland and Eggen had found that the current demand for sealed specimens polarized down to around -900mV vs Ag/AgCl was less than 1 mA/m^2 [17]. However, current density requirements for steel at damages must be taken into consideration in the total CP design. A reasonable assumption is that the coating failure of TSA should not be any larger than for organic coating, which is estimated to 1 %. In addition, TSA is much more robust than organic coating, which resulted in an estimated coating failure at 10% at the end of the lifetime for TSA [16]. The current demands for Al and AlZn coatings, sealed and unsealed, over an exposure time of 16 months and around 8 °C are shown in Figure 2.5. The figure shows that arc sprayed AlMg coating has a current demand at around 30 mA/m^2 after 1 month and less than 10 mA/m^2 after 16 months. The sealed

arc sprayed AlMg coating has a current demand around 1 mA/m^2 after one month and during the rest of the test period. Steel has, for comparison, a current demand around 30mA/m^2 after 16 months [17].

Fischer et al studied the influence of temperature on the current demand for TSA polarized to -1100 mV vs Ag/AgCl at 70-100 °C. After a month the current density had a mean value of 70 mA/m^2 and after a year the value had decreased to 30 mA/m^2 [14].

In addition to reducing the cathodic current demand, sealing of TSA-coatings will also reduce the current output under anodic polarization. While to the current output for an unsealed specimen is 500 mA/m^2, a sealed specimen has a current output between 30-200 mA/m^2. However, the current output for the sealed specimens is sufficient to achieve polarization of bare steel in a damage or holiday area and at the same time lowering the coating consumption of the TSA-coating, leading to an increase in the service life of the structure [16].

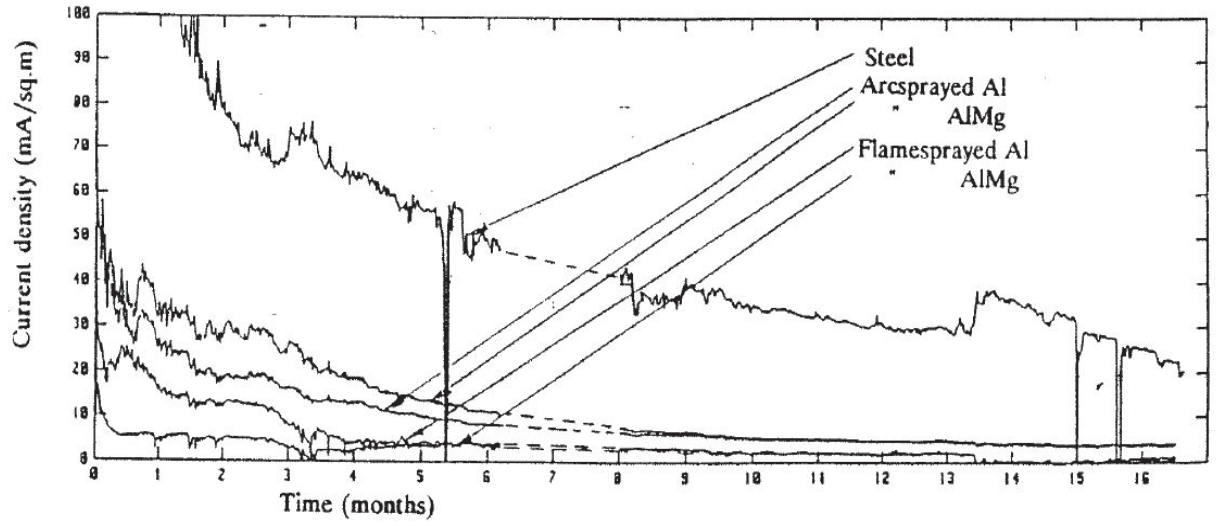

(a)

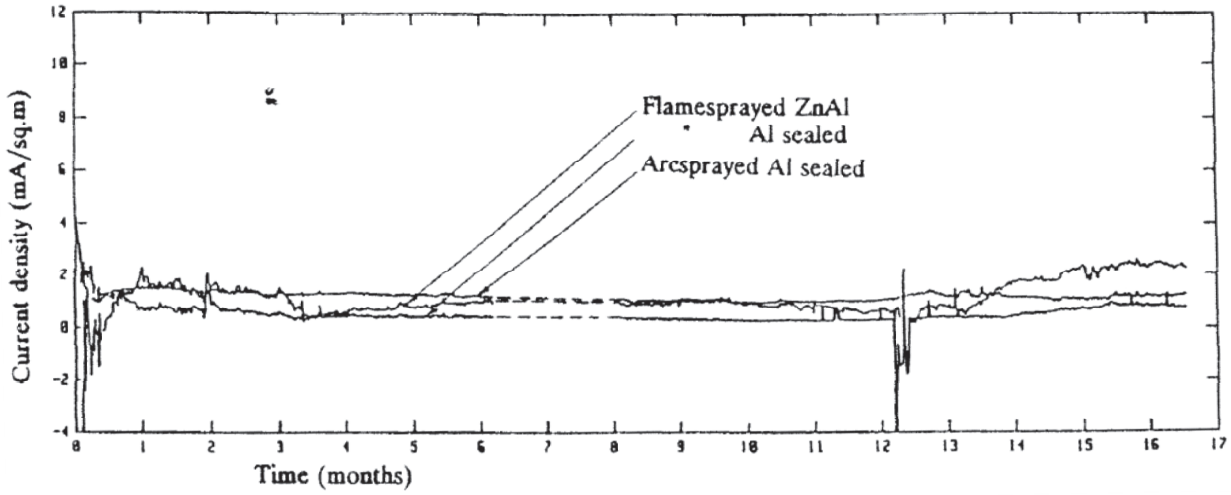

(b)

Figure 2.5: Cathodic current density of arc and flame sprayed Al coating, arc sprayed AlMg and steel (a) and flame sprayed ZnAl and arc and flame sprayed Al with sealer (b). All polarized to -1030 mV vs Ag/AgCl at a temperature around 8 °C [17].

2.3 Calcareous deposit formed during cathodic protection

2.3.1 Formation of calcareous deposit

In natural seawater the carbon dioxide system is given by equations (2.6) -(2.8) [11].

$$CO_2 + H_2O \rightarrow H_2CO_3 \quad (2.6)$$

$$H_2CO_3 \rightarrow H^+ + HCO_3^- \quad (2.7)$$

$$HCO_3^- \rightarrow H^+ + CO_3^{2-} \quad (2.8)$$

An increase in OH^-, as a result of cathodic protection, leads to a shift in the HCO_3^-/CO_3^{2-} ratio, increasing the formation of CO_3^{2-}, as can be seen from equation (2.9) [11, 19].

$$OH^- + HCO_3^- \rightarrow H_2O + CO_3^{2-} \quad (2.9)$$

The increase in OH^- can be due to cathodic protection, either from oxygen reduction, equation (2.10), or hydrogen evolution, equation (2.11) [11].

$$O_2 + 2H_2O + 4e^- \rightarrow 4OH^- \quad (2.10)$$

$$2H_2O + 2e^- \rightarrow H_2 + 2OH^- \quad (2.11)$$

When calcium and magnesium are supersaturated in seawater, they form calcium carbonate, $CaCO_3$, magnesium carbonate, $MgCO_3$ and $Mg(OH)_2$, as seen in equation (2.12), (2.13) and (2.14) respectively. Studies have found that Mg^+ is primarily found as $Mg(OH)_2$, with some $MgCO_3$ [11].

$$Ca^{2+} + CO_3^{2-} \rightarrow CaCO_3(s) \quad (2.12)$$

$$Mg^{2+} + CO_3^{2-} \rightarrow MgCO_3(s) \quad (2.13)$$

$$Mg^{2+} + 2OH^- \rightarrow Mg(OH)_2(s) \quad (2.14)$$

The solid products in equations (2.12)-(2.14) are known as calcareous deposits and they promote a physical barrier against oxygen diffusion, hence, decreasing the corrosion rate [20]. The different forms of calcareous deposits have different structure and form under different parameters, as will be reviewed in the following.

2.3.2 Microstructure of calcareous deposits

$CaCO_3$ mainly exists in two forms; calcite and aragonite [19]. Calcite has a rhombohedral shape with a certain space between each crystal, while aragonite spreads out like a flower and cover more of the surface, as seen in Figure 2.6 [20]. The structure makes the aragonite more protective to the substrate material. A study by Möller [20] showed that a steel surface covered with calcite would corrode between the rhombohedras. For the aragonite the area of exposed steel was negligible. $Mg(OH)_2$, forms aggregates of platelets, a very thin film which is difficult to detect [21]. The Mg rich deposit is sometimes refered to as brucite. The formation of a thin film of $Mg(OH)_2$ was confirmed by Deslouis et al who studied the formation of $Mg(OH)_2$ in the absence of $CaCO_3$ in artificial seawater and found that the structure of $Mg(OH)_2$ is a thin film in the range of micrometers [22]. The film is not significantly protective by itself and has a lower electrically insulating capability than $CaCO_3$ [23]. In addition, Mg^{2+} has an inhibiting effect on the nucleation and growth of calcite and the nucleation of aragonite [22]. Once aragonite is formed, Mg will not affect further growth. Consequently aragonite is the phase which is most likely to precipitate when magnesium ions are present [11]. $CaCO_3$ will be found as particles in a thin layer of $Mg(OH)_2$ [24].

During the introductory experiments, steel plates were exposed to seawater polarized to −1050 mV vs Ag/AgCl. The conditions were the same as will be described for the experiments done in connection to this thesis. Figure 2.7 shows particles with the typical calcite-structure with the rhombohedral shape, in addition to several small particles covering the surface as a blanket. The EDS-analysis showed that the Mg/Ca ratio was 0.7 for the large particles and 0.1 for the small particles. Over the whole area the Mg/Ca ratio was 0.2 [25].

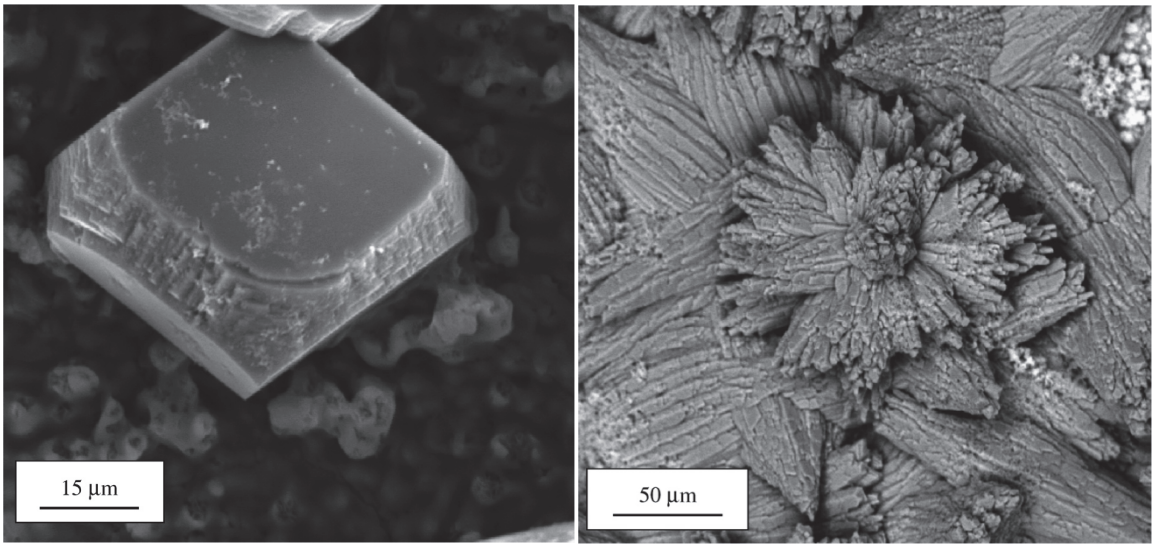

Figure 2.6: Calcareous deposit on steel surfaces formed during immersion for 21 days in an Mg^{2+} -free solution with the resulting calcite structure (left) and in an Mg^{2+}-containing solution with the resulting aragonite structure (right) [20].

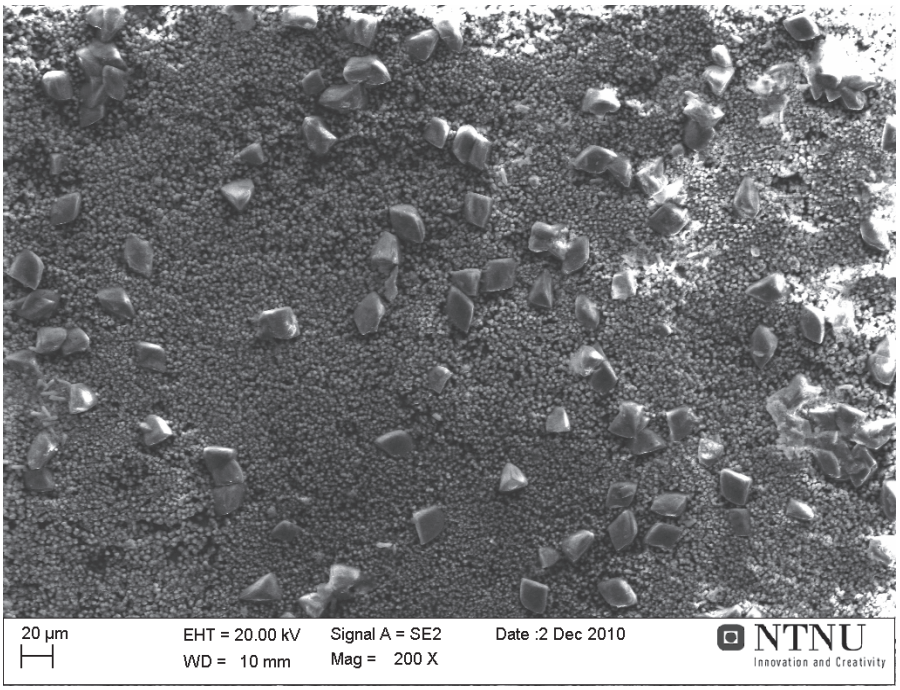

Figure 2.7: Calcareous deposit formed on steel polarized to -1050 mV vs Ag/AgCl in natural seawater for 6 weeks [25].

A study by Möller on the influence of Mg^{2+} on the formation of calcareous deposit on a freely corroding low carbon steel in seawater, showed that in artificial seawater with added Mg, aragonite was the only form of $CaCO_3$ found, while in a solution without Mg calcite was the only form [20]. This is confirmed by a number of scientists. Rousseau et al discovered that when the precipitation of $Mg(OH)_2$ in the presence of natural sediments was hindered because of low pH, the only form of calcareous deposit found was calcite [26].

Ben Amor et al found that an increase of Mg^{2+} concentration caused deposition of deformed calcite form, which was transformed to aragonite at larger Mg^{2+} concentrations [27]. Deslouis et al studied calcareous deposit in the absence of respectively $CaCO_3$ and $Mg(OH)_2$. They found that in the absence of Mg^{2+}, calcium carbonate deposition was observed in well define shapes of both calcite and aragonite. While in the absence of Ca^{2+}, $Mg(OH)_2$ precipitated under a rather amorphous form with a porous layer behavior [22]. This Mg containing layer could form even at potential values where $Mg(OH)_2$ normally can no deposit [22]. Barchiche et al found that the effect of Mg^{2+} was to inhibit both calcite and aragonite deposition and favor the formation of another compound, an unstable porous layer which may be the precursor of the brucite $Mg(OH)_2$ layer that forms at more cathodic potentials [28].

Figure 2.8 shows the influence of Mg^{2+} concentration on the forming of calcareous deposit [21]. The reference concentration is $[Mg^{2+}]_{ref}=5.5*10^{-2}$ mol/L. The trend is clear; the higher Mg^{2+} concentration, the longer the deposition time. As the potential for this experiment was -0.9 V SCE, the potential was too low to form $Mg(OH)_2$. That

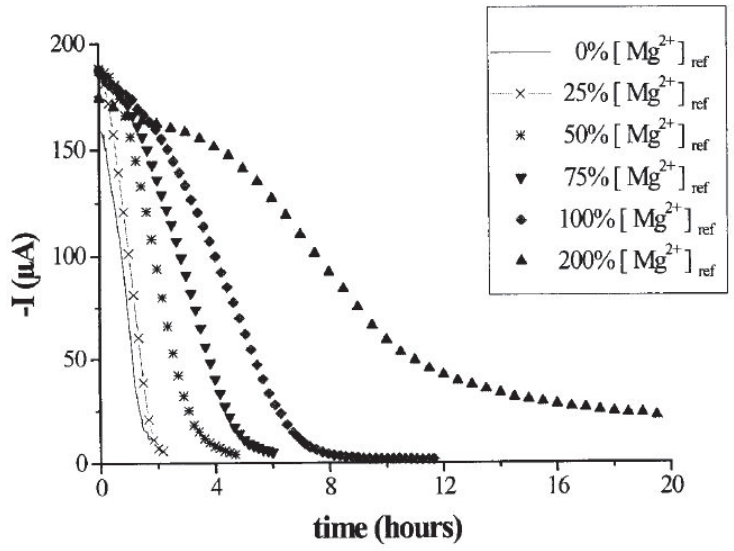

Figure 2.8: Influence of Mg2+ concentration on steel in artificial seawater at -0.9 V SCE.

indicates that it is not the $Mg(OH)_2$ that is preventing the formation of $CaCO_3$, it is rather the Mg^{2+} ions.

2.3.3 Factors influencing the formation of calcareous deposit

Several factors influence the formation of calcareous deposit; e.g. potential, current, pH, temperature, pressure, sea water chemistry, flow and time. Many studies have been performed with the purpose of clarifying the different factors and their interrelating properties. However, the results are varying and sometimes contradictory, as the experiments are not performed under the exact same conditions. Still, a short overview of the most important factors is found in the following.

Solubility of ions

The saturation of calcium and magnesium ions is an important premise for the precipitation of calcareous deposit. The solubility of these ions in seawater is influenced by depth, dissolved oxygen, temperature, salinity, pH, flow rate and pressure, and these parameters are again interrelated [3].

The solubility product for $CaCO_3$ is given in equation (2.15), while the solubility grade, Ω, is given in equation (2.16). The solubility in a given area can be calculated based on measurements of temperature, pressure, salinity and pH [29]. $[Ca^{2+}]$ and $[CO_3^{2-}]$ are the measured calcium and carbonate concentrations in seawater.

$$K_{sp} = \left[Ca^{2+} \right] \left[CO_3^{2-} \right] \quad (2.15)$$

$$\Omega = \frac{\left[Ca^{2+} \right] \left[CO_3^{2-} \right]}{K_{sp}} \quad (2.16)$$

The solution is saturated and calcareous deposit will precipitate if Ω > 1, but even if Ω < 1 calcareous deposit can precipitate if the production of carbonate is high enough to compensate for the dissolution.

Seawater is generally saturated with $CaCO_3$. The solubility product, K_{sp}, for calcite at 25°C and 3.5% salinity is $3.6*10^{-9}$, while for aragonite it is $6,7*10^{7}$ [11]. Hence, calcite will precipitate before aragonite. Studies has shown that precipitated calcite can be stable, i.e. it will not dissolve, down to Ω= 0.6 [29]. The solubility of $Mg(OH)_2$ is $4.5*10^{-10}$ and seawater is generally unsaturated with $Mg(OH)_2$.

Potential/current

When polarizing an electrode to a specified cathodic potential in aerated water, as is the case in cathodic protection, the current density will decrease with exposure time as the oxygen concentration polarization is invariably accompanying the polarization. The precipitation of calcareous deposit accompanies this polarization which, in turn, increases the extent of oxygen concentration polarization [11].

There is uncertainty concerning whether it is the current density or the potential that is the leading factor in determining the properties of calcareous deposit, as they are interrelated. Lowering the potential leads to an increase in current density and contrary. However, what is known, is that up to an optimal value, lowering the potential (or increasing the current density) will increase the concentration of $Mg(OH)_2$ relative to that of $CaCO_3$ [23]. Studies done by Barchiche et al showed that at 20 °C aragonite was formed between -0.9 and -1.1 V SCE, brucite and aragonite were formed at -1.2 V SCE and only brucite was formed at potentials lower than -1.3 V SCE [28]. Figure 2.9 shows the chronoamperometric curves at different potentials for steel in artificial seawater at 600 rpm [28]. The curves show two particular shapes, with a transition at -1.2 V SCE. The curves corresponding to the highest potentials has a steep slope in the beginning and is a typical curves of $CaCO_3$ deposition, while the curves at lower potentials starts with a plateau, and is typical curves of $Mg(OH)_2$ deposition. The difference of the potentiostatic curves for the two deposits shows, for one, that the protective properties are better at high potentials due $CaCO_3$ deposition, and, secondly, $Mg(OH)_2$ needs more negative potential than $CaCO_3$ to deposit.

Figure 2.10 shows the potentiostatic polarization curve for a steel specimen exposed to natural seawater polarized to -1050mV vs Ag/AgCl [25]. The curve has a steep

decrease in the beginning, indicating the formation of calcite. This was confirmed by the SEM image in Figure 2.7.

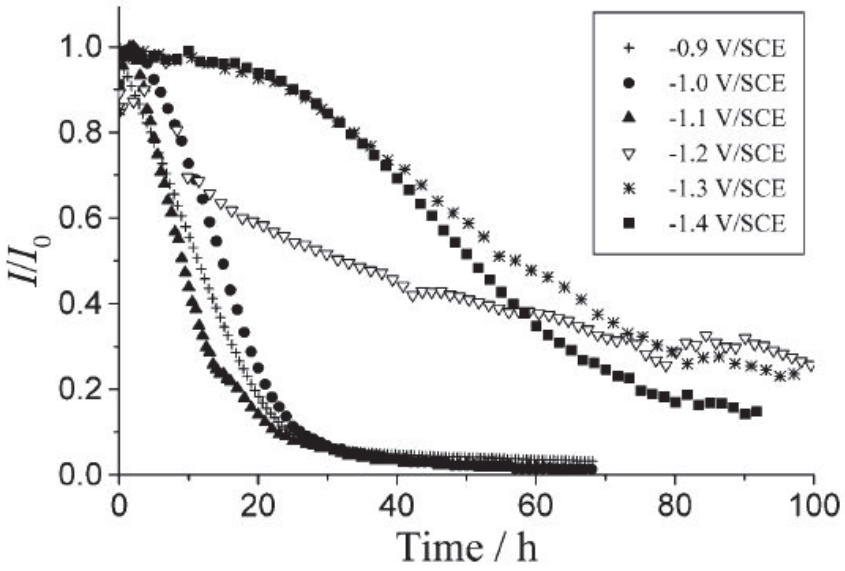

Figure 2.9: The effect of different potentials on the deposition of $CaCO_3$/$Mg(OH)_2$ [28]. The steep current curves represents $CaCO_3$ deposition, while $Mg(OH)_2$ deposition is represented by an initial stage before the decreasing in current. -1.2 V SCE seems to be the transition potential.

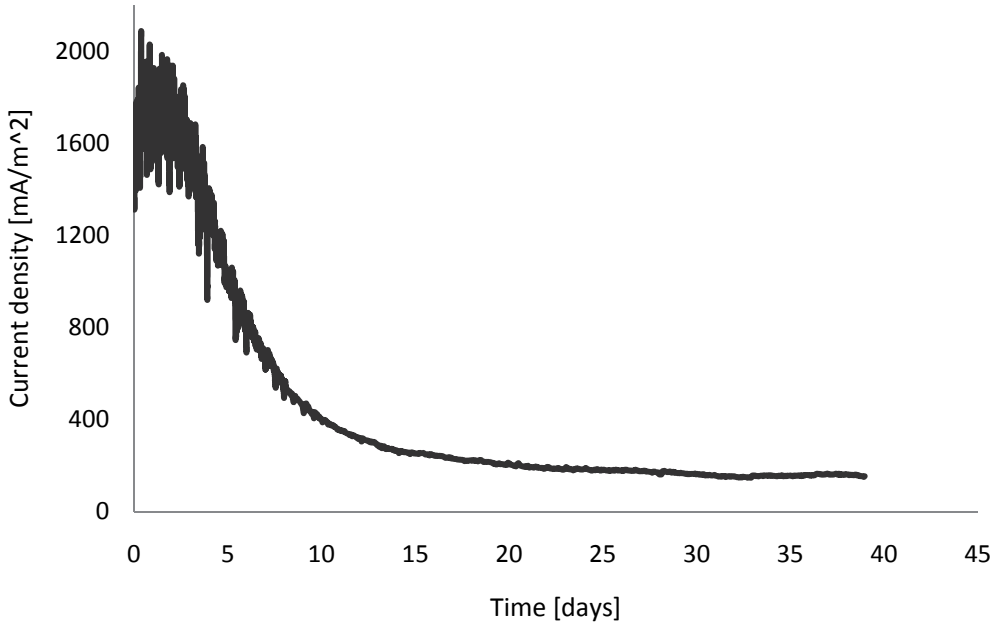

Figure 2.10: Potentiostatic polarization curve for a steel specimens in natural seawater polarized to -1050 mV vs Ag/AgCl [25].

Lowering the potential to a value where hydrogen evolution is the cathodic reaction affects the formation of a calcareous deposit. Barchiche et al found that formation of H_2 bubbles hinders the growth of aragonite crystals, as the bubbles induces cracks in the deposits and detachment of small fragments [30]. This was also investigated by Salvago et al [31]. During oxygen reduction, the deposit formed must be permeable to the ionic phase OH^- on the electrode surface, while during hydrogen evolution, the deposit must be permeable to the gas phase, H_2. In addition bubbles of hydrogen gas may mechanically hinder the formation of a protective deposit. Salvago et al found in their study that in the case of aluminum and its alloys, a consistent calcareous deposit could be observed after potentiodynamic tests performed at high current density and strong gas evolution. This was not the case for the other materials investigated, including steel. The hydrogen bubbles on the aluminum surface were macroscopically evident at potential lower than -1250 m V vs Ag/AgCl. At potentials below -2000 mV vs Ag/AgCl, the bubbles disappeared despite high current density [31].

pH

pH in seawater is between 7.5 and 8.3 [11]. However, pH is a function of the impressed cathodic current. According to equations (2.10) and (2.11) there will be an increase in pH for the electrolyte adjacent to the metal surface due to the production of hydroxyl ions [11]. Figure 2.11 is a schematic outline of how the pH immediate to the metal-electrolyte interface is determined by the rate of hydroxyl ion production and by removal due to diffusion, convection or both [11].

The increased pH immediate to the cathode surface due to cathodic protection is shown in several experiments and calculations, summarized by Hartt et al in [11]. Engell and Forchhammer found that pH on the surface of a cathodic protected steel plate in seawater was 10.9. Kobayashi found pH in the bulk solution to be 8.0, while it was 11.5 near the surface of the metal protected in artificial seawater. Salvago et al reported pH 10.76 at the cathode surface in artificial seawater, while the increase in pH at a cathode surface in natural seawater was smaller [31]. Deslouis et al calculated that for a potential of 0.5 V SCE the interfacial pH is close to 9.3, while at -1.0 V SCE the pH is 9.6 [32].

At increasing pH the growth and precipitation rates of $CaCO_3$ will increase [29]. $CaCO_3$ is thermodynamically stable in surface sea water, i.e. it is supersaturated in the ambient pH range. $Mg(OH)_2$, which is unsaturated in seawater, needs a pH higher than approximately 9.5 to precipitate [11]. Hence, an increase in pH by e.g. cathodic protection, is necessary for $Mg(OH)_2$ to form. Deslouis et al confirmed this in their study by finding that the critical value for $Mg(OH)_2$ to form was 9.3 [22].

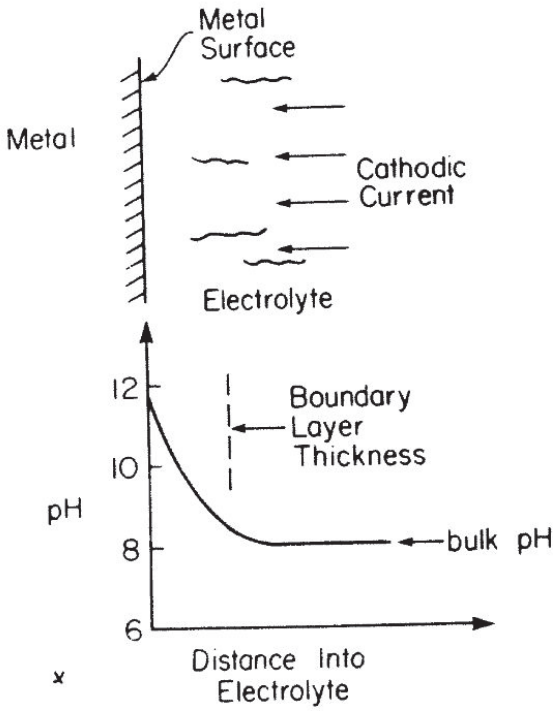

Figure 2.11: pH as a function of distance from electrode [11].

Temperature and pressure

The temperature in seawater affects both the pH and solubility of Mg and Ca. It decreases with depth and by 900 m depth in the Gulf of Mexico the temperature is 5°C [33]. The solubility of $CaCO_3$ increases with decreasing temperature, while the solubility of Mg decreases. That explains why it often is found higher Mg content at low temperatures [34]. In addition, pH increases at lower temperatures, hence favoring the precipitation of $Mg(OH)_2$.

This is confirmed in studies by Fischer et al, were calcite was the dominant mineral in seawater at 5°C and pH > 7, while aragonite was the dominant mineral at increasing temperature. In deep water, i.e. at low temperatures, magnesium calcite was the dominant mineral formed [29].

Stangeland reported in her master thesis that the Mg/Ca ratio for particles found on steel specimen polarized to -1 000 mV SCE at temperature between 0.3 and 0.8 °C was 1 and 0.6 [23].

Experiments done by Barchiche et al showed how temperature influences the formation of calcareous deposit. Figure 2.12 shows the current for specimens polarized to −1,0 V SCE (a) and -1.2 V SCE (b) at a rotation speed of 600 rpm in artificial seawater. At -1,0 V SCE only aragonite was formed. The current is halved after 7.5 hours at 30 °C, 15 hours at 20 °C and after 41 hours at 10 °C [30]. This indicates that the time for calcareous deposit to form, or rather a *protective* form of calcareous deposit, is much slower at 10 °C than both 20 °C and 30°C.

However, the same experiment performed with E= -1,2 V SCE, where the interfacial pH mainly controls the deposition, showed no apparent influence by the temperature, as shown in Figure 2.12b). In this case brucite $Mg(OH)_2$ and aragonite was formed, with increasing portion of brucite with increasing temperature. The increase of $Mg(OH)_2$ deposit at higher T is in contrast to the fact that the solubility of $Mg(OH)_2$ increases with increasing temperature. This was explained by the high interfacial pH due to the low potential, which facilitates formation of both $Mg(OH)_2$ and aragonite, so that the solubility of the compounds has a negligible effect. Since the formation of brucite depends closely on the interfacial pH, an increase in temperature, favoring water reduction, would favor the formation of $Mg(OH)_2$ [30].

Thermodynamic calculations by Fischer et al [29] showed that the effect of hydrostatic pressure has a major influence on the solubility of calcite. At 5 °C and 100 atm, corresponding to 1 000 m depth, the solubility of calcite will increase by 16% compared to at 1 atm, and at 1 000 atm, i.e. 10 000 m depth, the solubility will increase by nearly 500%. It is obvious from the calculations that calcite is unsaturated at large depths. However, the $CaCO_3$ saturation is not constant over an entire ocean area, but will depend upon local conditions of currents, temperature, and biochemical processes [29].

Fischer et al found in their study that calcareous deposits formed in deep water will be stable at depths down to at least 3000 m (or to where the degree of calcite saturation is 0.6 or higher). This makes the calcareous deposits stable in the North Sea at 65° and the Gulf of Mexico, where the saturation is 0.6 or higher [29].

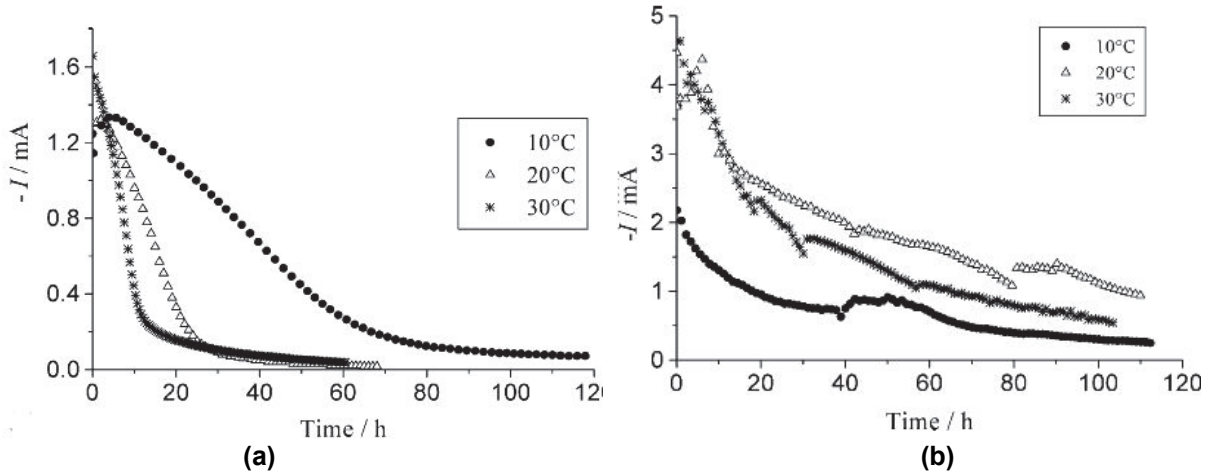

Figure 2.12: Effect of temperature for specimens polarized to (a) -1000 mV SCE and (b) -1200 mV SCE at a rotation speed of 600 rpm in artificial seawater [30].

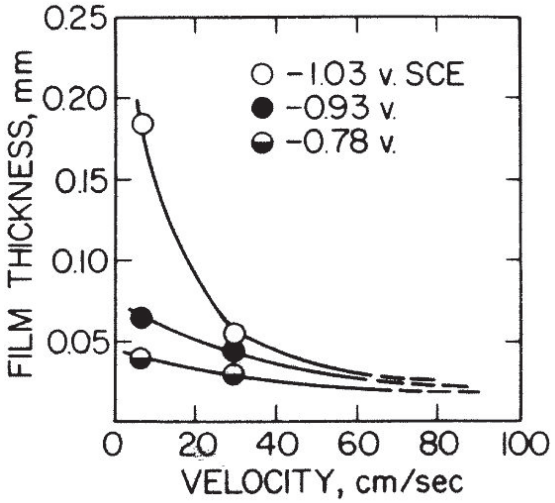

Figure 2.13: Thickness of calcareous deposit film as a function of seawater velocity [11].

Flow rate

The current requirement for a steel structure increases with increasing velocity. This is due to the increased availability of reactants near the surface as a consequence of a thinner diffusion layer and the increasing limiting current for oxygen reduction [23]. The increasing current demand would lead to increased pH. At the same time, it has been found that the thickness of the calcareous deposit is reduced with increasing velocity, with the trend shown in Figure 2.13 [11].

Seawater chemistry

Seawater chemistry is in most part about the dissolved oxygen and magnesium ion content. The Mg/Ca ratio is stable in seawater reported to be 5.2 mol/mol or [35]. The Mg/Ca ratio has generally been related to the protective properties of the calcareous deposit. In addition to the inhibiting effect Mg^{2+} ions have on the formation and growth of calcite and aragonite, other ions present in seawater also contribute. The growth rate of both calcite and aragonite is inhibited by the presence of phosphate, sulphate and by organic constituents. Aragonite is inhibited by the PO_4^{3-} ion, while calcite is inhibited by both PO_4^{3-} and HPO_4^{2-} ions [29]. Also sulphate ions, which is the main anionic species in seawater after Cl^- ions, influences the deposition [30]. Barchiche et al found that the presence of SO_4^{2-} anions proved to hinder the deposition of $CaCO_3$. This was proven by the fact that in a solution of artificial seawater with SO_4^{2-} only less than half of the electrode surface was covered with calcareous deposit, whereas without the SO_4^{2-} anions, the surface was totally covered [30].

The presence of clay in seawater must also be considered. Deslouis et al found that the montmorillonite particles, which are the most widely used material for fundamental studies, significantly delayed the onset of calcareous deposition. Once

the deposition started, however, the kinetics of deposition is unchanged relative to the situation without clay particles [36].

2.4 Methods used to characterize calcareous deposits

To investigate the calcareous deposit, several methods can be used. During the exposure, potentiostatic and potentiodynamic polarization can be performed. Potentio*static* polarization is applying a constant potential, while measuring the corresponding current as a function of time. During potentio*dynamic* polarization, the potential is changed in steps of a certain size in with a certain holding time, while measuring the corresponding current. The results from the polarization give information about the precipitation of calcareous deposit and how protective the deposit is. In addition, the potentiodynamic polarization curves gives information about what kind of reduction reactions that are happening on the surface.

A Scanning Electron Microscope, SEM, can be used to investigate the surface of the specimens. The microscope gives information about topography and crystallography. In addition, chemical composition can be found using EDS, Energy-dispersive X-ray Spectroscopy. The EDS detector, made of SiLi, can analyze the whole spectra at the same time and detects more photons than e.g. the wavelength dispersive spectrometer, WDS, even at low beam currents. EDS is suitable of identifying elements at concentrations higher than 0.5-1% [37].

3 Experimental work

3.1 Test specimens

Experiments were performed on 5 different materials, with 7 different situations in all.

1. Steel with thermally sprayed aluminum

The specimens were made out of a steel plate sprayed with thermally sprayed aluminum. Wire arc spraying was the method being used and the coating was 100 – 200 µm thick. The alloy was AlMg5, with 95% Al and 5 % Mg. After the coating was applied, the plate was cut in pieces of 35 x 60 mm. The work was performed at Scana Offshore Vestby AS. Next, the back and sides of the specimens were painted with an organic coating, Carbomastic 18 FC, to avoid exposure of the bare steel. 10.

2. Steel with thermally sprayed aluminum – sealed

Since appliance of sealant on TSA is recommended practice for applications submerged in seawater, a silicon sealer was applied on two of the TSA specimens. This was in order to compare the two cases, sealed and unsealed TSA. As mentioned above, the rest of the TSA samples were not applied sealant. This was in order to hasten the reactions on the surface. The organic sealant will gradually degrade, resulting in the same reactions than without sealant after some time (in the order of years).

3. Long term exposure of TSA specimens

To study the long term effect of exposure to cathodic protection in seawater, introductory experiments still submerged in seawater when the present experiments began were investigated. The specimens were prepared similar to the specimens described above and polarized to the same potential as the new experiments. The specimens had been submerged for 4 months when taken out of the tub.

4. Aluminum plate of alloy AA5082

This alloy is also known as an AlMg5 alloy, i.e., it contains up to 5% magnesium. For the rest of the composition, see Table 3.1. This alloy is close to the alloy used for the TSA specimen. For these specimens it will be easier to locate the intermetallic particles, as the surface is smooth compared to the TSA surface. The extruded plate was cut in pieces of 35x60 mm and submerged in as-received condition.

Table 3.1: Composition of the alloy AA5082 and the impurity limits for AA1050.

	Mg	Si	Fe	Cu	Mn	Cr	Zn	Ti
AA5082	4.0-	0.2	0.35	0.15	0.15	0.15	0.25	0.06-0.20
AA1050	0.05	0.25	0.4	0.05	0.05	-	0.05	0.03

5. Aluminum plate of alloy AA1050
Earlier work on TSA specimens showed that the calcareous deposit mainly consisted of $Mg(OH)_2$ [25]. To see whether the magnesium comes from the seawater or the alloy, plates of an alloy without magnesium will also be submerged. Aluminum alloy AA1050, which contains up to 99.5% aluminum with maximum 0.05% Mg, was therefore chosen. The impurity limits for the alloy are found in Table 3.1. Alloys containing 0.1 to 1% impurities are generally known as *commercially pure aluminum* and the impurities mainly consist of iron and silicon as insoluble particles. Al99.5 alloys are also commonly used alloy for TSA.

The extruded plate was cut in pieces of 35x60 mm and submerged in as-received condition.

6. Aluminum plate with 99.99% aluminum.
To verify the theory of the intermetallic particles acting as cathodic sites were the calcareous deposit precipitates pure aluminum plates with 99.99% aluminum were also investigated. This *refined aluminum* is produced by electro-refining the commercially pure metal in the three layer cell and should contain a minimum of intermetallic particles [4].

The extruded plate was cut in pieces of 35x60 mm and submerged in as-received condition.

7. Potentiodynamic polarization of TSA specimens
During the exposure to seawater potentiodynamic polarization curves were recorded almost weekly on four specimens with thermally sprayed aluminum, two with sealer and two without. The potential at start was -1050mV vs Ag/AgCl and then changed in steps at 25 mV in the positive direction with a dwell time of 5 minutes. The recording ended when the current density drew near the corrosion current, i_{corr}, correspondingly around -900 mV vs Ag/AgCl. Afterwards, the potential was set back to -1050 mV vs Ag/AgCl again.

In order to electrically connect the specimens to the potensiostat an electric wire was fasten to the specimens. This was done by fastening the electric wire to a fastener with a hole, drilling a hole on the upper part of the specimen and threading and

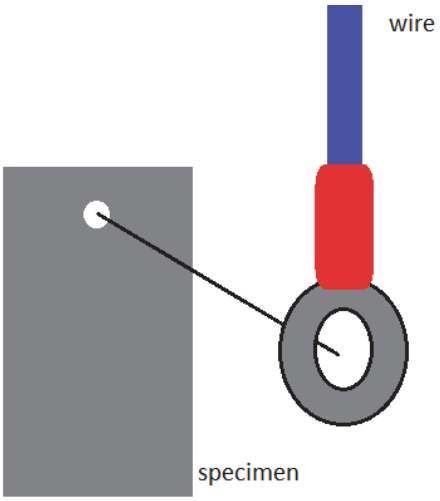

Figure 3.1: Fastening of electrical wire to the specimen. The rivet goes through the two holes, as marked by the black line.

tightening a rivet through the two holes, as shown in Figure 3.1. The electrical conductivity was tested using a multimeter.

Before exposure the specimens were degreased in acetone and rinsed in ethanol.

3.2 Exposure to seawater with cathodic protection

The experiments were performed at SEALAB Brattøra in Trondheim. The specimens described above were exposed to natural seawater, taken from 80 m deep in the Trondheimsfjord. The water, with a temperature at 8-12 °C, was filtered before entering the tub where the specimens were mounted. The circulation of the seawater was so slow, that the conditions in the tub can be described as nearly stagnant. The specimens were exposed for 6 weeks.

Due to practical reasons, the specimens were divided in two tubs; the aluminum plates and the sealed TSA samples were placed in one tub, while the unsealed TSA specimens and the specimens used for potentiodynamic polarization curves were placed in the other. The experimental parameters in the two tubs were in principle the same.

The specimens were coupled to a potensiostat and polarized down to -1050mV vs Ag/AgCl. A resistance of 10 ohms was connected between the working electrodes (the specimens) and the platinum counter electrodes. The current was calculated by measuring the potential drop over the resistance and applying Ohm's law. Se Figure 3.2 for the setup. The current consumption and potential was recorded by the computer program KorrosjonsLogger Versjon 1.1©. It was possible to follow the current development in situ during the whole period.

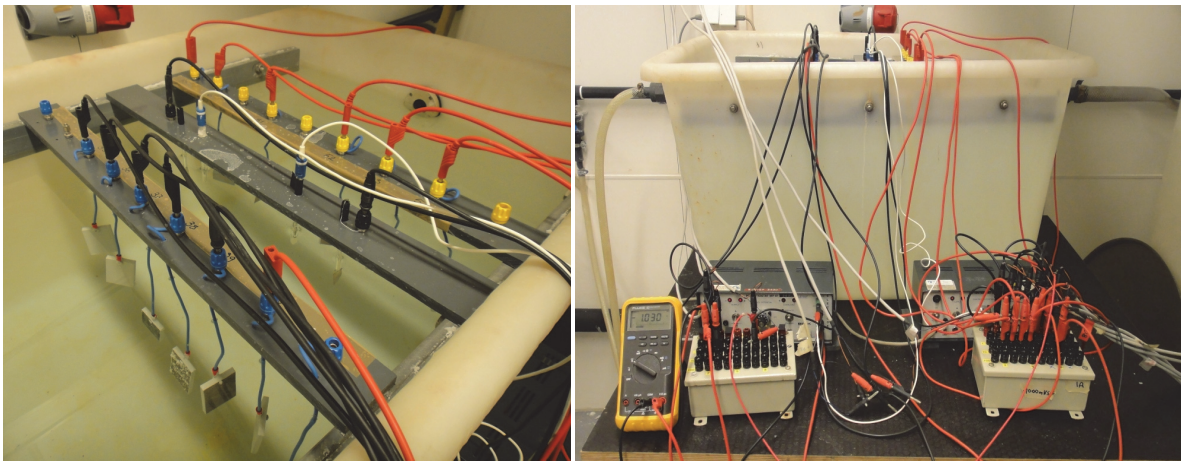

Figure 3.2: Experimental setup for the test specimen.

3.3 Examination of the specimens

After 6 weeks exposure the specimens were taken out of the tub and rinsed in water and acetone. Subsequently they were examined visually in the LVFESEM (Low vacuum field emission scanning electron microscope) Zeiss Supra 55VP and the FESEM (field emission scanning electron microscope) Zeiss Ultra, 55 Limited Edition. The use of two different SEM was due to a malfunction of one of them during a period. The composition on the surface was determined using EDS (Energy Dispersive Spectroscopy). The SEM images were taken with varying magnification at 10-15kV and a working distance of 10 mm.

It was emphasized on studying the intermetallic particles, to find their composition and see whether the amount and composition of calcareous deposit to be found there, agrees with the theory.

For the investigation of the TSA structure, the TSA surface was grinded using SiC paper from 320 grit to 2400 grit and then polished with Struers MD*Dac* plates with grain size from 3μm to 1 μm.

To examine the cross sections, the specimens were cut using Struers Discotom-5 with Struers High Quality Cut of Wheels number 50A25 for the TSA specimens and 20S25 for the aluminum plates. Afterwards the cross section was grinded and polished as described above.

4 Results

4.1 Potentiostatic polarization curves

4.1.1 TSA specimens –sealed and unsealed

The potentiostatic polarization curves show the development of the current density needed to keep the potential of the specimens at -1050 mV vs Ag/AgCl over time. Figure 4.1 shows the current density for the TSA specimens, sealed and unsealed. The curve for the unsealed TSA (light blue) is the average of five specimens, while the curve for the sealed TSA specimen is the average of two specimens. In addition to the values from the present experiments, results from earlier work done by the author is also included [25]. All the curves which the average is based on, including the curves for AA5082 and AA1050, are found in Appendix A.

As seen in Figure 4.1 the results for the TSA samples from the present experiments has clearly the highest current demand. After 38 days the current density is 80 mA/m^2, i.e., twice the value of the TSA from earlier work [25]. The difference in current density between the two curves for unsealed TSA specimens are, at the most, 60 mA/m^2. Still, the shape of the two curves is quite similar, with a steep slope the first 10 days of exposure before the current density increases slightly after 15 days. After 30 days, the current density for the TSA specimens from the present experiments decreases, while the other unsealed TSA specimen has a quite stable current density.

It should be reminded that the TSA samples from current and past experiments are prepared in the same way, has the same alloy composition and are polarized to the same potential. Still there is an important difference though; the temperature of the seawater. The temperature in the seawater was measured weekly. Two different tubs were used, but the water in both tubs came from the same place. One of the tubs had a relatively constant temperature at 10-12 °C during the whole exposure -the same temperature as found in earlier work by the author. In the tub were the TSA samples and the samples for potentiodynamic polarization curves were exposed, however, the temperature was 17-18 °C, before decreasing to around 12 °C after 30 days. This was unintended and could be due to a stop in the circulation of the water.

Figure 4.2 shows the same curves as Figure 4.1, but only for the first day of exposure. The figure shows the initial increase of current density as described by Gundersen and Nisancioglu in Figure 2.3 [10] for the TSA specimen from the present experiment, but not for the TSA from earlier work or the sealed TSA. In the case of the TSA from earlier work it is uncertain whether the logging started in time.

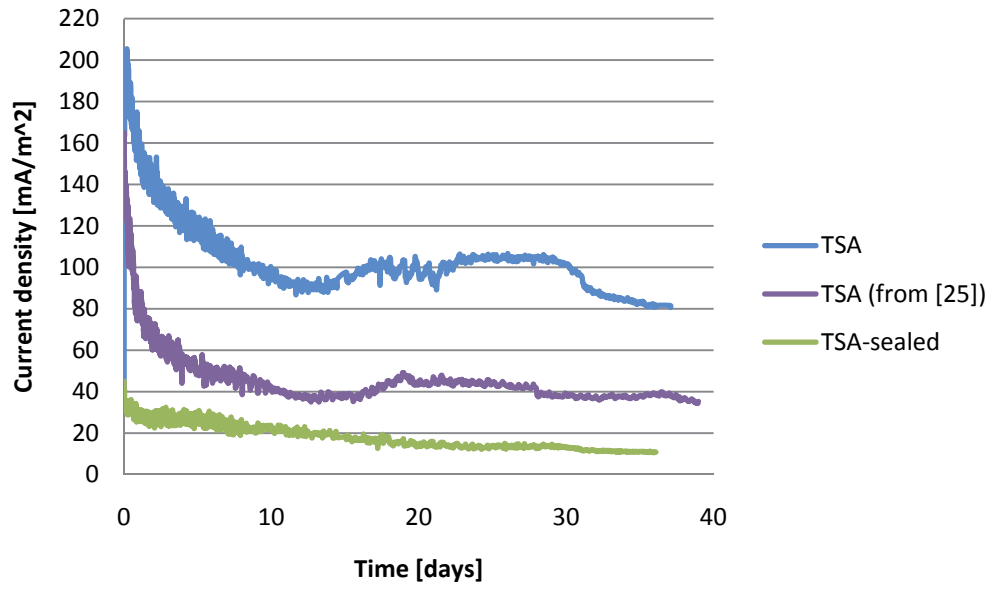

Figure 4.1: Potentiostatic polarization curves for TSA specimens polarized to-1050 mV vs Ag/AgCl . The blue and green line are from current experiments, while the purple is from earlier work [25].

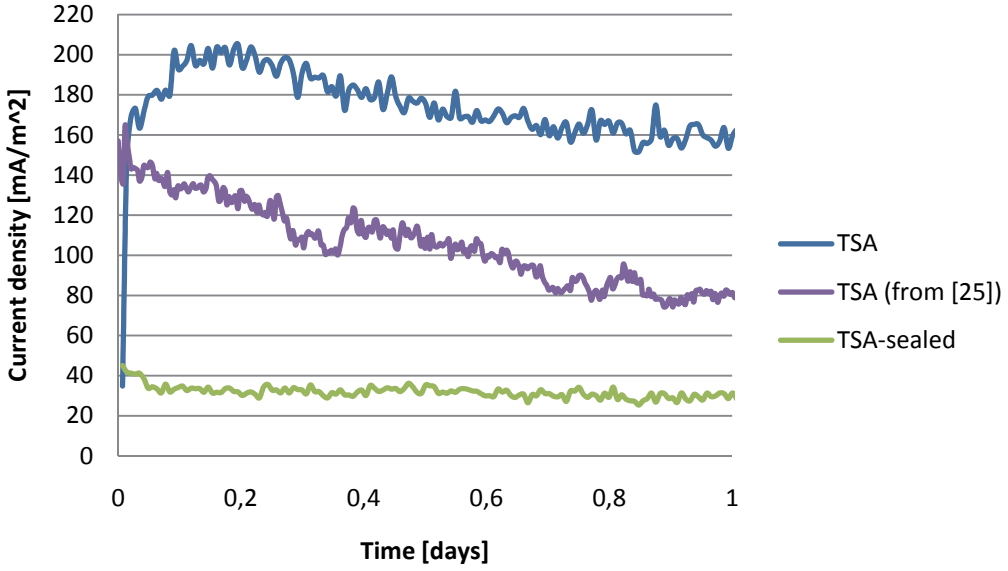

Figure 4.2: First day of exposure to cathodic protection in seawater for the same specimens as above.

4.1.2 Effect of sealer on the current demand

As mentioned in the theory, TSA is normally not used in seawater without a sealer. The effect of sealer on the current demand is evident from figure 4.1. The current density for the sealed TSA sample after 38 days is 10mA/m^2 -8 times lower than the unsealed specimens from the current experiments, or four times of the earlier work [25].

The duration of exposure was not long enough to see any degradation of the sealer.

4.1.3 Long term exposure of TSA specimen

Figure 4.3 shows the current density for the specimen that was exposed in natural seawater with cathodic protection for 4 months. As mentioned earlier, this specimen was submerged last fall, and taken out of the tub when the new experiments began. The current demand for the long term TSA follows the same behavior as the TSA specimens from Figure 4.1; it decreases fast during the first days, increases slightly again after 15 days and then decreases slowly. After 40 days, the current density was around 40 mA/m^2, like the TSA specimen from earlier work. After 4 months the current density was 25 mA/m^2.

Between 60 and 120 days exposure there was a malfunction in the logging program. However, as the value of the current density is just a few mA lower at 120 days then at 60 days and looks quite stable, it is assumed that the current demand has been relatively stable during this period as well.

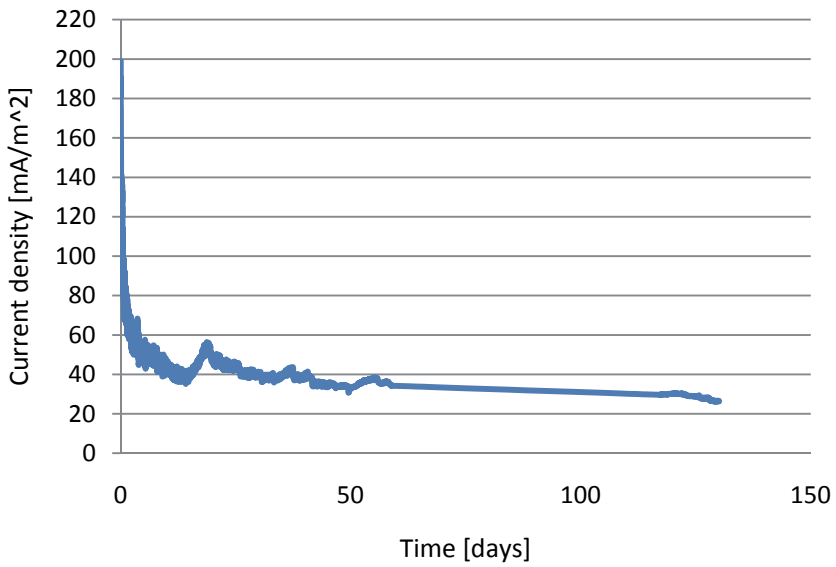

Figure 4.3: Potentiostatic polarization curve for a TSA specimen exposed to seawater, polarized to -1050 mV vs Ag/AgCl, for 4 months.

4.1.4 Aluminum alloys

Figure 4.4 shows the potentiostatic polarization curves for aluminum plates of alloys AA5082, AA1050 and Al99.99. After 30 days the current densities for the aluminum plates were 43 mA/m^2, 21 mA/m^2 and 7 mA/m^2, respectively. The tendency for the aluminum alloys is that the more alloying elements, the higher current density.

The curves representing the alloys AA5082 and AA1050 do not follow the same exponential decrease as the sketch in Figure 2.4, but still have the initial current peak. The initial peak for the specimen of AA5082 is difficult to see in Figure 4.4, but is visible in Figure 4.5 where only the first two days are shown. The peak for AA5082 is pointier, and takes place in the order of a couple of hours, while the peak for the alloy AA1050 lasts for nearly a day (up and down).

The current density curve for alloy Al99.99 does not have this initial increase in current density, but has a steep slope in the beginning, decreasing from 115 mA/m^2 to 20 mA/m^2 in only 3 days. The curve actually has more similarity to the curve representing a steel specimen in Figure 2.10.

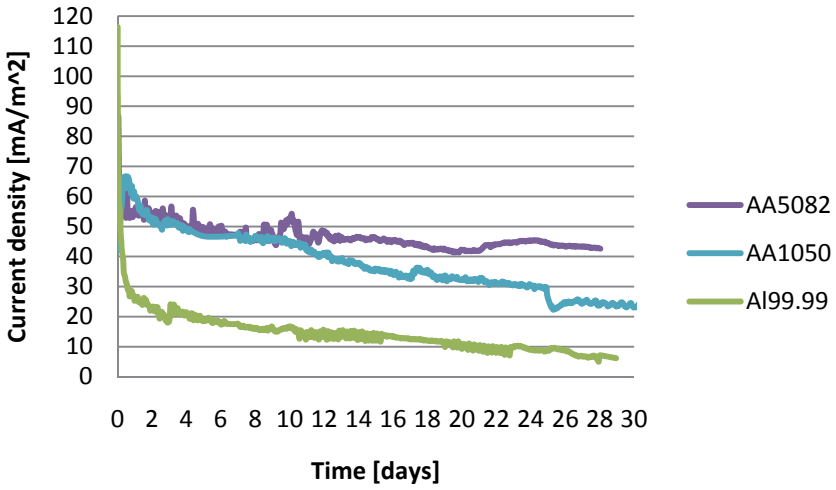

Figure 4.4: Potentiostatic polarization curve for aluminum alloys AA5082, AA1050 and Al99.99. An initial peak in current density is visible for the alloy AA1050.

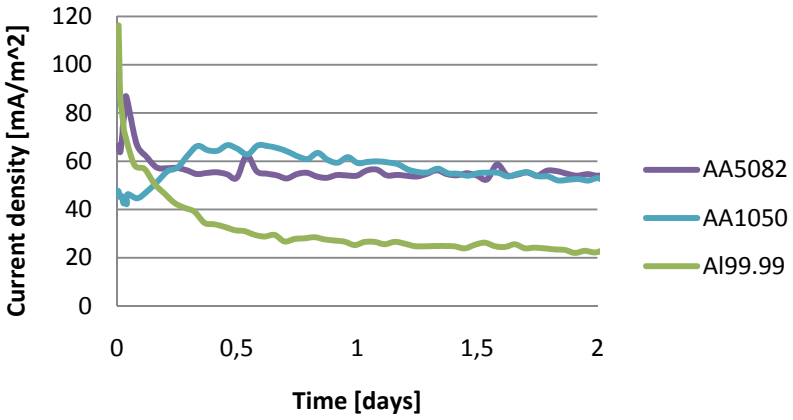

Figure 4.5: The first two days of exposure for the aluminum plates of alloy AA5082, AA1050 and Al99.99. At this magnification the peak at the beginning of the exposure is visible for the alloy AA5082.

4.2 Potentiodynamic polarization curves

Potentiodynamic polarization curves were recorded for TSA samples with and without sealer and the results are shown in Figure 4.6. As was the case for the potentiostatic polarization curves, the current density for the potentiodynamic polarization curves decreases with time and the current density for the sealed specimens are much lower than for the unsealed specimens. The last curves reach the corrosion current, i_{corr}, at a lower potential than the curves corresponding to freshly exposed surfaces.

These specimens were placed in the same tub as the TSA specimens, i.e. the temperature was 16-18°C.

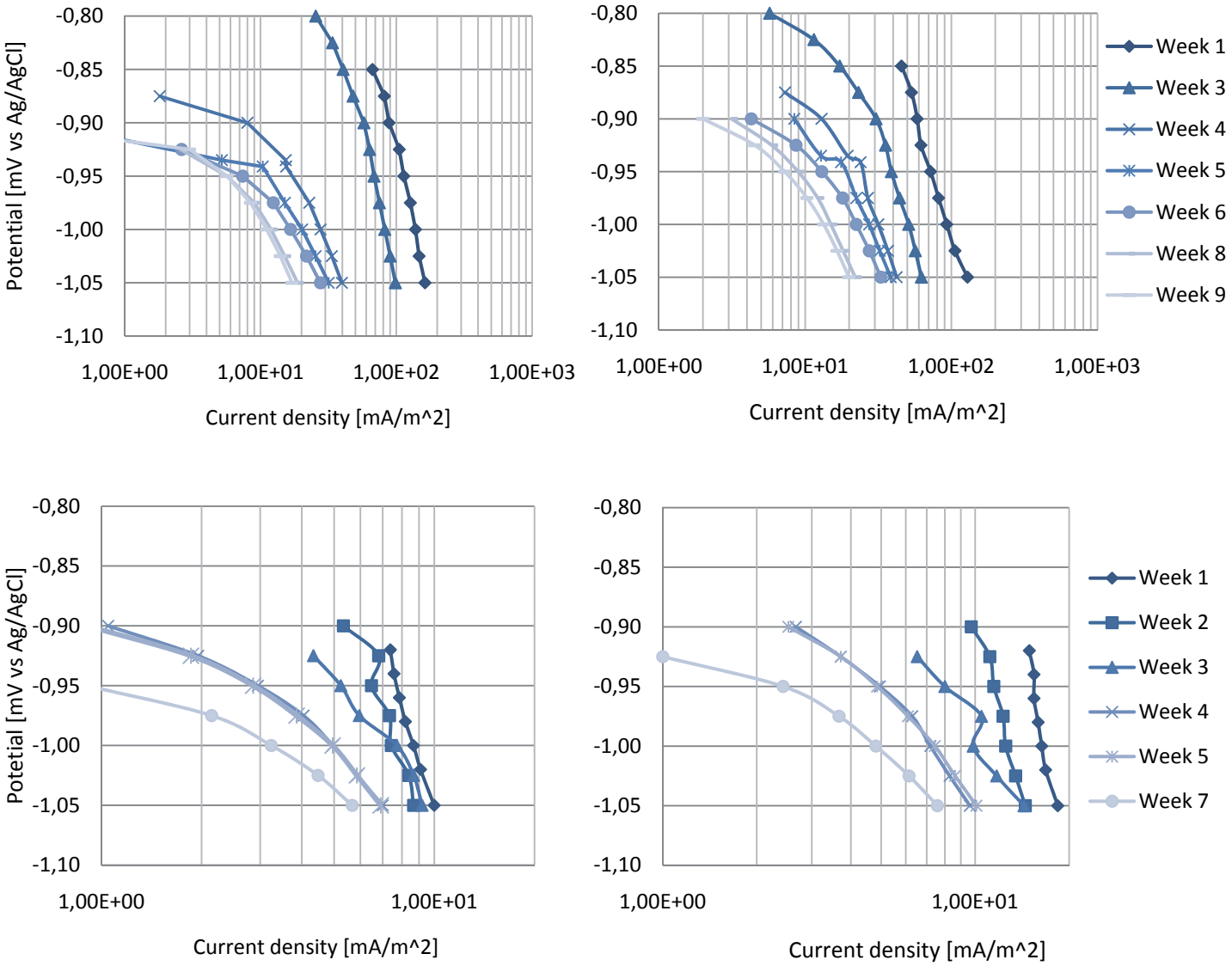

Figure 4.6: Potentiodynamic polarization curves for four different specimens with thermally sprayed aluminum. The two on top without sealing and the bottom two are sealed samples. Notice that the scales are logarithmic.

4.3 SEM images and EDS analyses

4.3.1 Surface characterization of thermally sprayed aluminum

The surface of thermally sprayed aluminum, as showed in Figure 4.7 is rough and it is obvious that the metal has been “splashed” all over the surface. It is not possible to see any intermetallic particles on the surface.

Figure 4.8 shows the TSA surface after polishing the surface, revealing the structure of the coating. The need for a sealer seems obvious looking at the surface. There are several pores, the largest around 10-20 µm in diameter. However, as the coating consist of several layers over a thickness of 200 µm the pores do probably not go all the way through the substrate material.

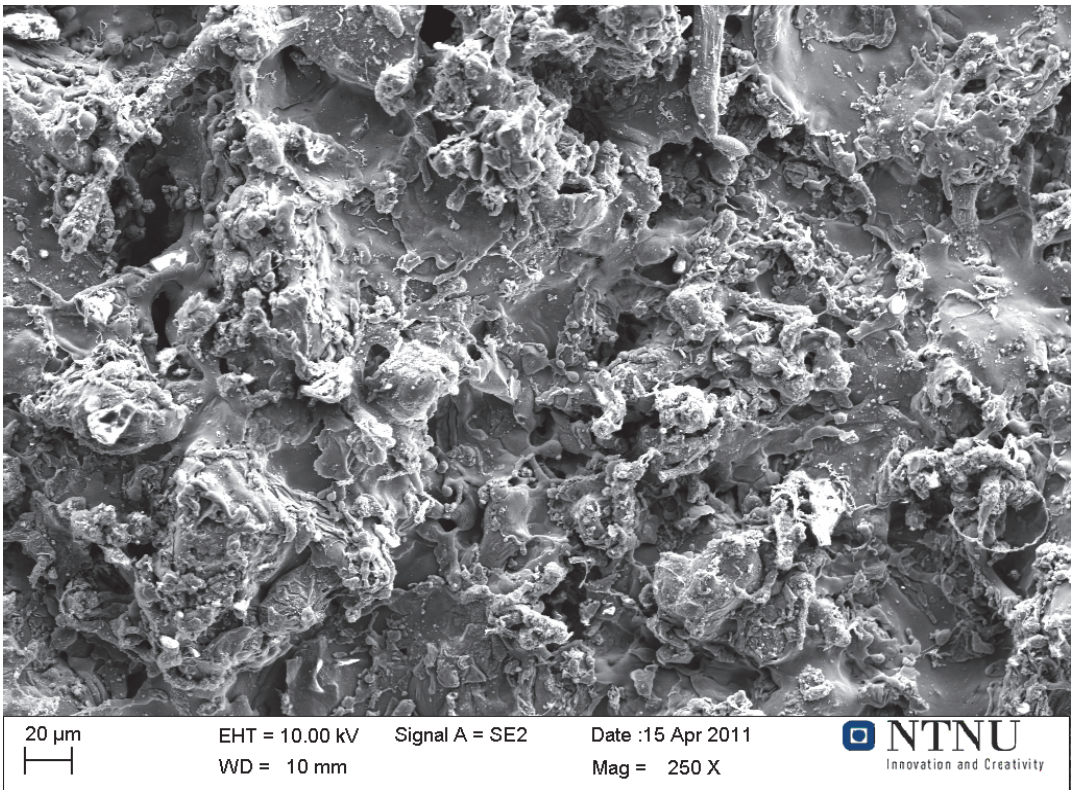

Figure 4.7: Surface of a TSA specimen before exposure, taken with 250x magnification.

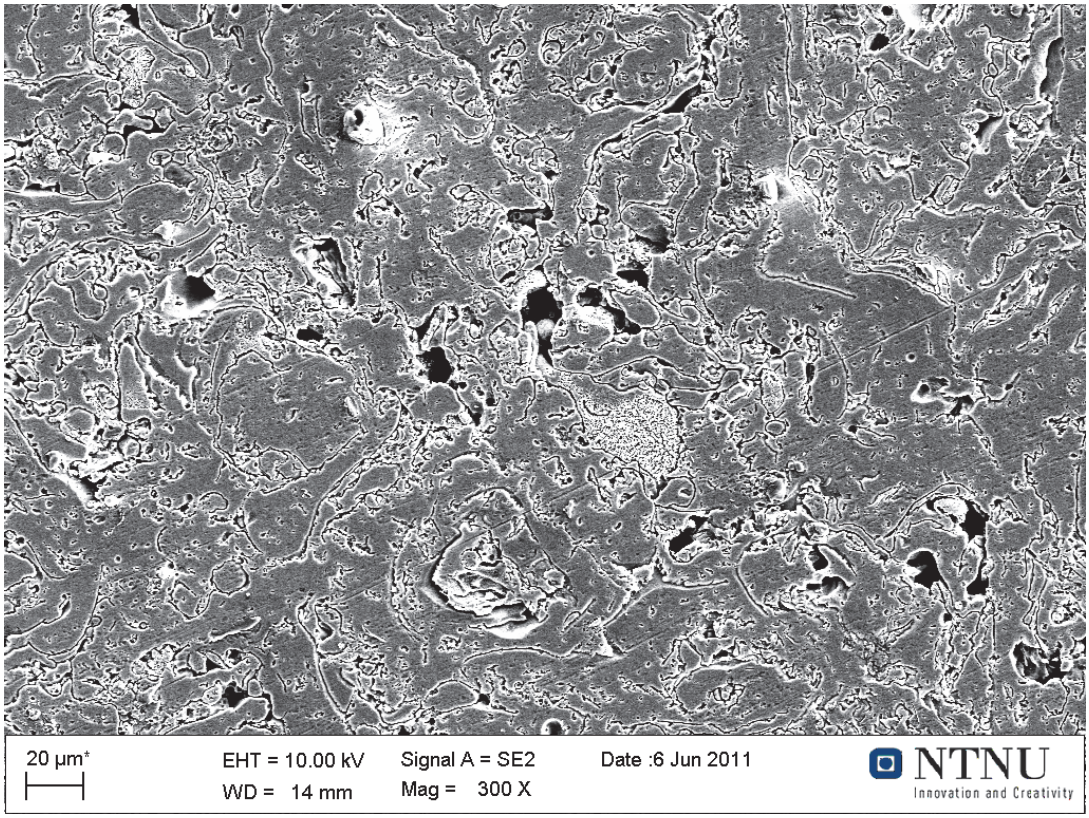

Figure 4.8: Surface of TSA specimen after grinding and polishing, taken with 300x magnification.

4.3.2 EDS-analysis of the TSA surface

Figure 4.9 shows an unexposed TSA specimen with the area being analyzed inside the yellow rectangle. The result is shown in Table 4.1 with the corresponding spectrum in Figure 4.10. The surface consists of 3.4 wt% Mg in addition to Al, C and O. The magnesium content is perhaps the most interesting since, as it will be shown later, the Mg content increases after exposure to seawater and cathodic protection.

Figure 4.11 shows the surface of a TSA specimen exposed in seawater with cathodic protection for 6 weeks. The surface looks rougher than before exposure. There are several bright spots which indicate substrates with poor conductive properties, i.e. corrosion products or calcareous deposit. Most of the bright spots are located on peaks of the surface. However, that may be due to the peaks being more exposed to the electron beam. Areas which before exposure were relatively smooth show cracks in the surface.

The EDS analysis of the marked area shows that there are several types of elements on the surface, as shown in Figure 4.12 and Table 4.2. In addition to the elements found on the unexposed TSA surface, Ca, Si, Cl, Na, P and S are also present, all of which are naturally present in seawater. In addition to the new elements, the biggest difference from the unexposed specimen is the increase in Mg and O content. The Mg content is increased from 3.4 wt% to 9.3 wt%, while the oxygen content is increased from 16.9 wt% to 40.6 wt%. The calculated Mg/Ca mol ratio is 15.3. However, subtracting the Mg content initially found at the TSA surface gives an Mg/Ca ratio at 9.7.

In Figure 4.13 and Figure 4.15 a smaller area is marked for EDS analysis. It seems like something has precipitated on the surface, as the surface looks rugged, although a typical structure is not seen. The two marked areas look quite alike, however, the EDS analysis shown in Table 4.3 and Figure 4.14 and Table 4. 4 and Figure 4.15 respectively, show that the Mg/Ca ratios for the two areas are quite different. The area in Figure 4.13 has an Mg/Ca ratio at 5.4, while the area in Figure 4.15 has an Mg/Ca ratio at 22.1. Both values are adjusted for initial Mg content.

Figure 4.17 shows the TSA surface after 4 months exposure to cathodic protection in seawater. According to the EDS analysis in Table 4.5, the Mg content is slightly higher than after 40 days, with 10.1 wt %. The Ca content is about the same, at 0.9 wt%, giving an Mg/Ca ratio at 18.5, or 12.3 after adjusting for initial Mg content. However, the EDS analysis in Table 4.6 and Figure 4.20, of a smaller area shown in Figure 4.19 reveals a higher Mg content and a lower Ca content, resulting in an Mg/Ca ratio at 36.0 after adjusting for initial Mg content. Fe was not detected.

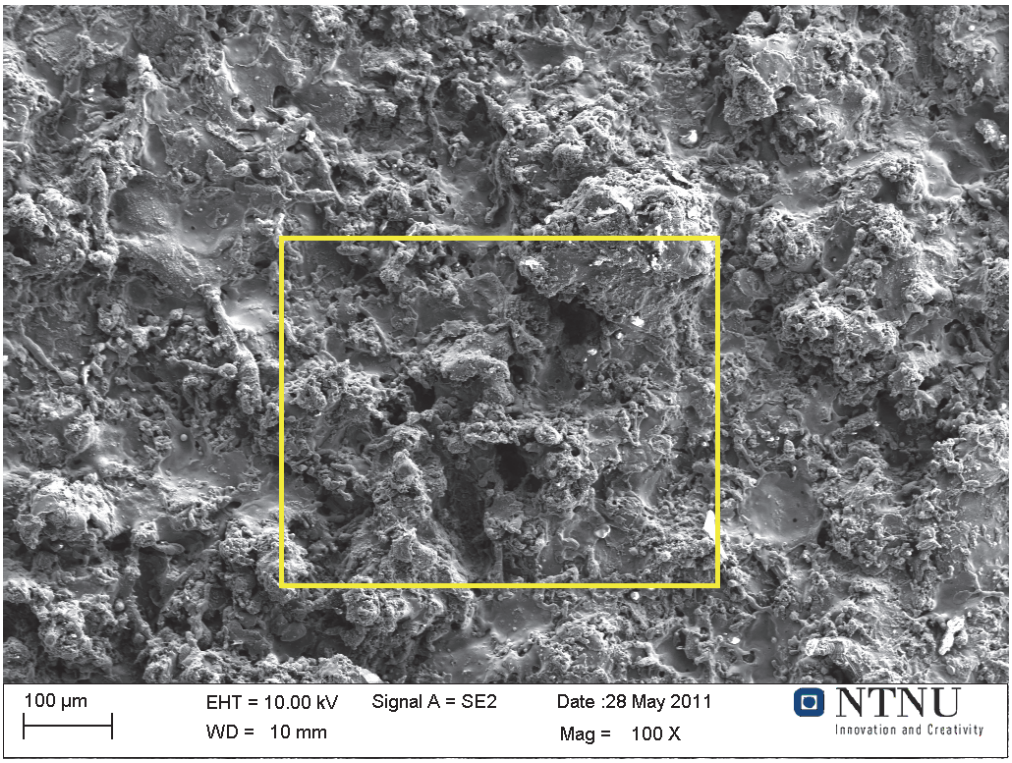

Figure 4.9: Surface of unexposed TSA. The EDS analysis is taken inside the rectangle.

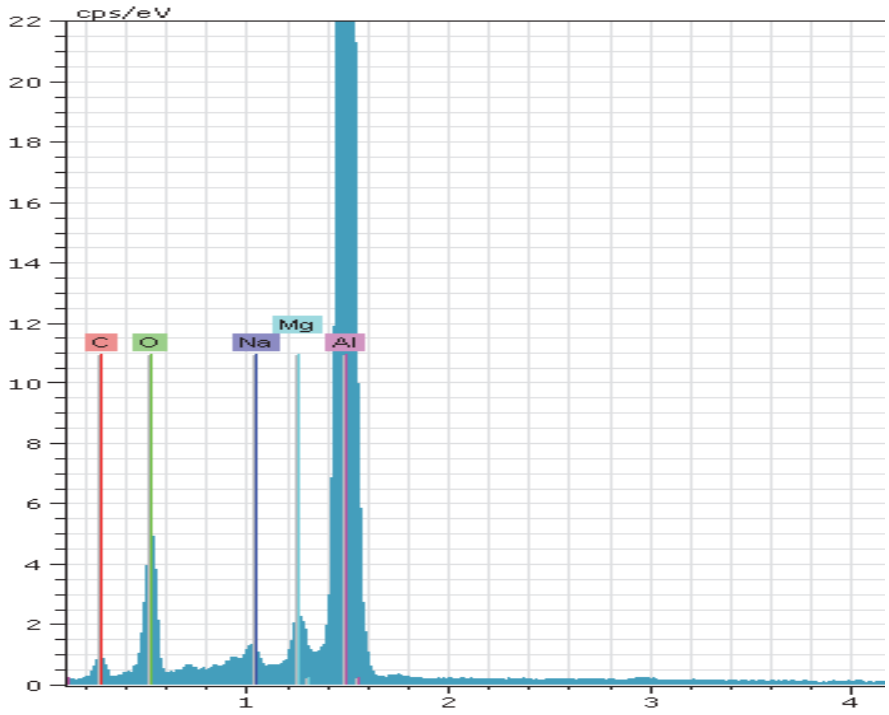

Figure 4.10: EDS-spectra for the unexposed TSA specimen in Figure 4.9.

Table 4.1: EDS analysis of the unexposed TSA surface from Figure 4.9.

Element	C	O	Mg	Al
[wt.%]	12.8	16.9	3.4	86.9

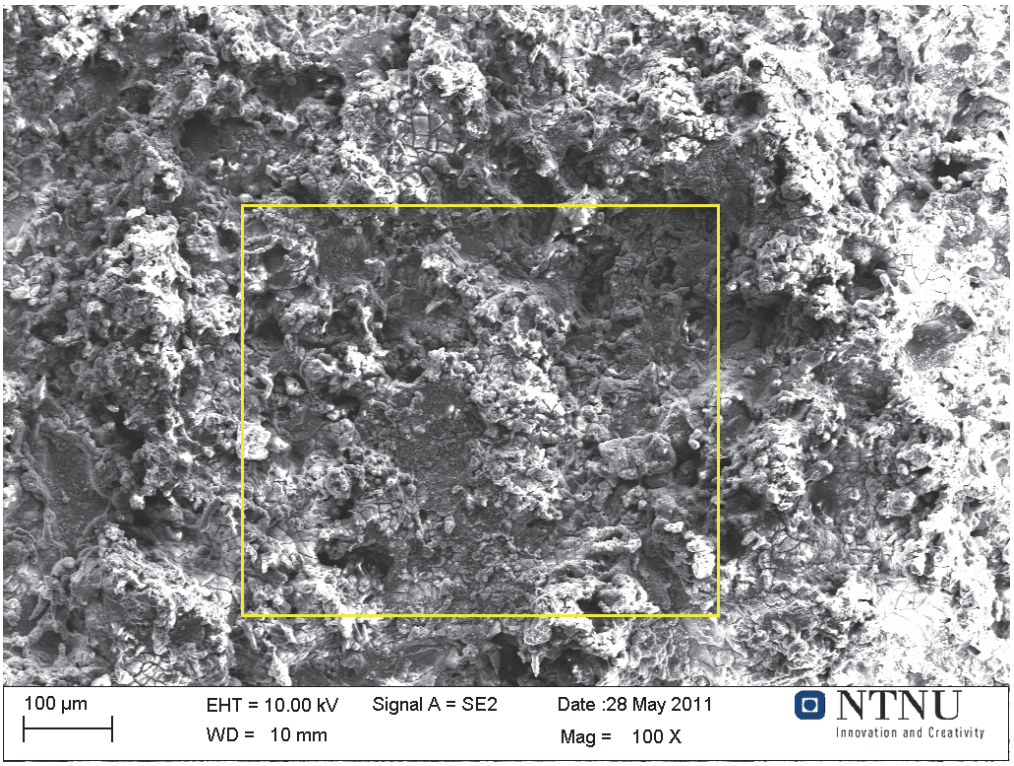

Figure 4.11: Surface of a TSA specimen after 6 weeks exposure to seawater with cathodic protection. The bright spots indicate calcareous deposits.

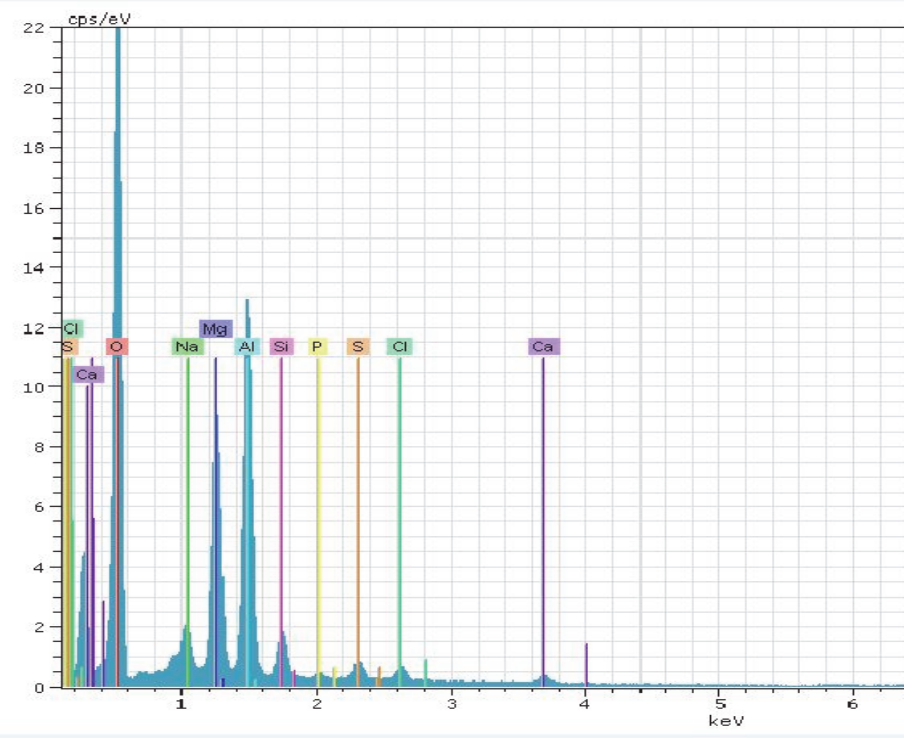

Figure 4.12: EDS spectrum of the TSA surface shown in Figure 4.11.

Table 4.2: EDS analysis of the TSA surface shown in Figure 4.11.

Element	Al	Mg	Si	O	Ca	Na	Cl	P	S
[wt.%]	14.9	9.3	2.6	40.6	1.0	2.9	1.0	0.2	1.0

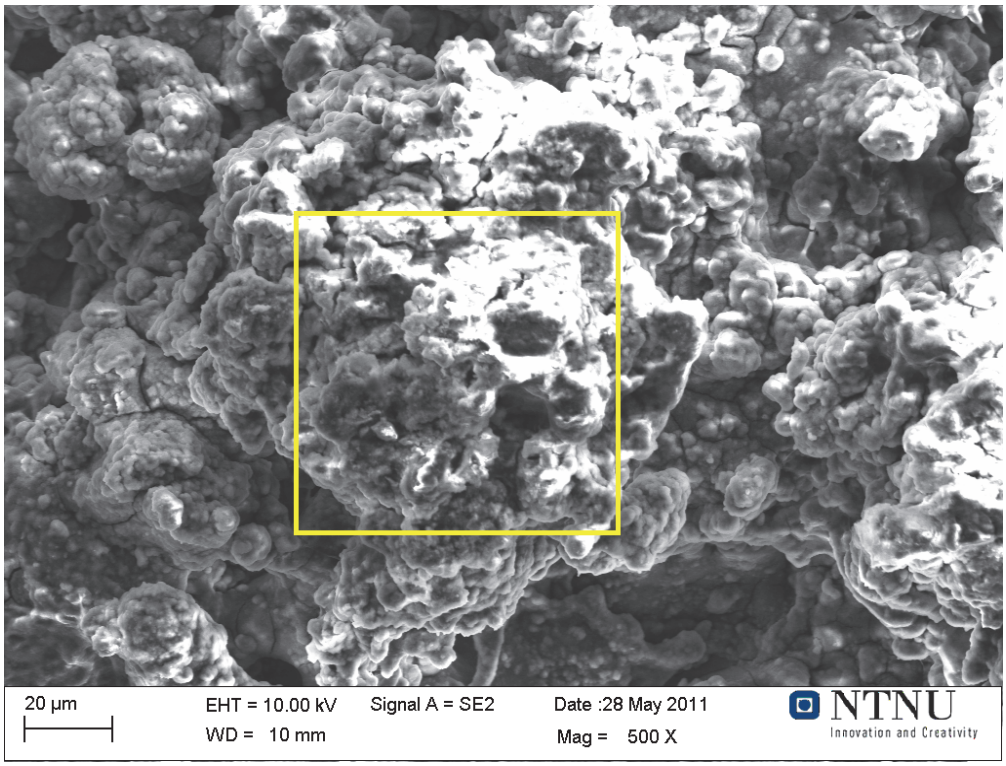

Figure 4.13: Image of a TSA surface after 6 weeks exposure, taken with 500x magnification. It seems like something has precipitated, although not with a familiar structure.

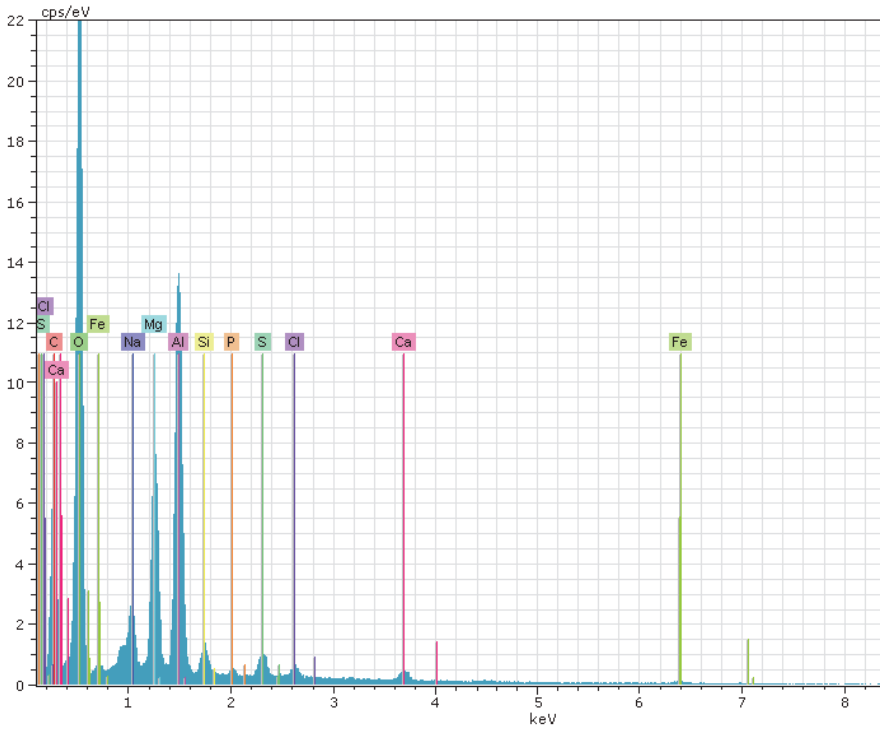

Figure 4.14: EDS spectrum of the marked area in Figure 4.13.

Table 4.3: EDS-analysis of marked area in Figure 4.13.

Element	C	O	S	Mg	Al	S	Cl	Ca	Fe
[wt.%]	19.0	42.6	3.1	7.0	13.2	1.3	0.7	1.1	3.1

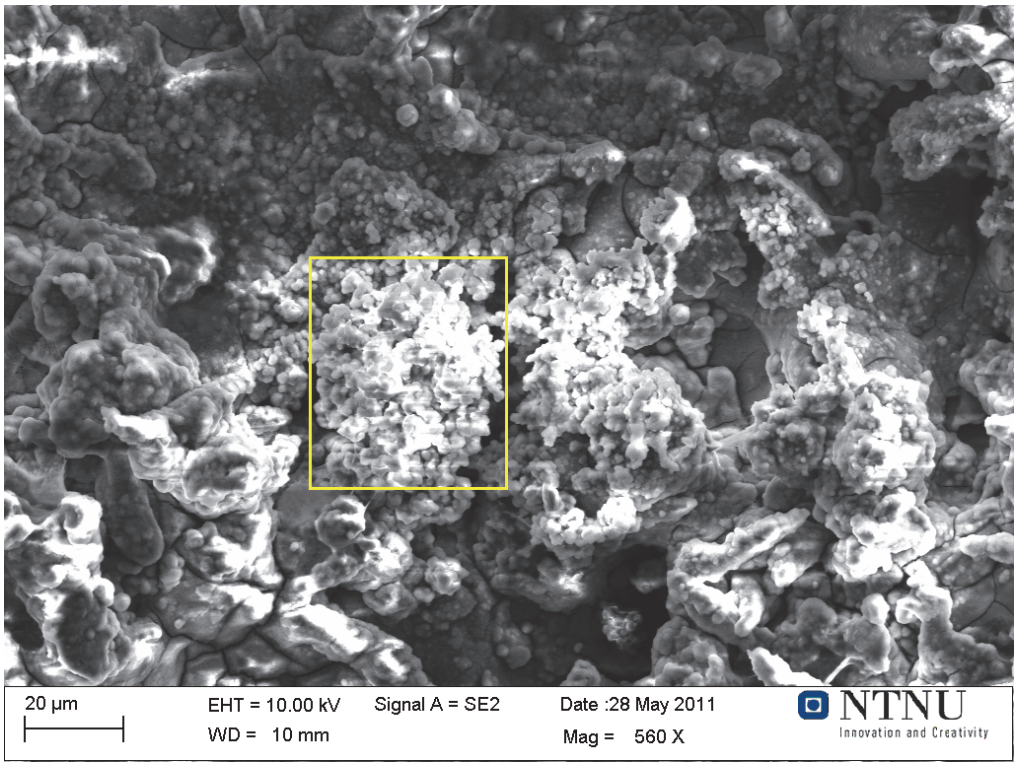

Figure 4.15: Image of a TSA surface exposed for 6 weeks, taken with 560 x magnification. It looks like something has precipitated at the area inside the yellow rectangle.

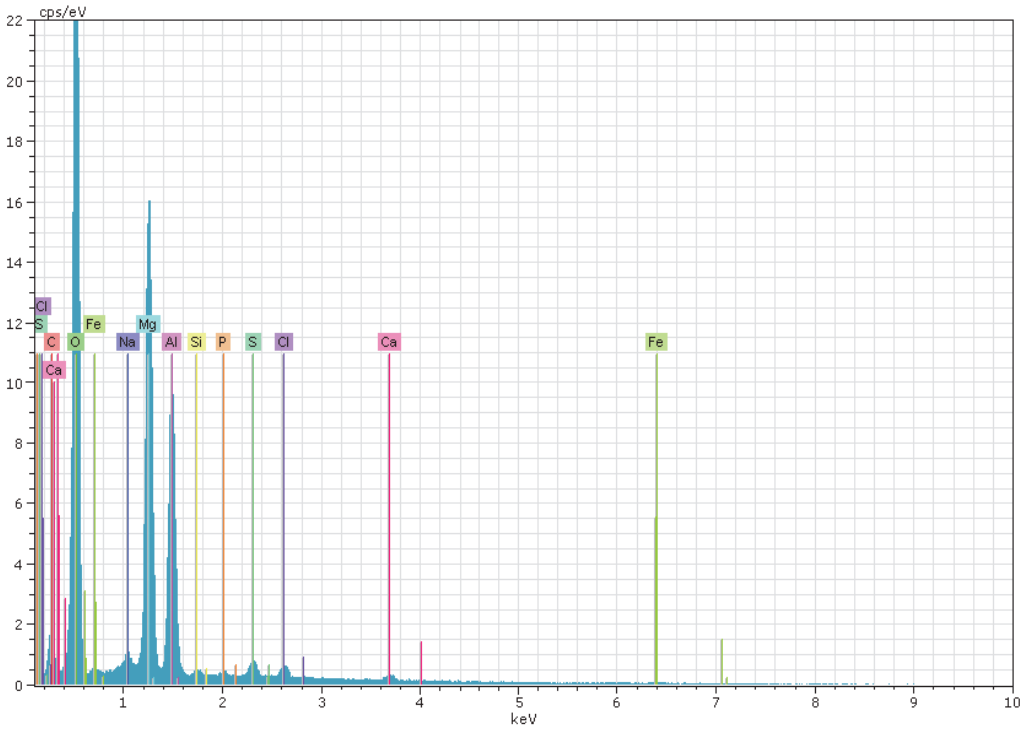

Figure 4.16: EDS spectrum of the small area marked in Figure 4.15.

Table 4. 4: EDS analysis of the small area marked in Figure 4.15.

C	O	Na	Mg	Al	Si	P	S	Cl	Ca	Fe
4.8	44.4	0.8	14.1	10.1	0.1	0.1	0.7	0.7	0.8	2.2

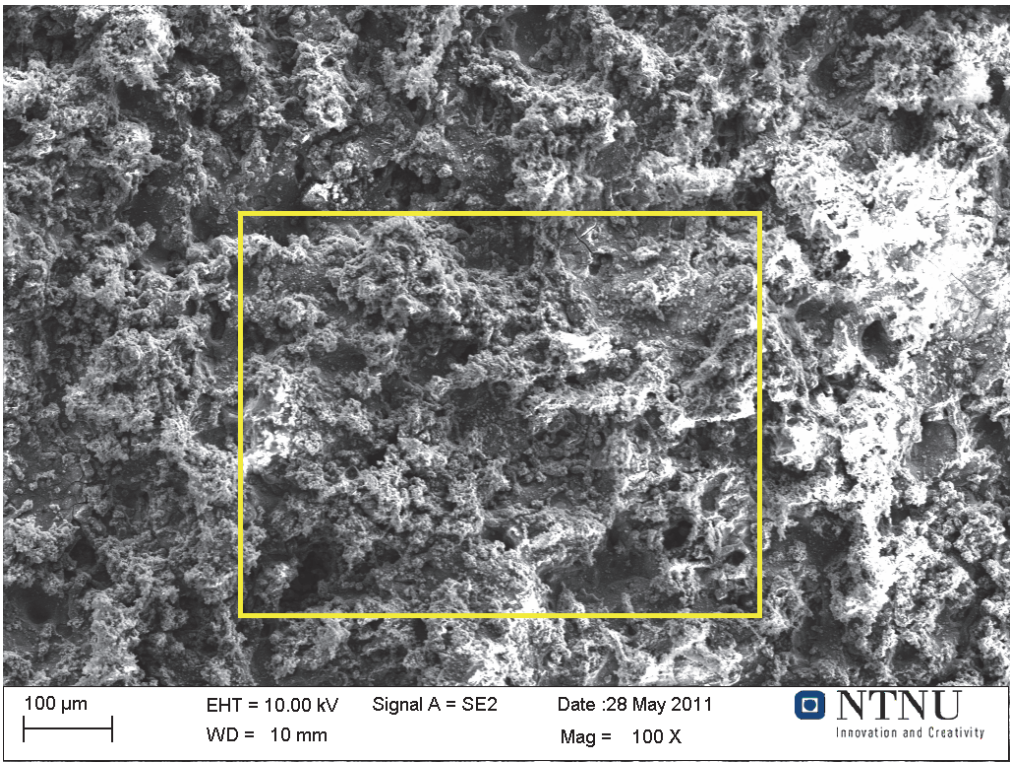

Figure 4.17: TSA surface after 4 months exposure. The white areas indicate calcareous deposit, although a familiar structure is not seen.

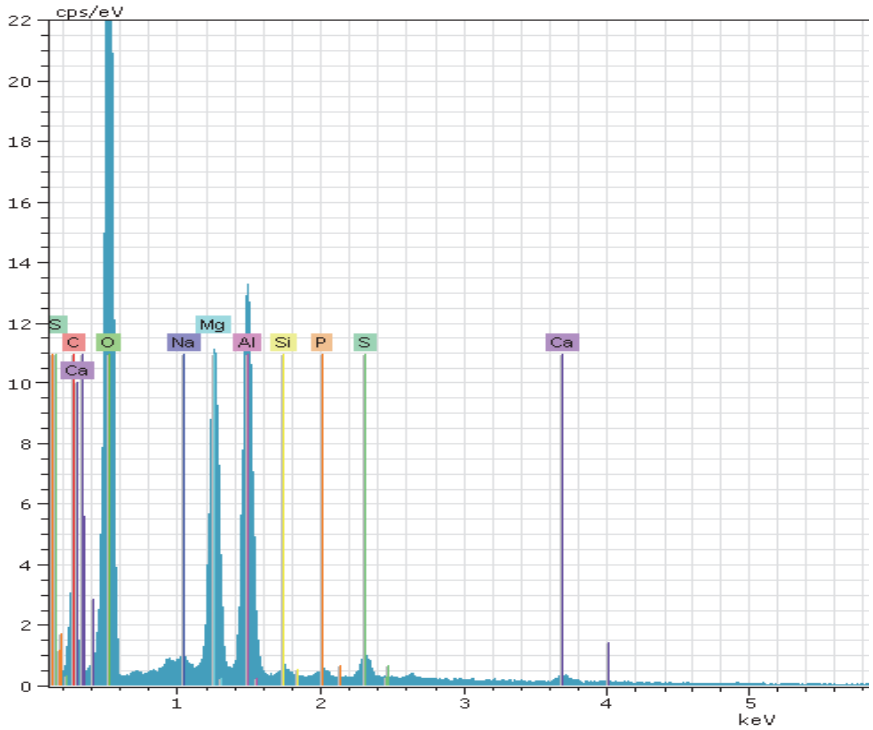

Figure 4.18: EDS - spectrum of the TSA specimen exposed for 4 months from Figure 4.17.

Table 4.5: EDS analysis of the TSA specimen exposed for 4 months from Figure 4.17.

Element	C	O	S	Mg	Al	Si	Ca
[wt.%]	10.1	47.7	1.3	10.1	13.3	0.4	0.9

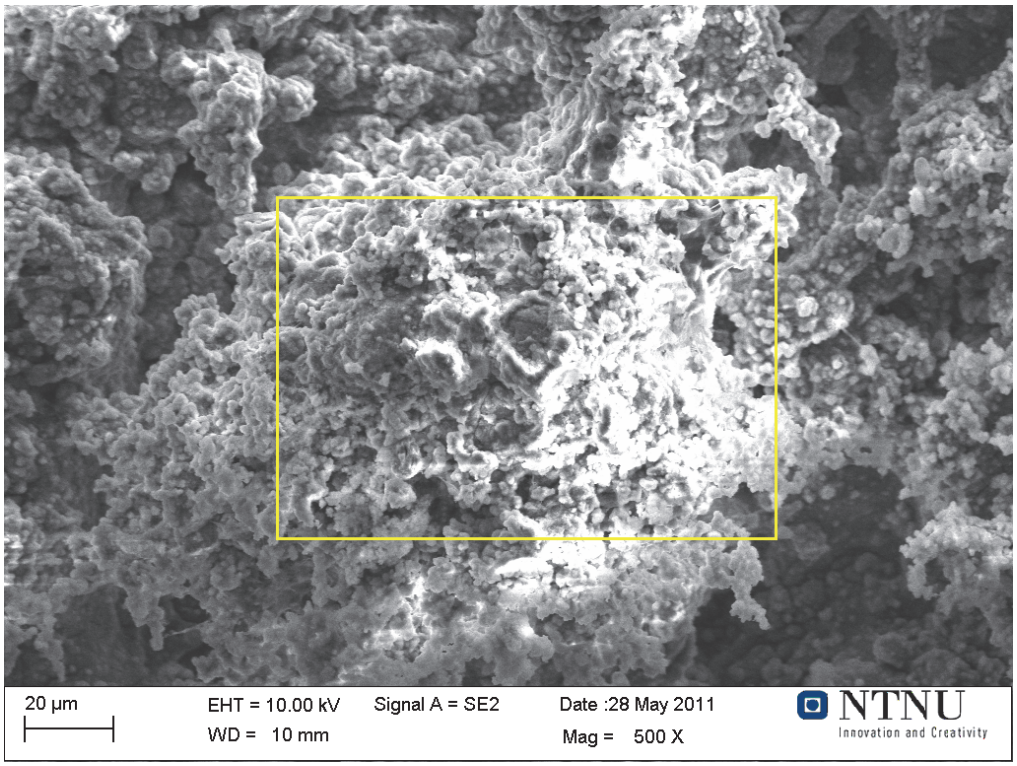

Figure 4.19: Small area of a TSA surface exposed for 4 months. The brightness indicates non-conductive material, i.e. calcareous deposit.

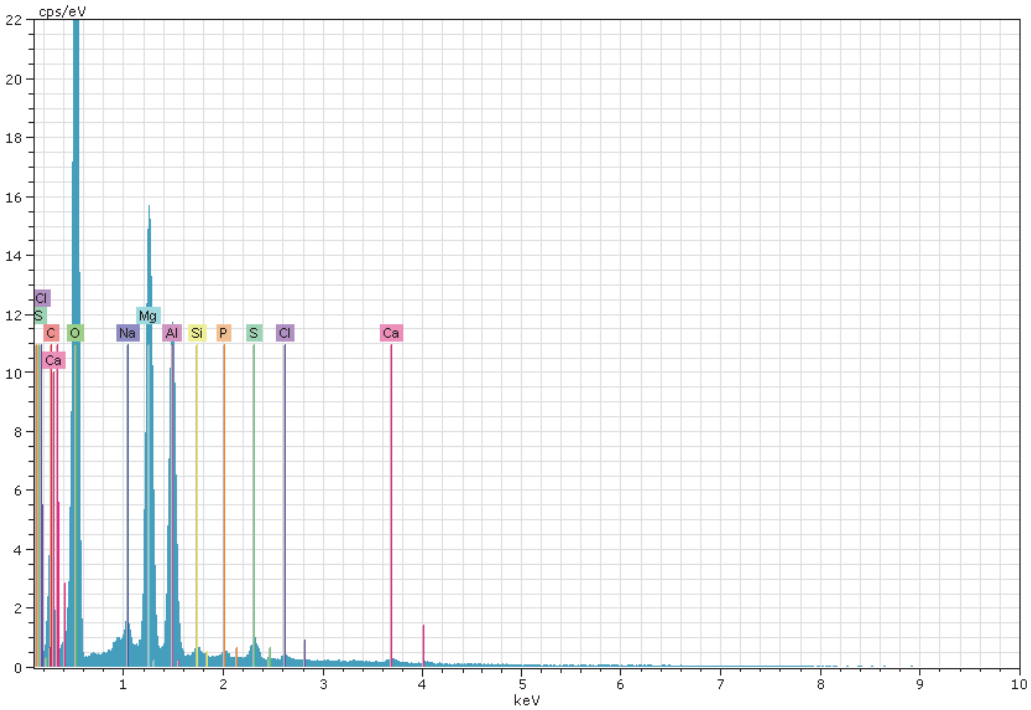

Figure 4.20: EDS spectrum of the area marked in Figure 4.19 of a TSA surface exposed for 4 months.

Table 4.6: EDS analysis the area marked in Figure 4.19 of a TSA surface exposed for 4 months.

Elemen	C	O	Na	Mg	Al	Si	P	S	Cl	Ca
wt%	12.0	52.8	2.0	14.3	12.1	0.5	0.3	1.0	0.3	0.5

4.3.3 TSA surface with sealer

Figure 4.21 shows the sealed surface with 200 X magnification, after 6 weeks exposure to seawater. The surface is partly covered with particles and a film can vaguely be seen. EDS analyses of the whole area and at one particle were therefore performed. Figure 4.22 shows the EDS spectra for the area inside the red rectangle, (a), and the particle, (b), while Table 4.7 shows the corresponding values. The EDS analysis shows that the surface mostly consists of Al, Si, C and O. As the sealer is organic and Si based, the relatively high Si, O and C content is expected. The relatively low Al and Mg content indicate that the sealer has covered the surface.

Somewhat the same values was detected at the particle, with slightly increase of Si and K, in addition to Fe. Although the specimen has been exposed to seawater for 6 weeks, none of the salts found at the other specimens, e.g. Ca, P and S, were found on the sealed surface.

It is not possible to see whether the sealer has penetrated through the surface, just by investigating the surface. Therefore, the surface was grinded and polished to see if sealer was found further down in the coating. Figure 4.23 shows the sealed TSA surface after grinding and polishing. The sealer does not seem to have filled the pores. The EDS analysis of the marked area in Figure 4.24 confirms that sealer is not present. Figure 4.25 and Table 4.8 shows that the main element on the polished surface is Al. Only 0.15 wt% Si detected. An Mg content of 0.95 wt% was lower than expected.

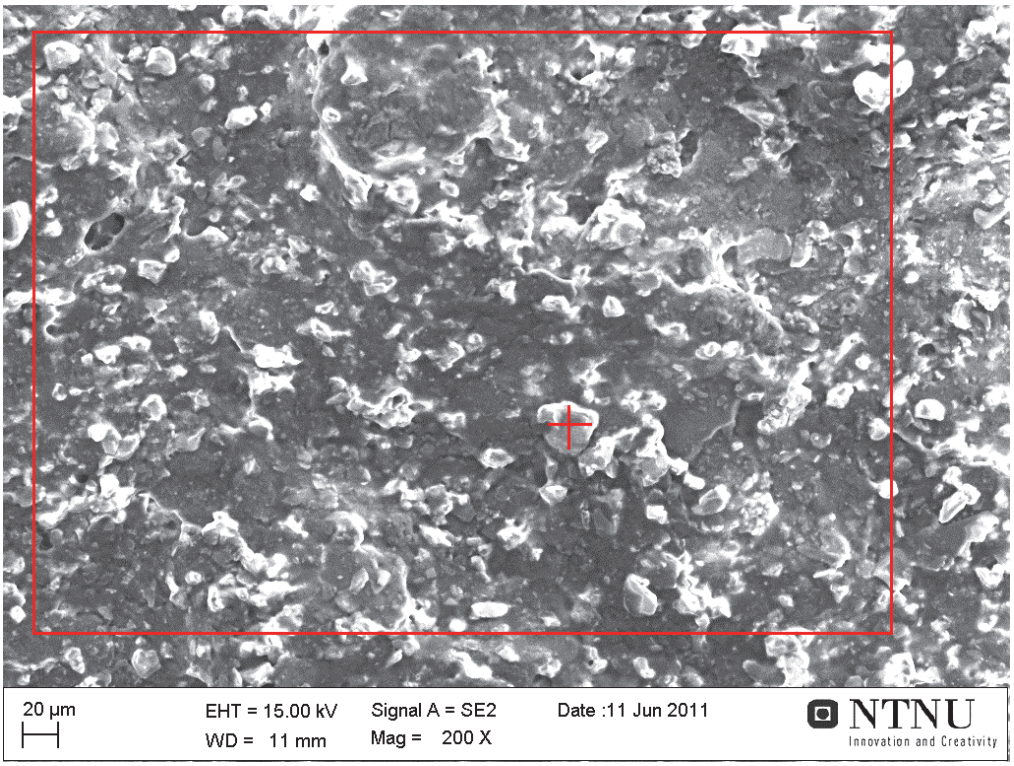

Figure 4.21: TSA with sealer after exposure to seawater for 6 weeks, polarized to -1050 mV vs Ag/AgCl.

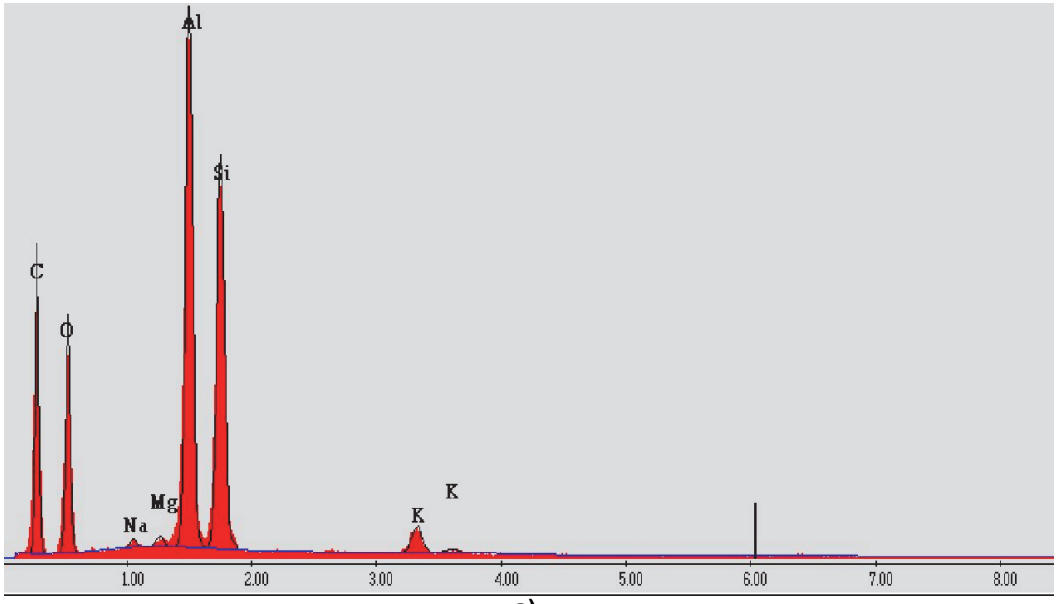

a)

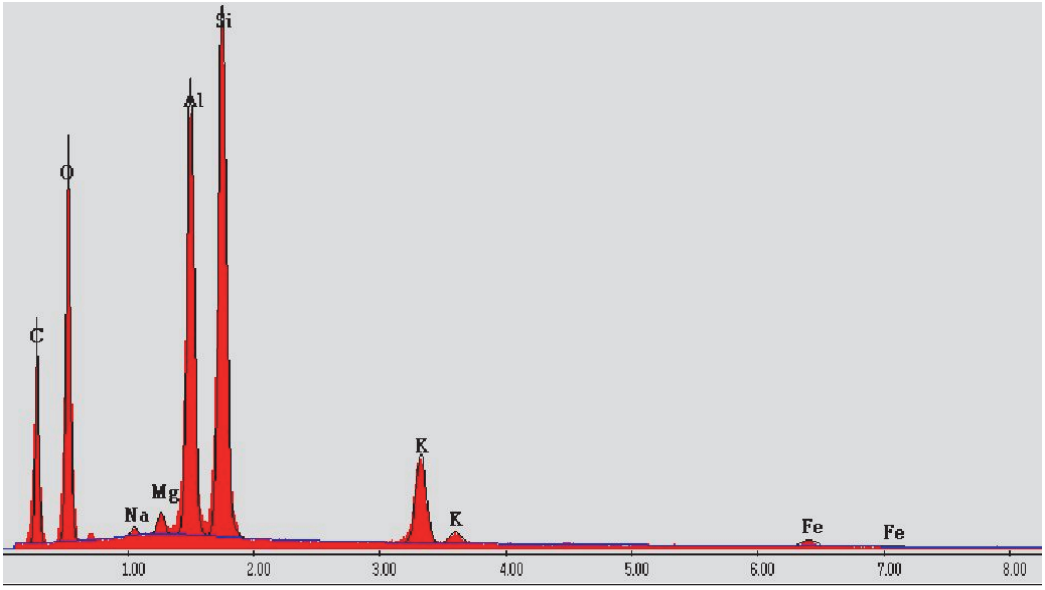

b)

Figure 4.22: EDS spectra of the area (a) and particle (b) in Figure 4.21.

Table 4.7: EDS-analysis of the area (a) and particle (b) in Figure 4.21.

Element	Al	C	O	Mg	Si	Fe	K	Na
Area (a)	17.39	45.97	19.27	0.30	14.92	-	1.86	0.30
Particle (b)	13.53	32.14	27.09	0.59	18.62	1.95	5.79	0.29

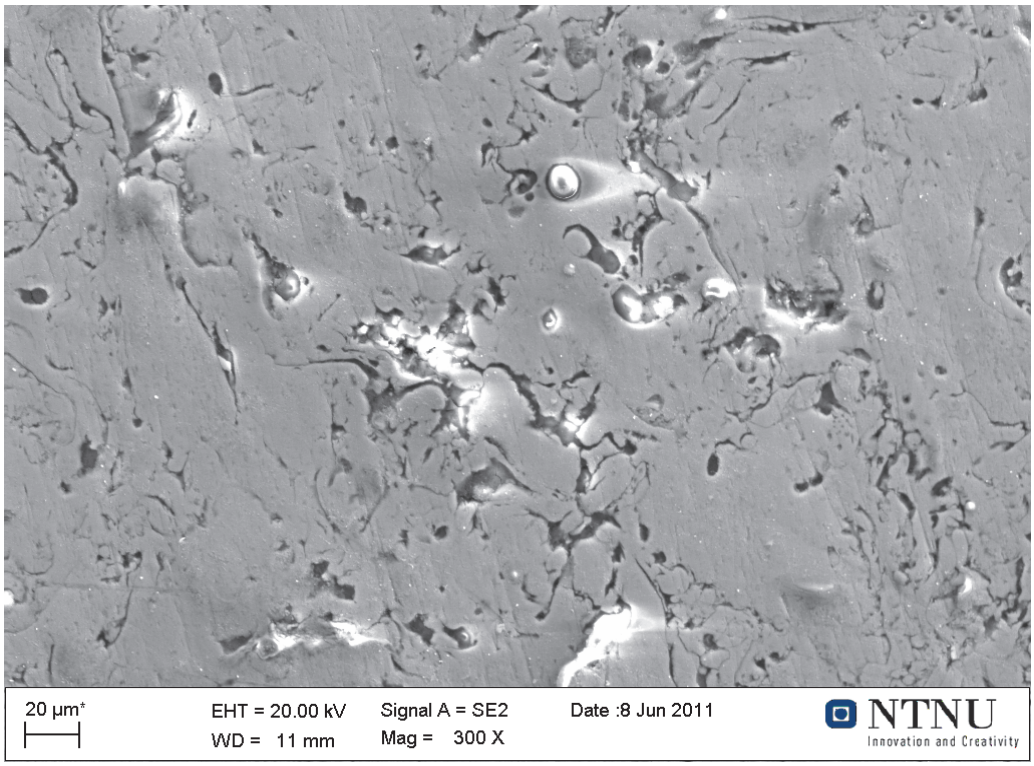

Figure 4.23: The sealed TSA surface after polishing.

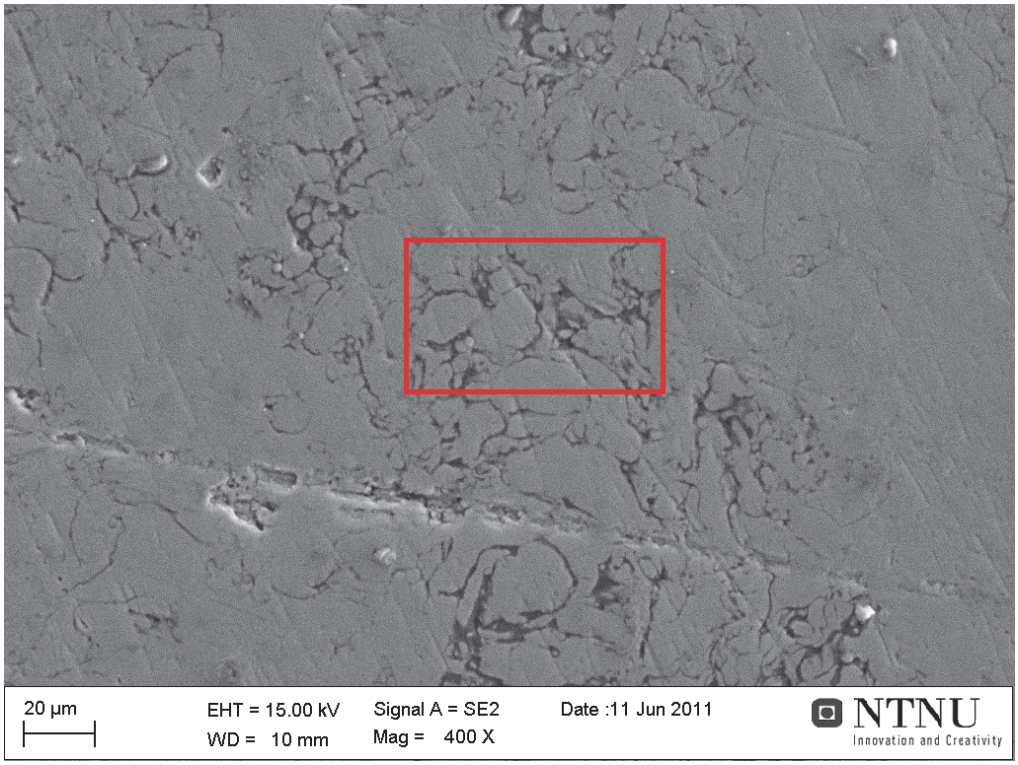

Figure 4.24: Polished sealed TSA surface with a marked area for EDS analysis.

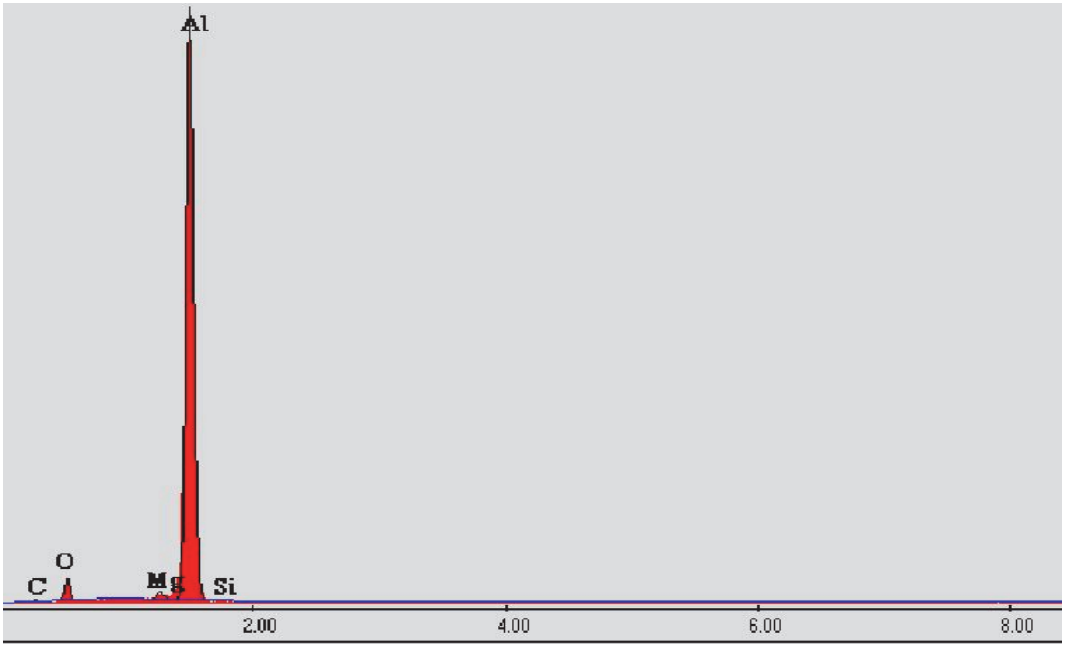

Figure 4.25: EDS spectra of the marked area in Figure 4.24.

Table 4.8: EDS analysis of the polished TSA surface in Figure 4.24

Element	Al	C	O	Mg	Si
wt%	91.24	0.87	6.79	0.95	0.15

4.3.4 Aluminum alloys

Plates of different aluminum alloys were investigated before and after exposure to seawater. The emphasis was on the intermetallic particles which were analyzed with EDS. Figure 4.26 shows a cross section of the aluminum alloy AA5082 before exposure. This is a similar alloy to the TSA specimens. EDS analysis of the particles, Table 4.9 (EDS spectra not available), showed that they mainly consist of Fe and Mn, probably as $(FeMn)Al_6$, but also as $FeAl_3$. Hence, the particles will be cathodic to the matrix. The Mg content found on the particles was between 0.9 and 3.7 wt%, with an average of 1.65 wt%. The matrix has an average Mg content at 4.0 before exposure, as shown in Figure 4.27 and Table 4.10.

After 6 weeks exposure to cathodic protection in seawater the particles look like they have been dug out of the matrix, as shown in Figure 4.28 and Figure 4.29. There are visible pits in the interface between the particle and the matrix, and in Figure 4.29 one of the particles has fallen out.

The EDS analysis of the points on the AA5082 specimen marked in Figure 4.28 is shown in Table 4.11 (EDS spectra not available) and shows an Mg content between 5.2 and 9.5 wt% and a Ca content from 1.1 to 2.0 wt% at the particles. The Mg/Ca ratio for each particle gives an average Mg/Ca ratio of 8.0, after adjusting for the average Mg content for the particles found before exposure. The Mg/Ca ratio at the

matrix ranges from 1.8 to 5.5 wt% and show an Mg/Ca ratio of 3.0, i.e. lower than before exposure.

The Fe content is no longer detectable in some particles and around 2.5 wt % where it is found. The C content is remarkable high, varying from 30 to 66 wt% at the particles, while only between 8 and 12 wt% on the matrix.

Figure 4.30 (1)-(4) shows the EDS spectra for the areas marked in Figure 4.29, with the corresponding values in Table 4.12. The Mg content is lower than the particles above, with 3.14 and 3.95 wt%, respectively for the two particles analyzed. With Ca content 1.01 and 1.77 wt%, the Mg/Ca ratio is 2.5 and 2.2. Fe is found in one of the particles, significantly lower amount than found in the particles before exposure (2.94 wt%).

The Mg content at the pit and matrix, marked (3) and (4), is slightly higher than at the particles, with 4.8 and 4.2 wt%, respectively. Ca was not detected in the pit or the at the matrix, so the Mg/Ca ratio is not defined. C, on the other hand, was found in the matrix, but not in the pit. The C content at the matrix was much lower than at the particles. In addition the O content is much lower in the matrix and pit, than the particles.

The sample made of aluminum alloy AA1050 have no visible particles at 200X magnification before exposure to cathodic protection in seawater, as seen in Figure 4.31. After exposure the surface has both visible particles and pits, as shown in Figure 4.32. The EDS analyses of the marked points is shown in Table 4.13 and Figure 4.33. The particles (1) and (2) have first of all a high Mg content. This alloy initially contains 0.05 wt% Mg, and while Mg was not detected at the matrix, the EDS analysis shows 8-9 wt% Mg at the particles. However, the Ca content is also quite high at the particles, with 3.65 and 2 wt% Ca, which gives a Ca/Mg ratio at 3.7 and 7.8. Ca is not detected on the matrix, either.

Also notice that both the O and C content are lower at the matrix, than at the particles. S and P are only detected at the particles.

Figure 4.34 shows the surface of the aluminum alloy Al99.99 before exposure with no particles seen, as it should not be. Figure 4.35 shows the surface after exposure, and it looks quite the same. Some particles and pits are seen, although this could be contaminations. The EDS analysis in Figure 4.36 and Table 4.14 shows that the only elements detected are Al, O, C and barely Si (0.13 wt%). The Si content found is within the impurity limit of the alloy.

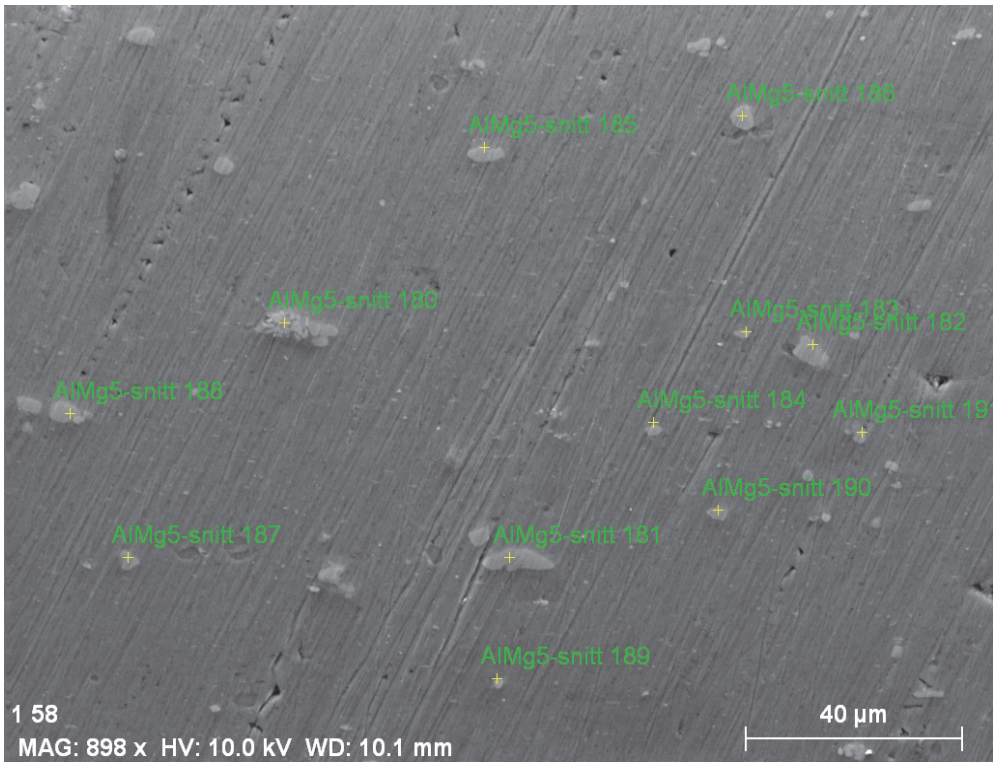

Figure 4.26: Particles in aluminum alloy AA5082 before exposure.

Table 4.9: EDS analysis of the particles in an unexposed AA5082 alloy shown in Figure 4.27.

Particle tag	C	O	Mg	Al	Si	Mn	Fe
AlMg5-snitt 180	2.5	-	1.3	55.5	0.5	-	34.5
AlMg5-snitt 181	-	-	0.9	63.3	-	8.2	20.8
AlMg5-snitt 182	-	-	1.5	66.5	-	6.1	19.4
AlMg5-snitt 183	-	-	1.9	68.3	-	10.8	11.1
AlMg5-snitt 184	-	1.5	3.0	67.1	-	-	7.2
AlMg5-snitt 185	-	1.5	2.4	70.4	-	6.9	17.6
AlMg5-snitt 186	-	-	0.8	64.5	-	8.0	24.1
AlMg5-snitt 187	-	1.8	0.8	58.4	-	-	22.8
AlMg5-snitt 188	-	-	0.7	63.8	-	8.5	24.6
AlMg5-snitt 189	-	0.9	3.7	75.9	-	3.5	20.3
AlMg5-snitt 190	-	-	1.0	64.2	-	6.7	21.2
AlMg5-snitt 191	-	-	1.8	66.7	-	6.7	18.9

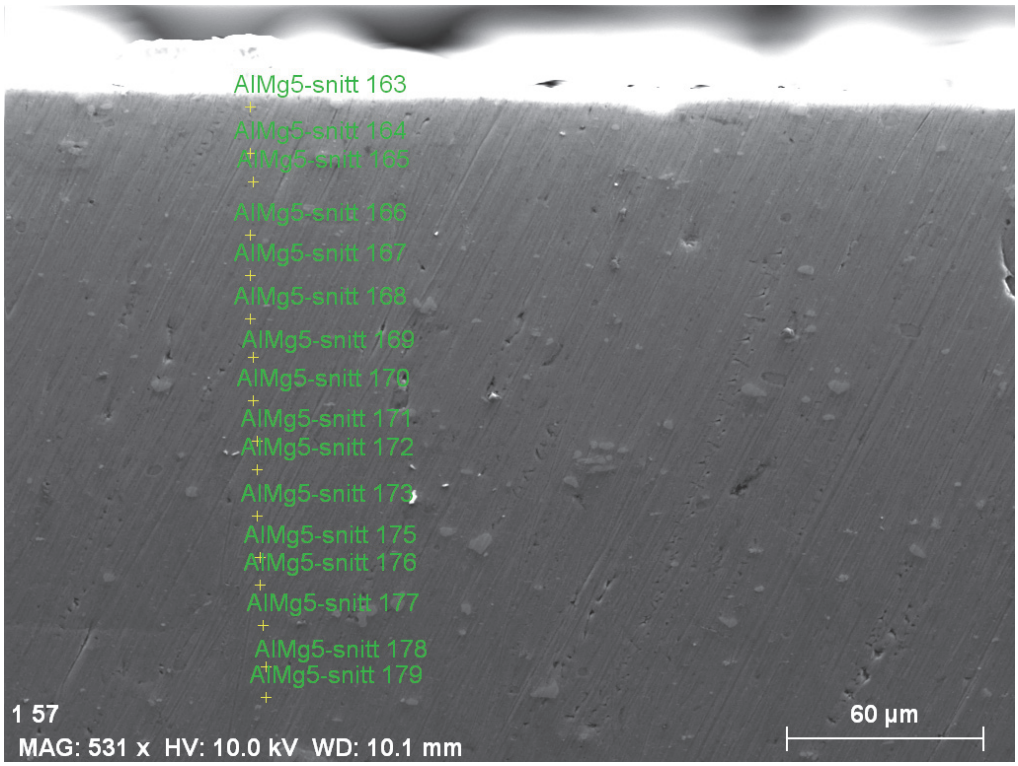

Figure 4.27: Image of a cross section of an unexposed AA5082 specimen, with marked points for EDS analysis of the matrix.

Table 4.10: EDS analysis of the points marked in Figure 4.27

Element	C	O	Mg	Al	Mn
AlMg5-snitt 163		1.5	3.7	72.8	
AlMg5-snitt 164		2.9	4.0	78.2	
AlMg5-snitt 165		1.8	4.0	71.5	
AlMg5-snitt 166		1.4	3.4	66.3	4.8
AlMg5-snitt 167		2.1	3.7	74.0	
AlMg5-snitt 168		1.2	4.1	77.0	
AlMg5-snitt 169	6.8	1.5	3.9	73.0	
AlMg5-snitt 170	4.8	2.1	4.2	80.8	
AlMg5-snitt 171		2.3	3.7	73.9	
AlMg5-snitt 172		1.2	4.2	76.7	
AlMg5-snitt 173		1.2	4.3	81.7	
AlMg5-snitt 175		3.7	4.3	78.5	
AlMg5-snitt 176		2.4	4.1	74.1	
AlMg5-snitt 177		2.0	4.2	82.3	
AlMg5-snitt 178		2.4	3.9	72.1	
AlMg5-snitt 179		2.5	4.1	77.4	

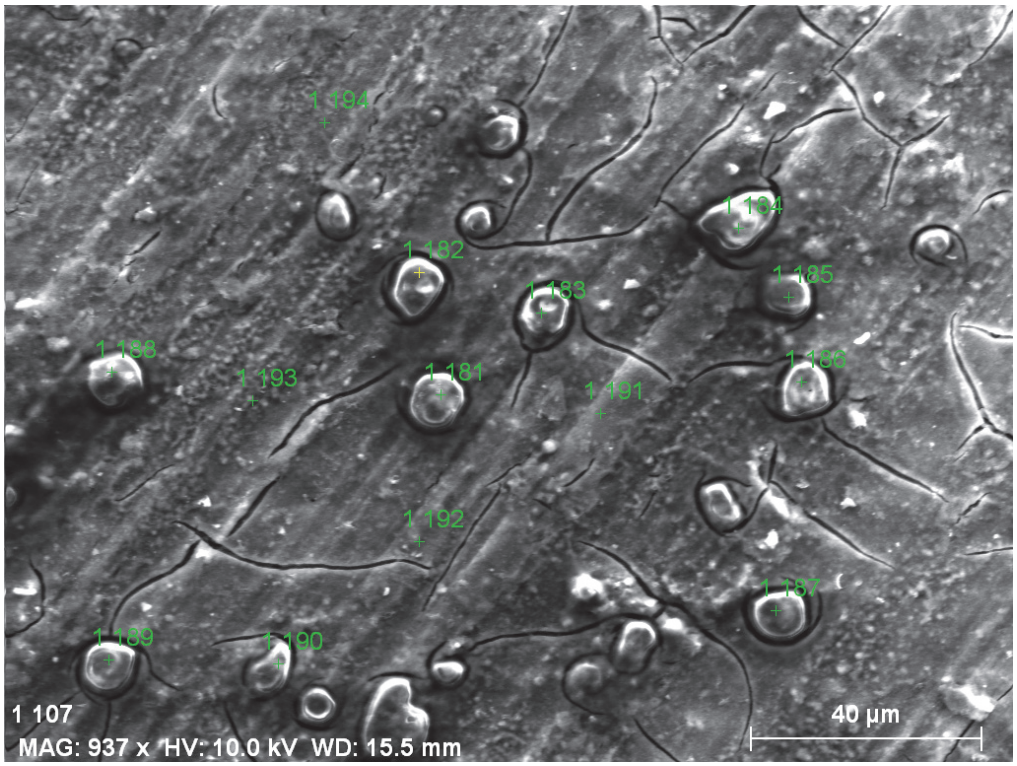

Figure 4.28: Particles on the surface of AA5082 after 6 weeks exposure to seawater.

Table 4.11: EDS analysis of particles and matrix (marked with grey color) from Figure 4.28. The values are in wt%.

Point	C	O	Na	Mg	Al	Si	Ca	Fe
1 181	55.6	27.8	0.8	5.2	5.1	0.7	1.3	
1 182	32.3	38.7	0.5	7.4	9.6	0.5	1.7	
1 183	30.5	32.3	0.3	7.6	8.0	0.4	1.5	
1 184	45.1	23.7		6.0	4.9		1.1	
1 185	45.8	25.9	0.5	6.2	7.7	0.4	1.2	2.4
1 186	46.6	42.0	1.0	9.5	12.6	0.9	1.4	
1 187	44.9	25.6	0.3	5.2	5.5	0.4	1.4	
1 188	66.0	37.5	0.9	6.7	5.2	0.5	1.1	2.5
1 189	30.4	51.7	0.8	8.4	12.8	4.0	1.7	
1 190	34.8	38.3	0.6	6.6	16.2	0.8	1.5	
1 191	8.6	23.7		3.5	44.1	0.6	2.0	
1 192	11.7	20.7		2.9	46.2	0.5	1.3	
1 193	9.3	12.6		3.3	53.6	0.1	0.6	
1 194	11.2	17.4		3.0	47.4	0.3	0.9	

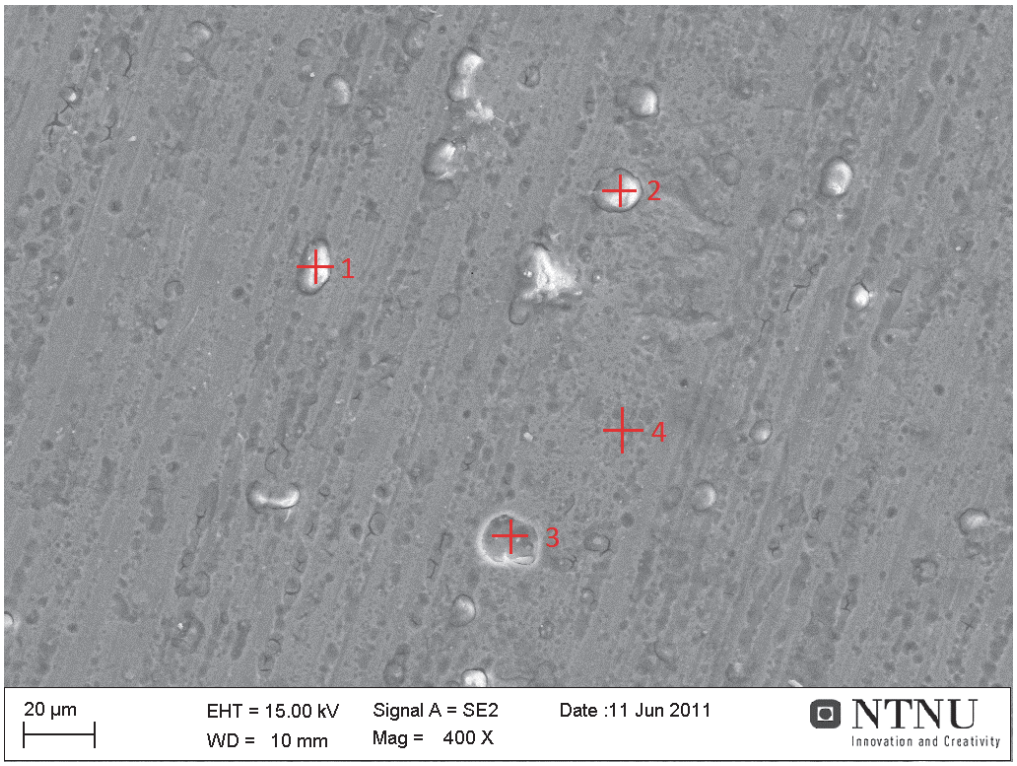

Figure 4.29: SEM image of AA5082 after 6 weeks exposure with marks for the EDS analyses.

Table 4.12: EDS analysis of the marked areas in Figure 4.29. The values are in wt%.

	Al	C	O	Mg	Si	Ca	Fe	P	S
1	14.73	63.07	12.58	3.14	0.34	1.01	2.94	0.84	1.36
2	8.83	68.39	13.83	3.95	0.47	1.77	-	1.32	0.47
3	94.09	-	1.10	4.81	-	-	-	-	-
4	74.51	13.51	7.80	4.18	-	-	-	-	-

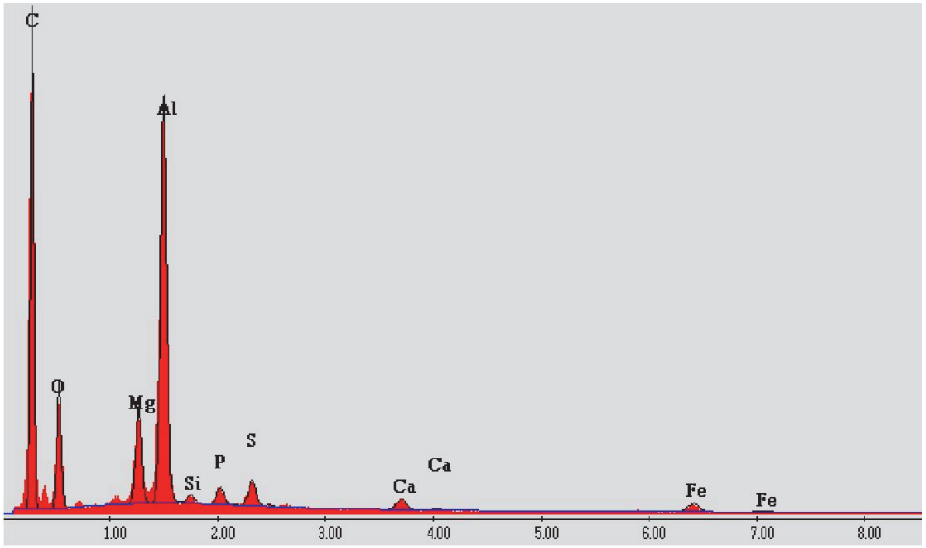

(1)

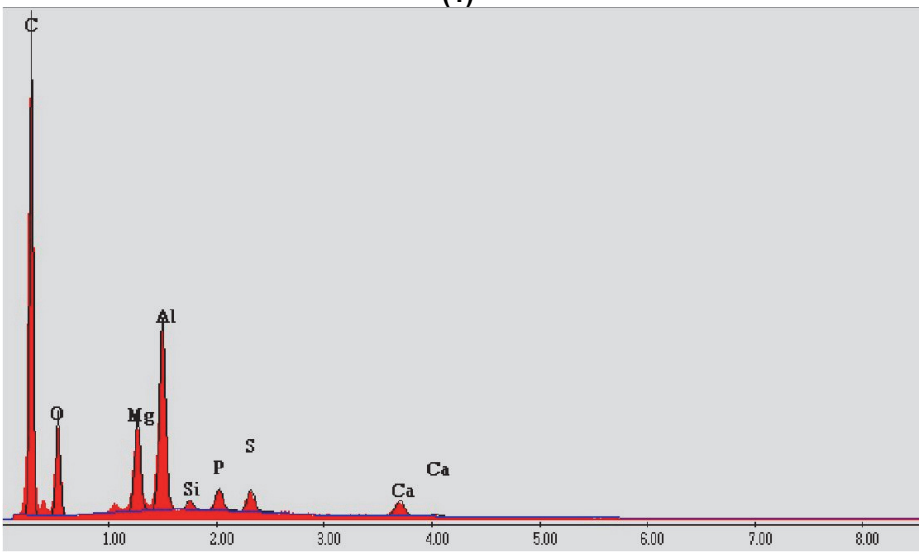

(2)

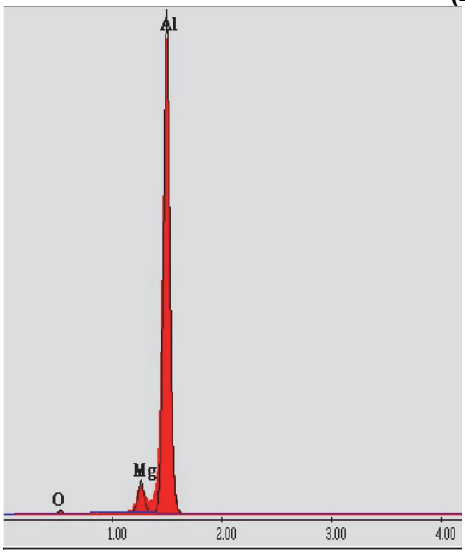

(3)

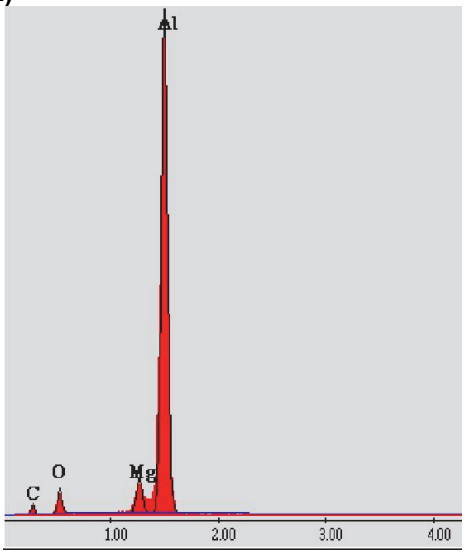

(4)

Figure 4.30: EDS spectra of the points marked in Figure 4.29.

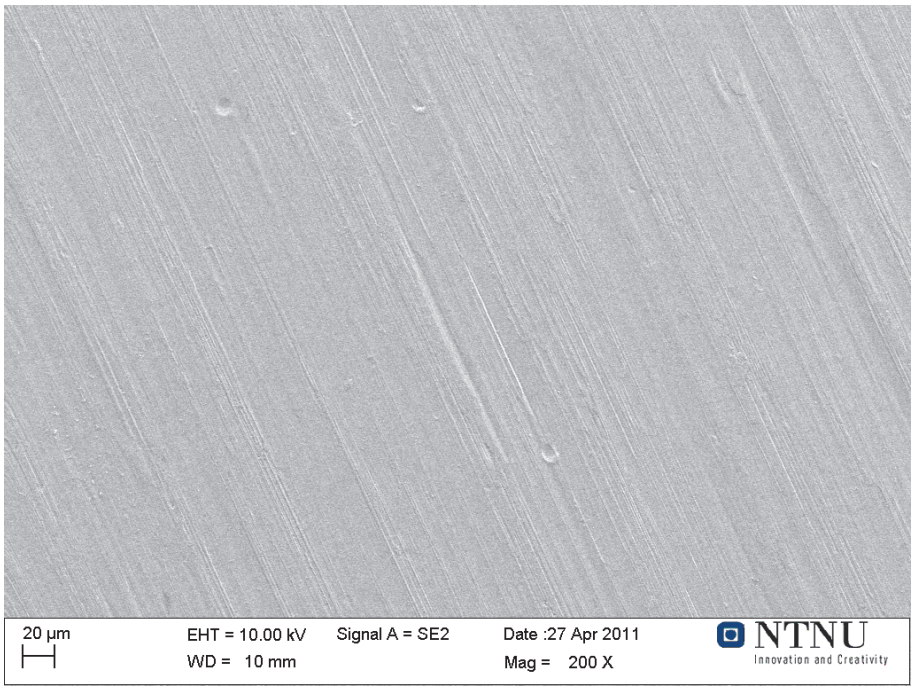

Figure 4.31: Surface of aluminum alloy AA1050 before exposure to seawater.

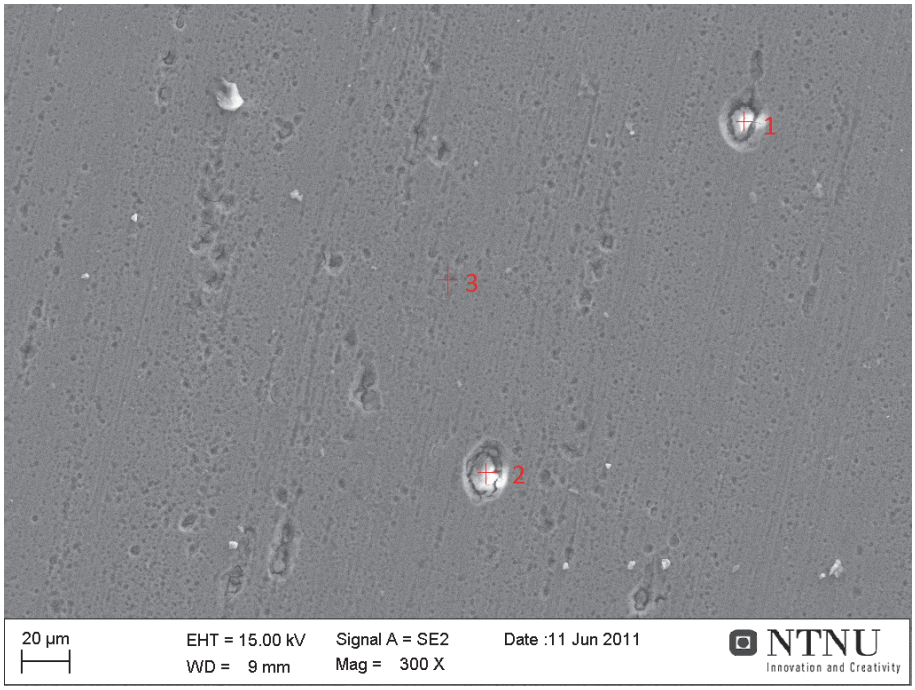

Figure 4.32: Surface of aluminum alloy AA1050 after 6 weeks exposure to seawater. The particles have been dug out of the matrix.

Table 4.13: EDS-analysis of the particles in Figure 4.32.

	Al	C	O	Mg	Si	Ca	Fe	P	S	Na	Cl
1	34.43	10.10	25.60	8.14	0.85	3.65	4.73	0.92	3.18	1.02	7.38
2	20.83	16.42	38.65	9.50	0.54	2.00	3.20	0.60	1.99	1.24	5.04
3	88.25	3.40	8.34	-	-	-	-	-	-	-	-

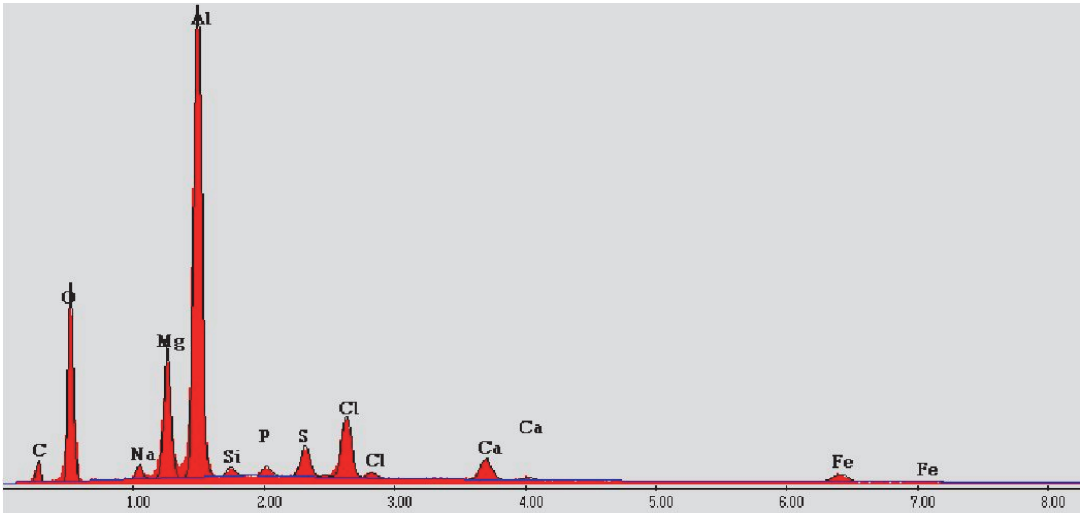

1)

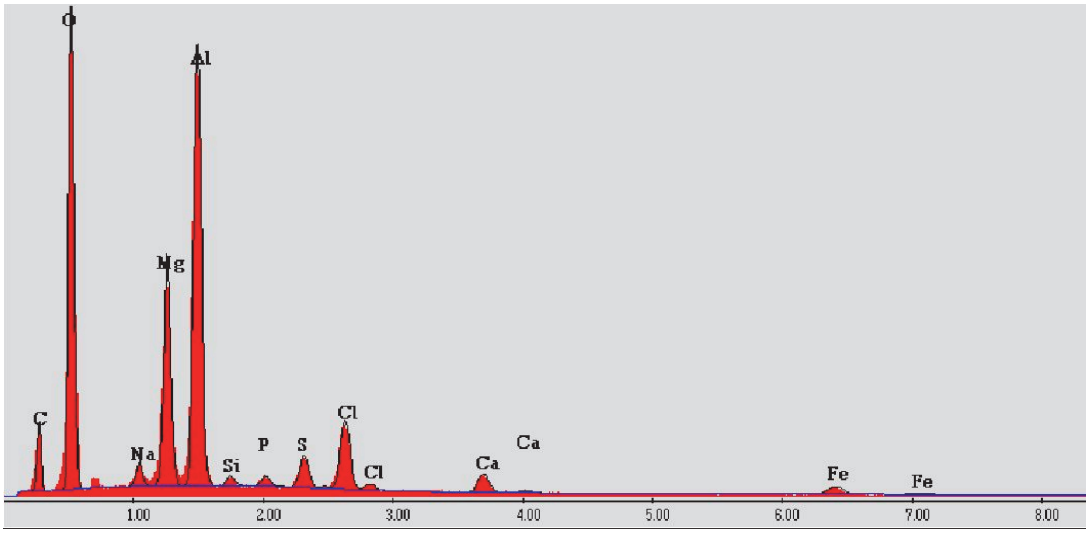

2)

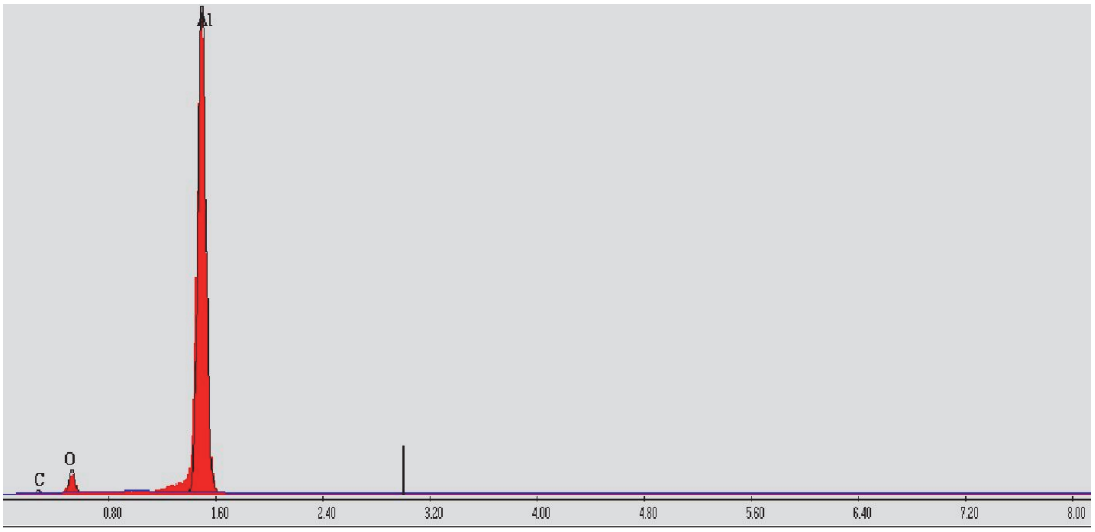

3)

Figure 4.33: EDS spectrum of respectively particle labeled 1, 2 and 3 on the AA1050 specimen in Figure 4.32.

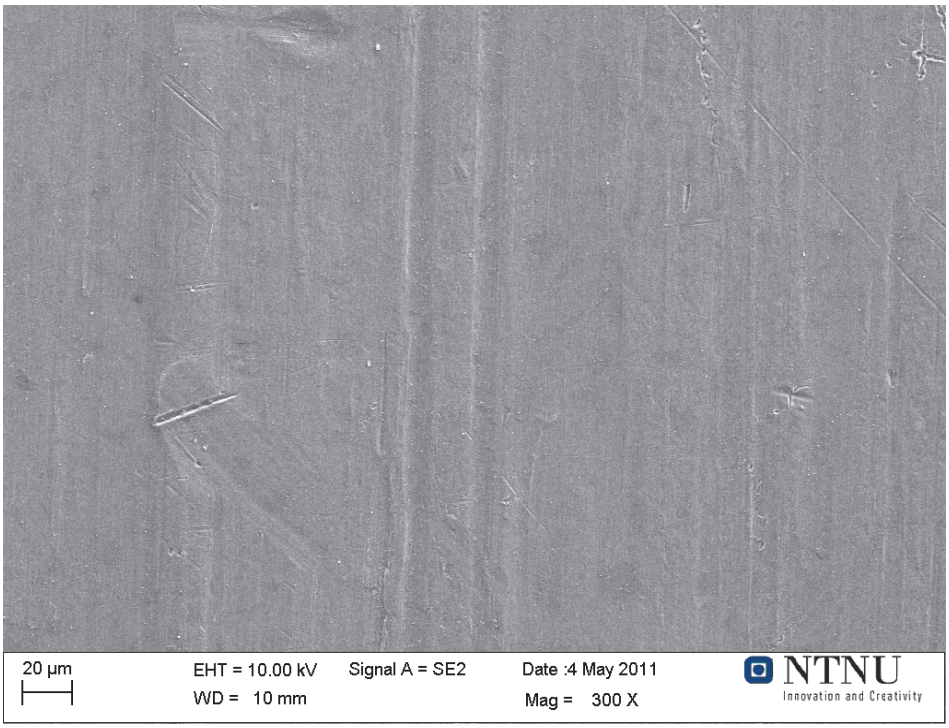

Figure 4.34: Surface of aluminum alloy Al99.99 before exposure.

Figure 4.35: Surface of aluminum alloy Al99.99 after 6 weeks exposure. No visible difference in the surface.

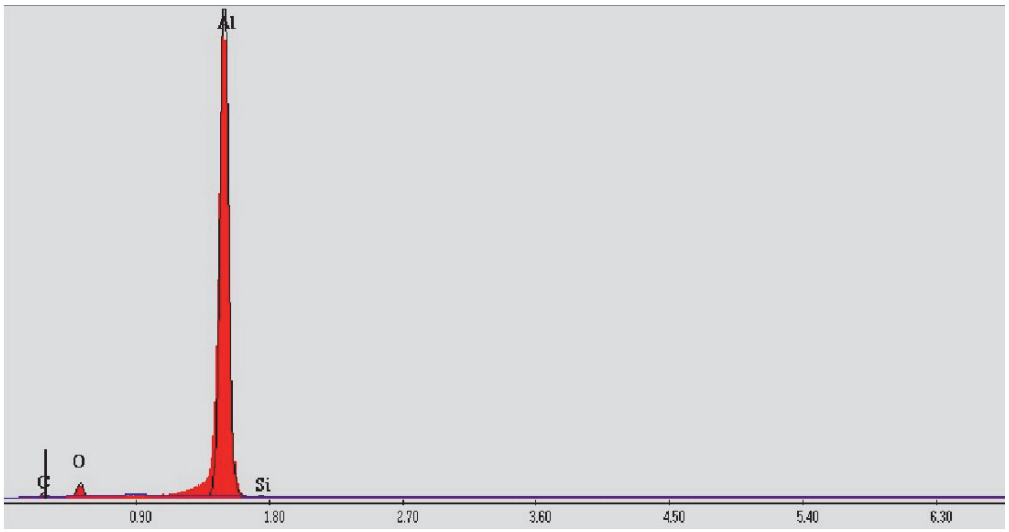

Figure 4.36: EDS spectrum for the area of Al99.99 in Figure 4.35

Table 4.14: EDS-analysis of the area of Al99.99 in Figure 4.35.

Element	Al	C	O	Si
wt%	88.52	6.15	5.20	0.13

4.4 Cross sections of specimens

The TSA specimens were cut in half and the cross section investigated to see whether diffusion of oxygen through the surface had occurred. tHe sanokes investigated were TSA prior to exposure to seawater, for comparison, and TSA exposed to seawater for respectively 6 weeks and 4 months. As the steel under the TSA is so much harder than the TSA, grinding and polishing the surface was difficult, as will be shown by the pictures. It was not possible to detect any pores in the structure, as the aluminum is so soft that any possible pore was erased. In addition, there was not seen any well-defined trend for the O content for any of the samples. This also applies to the sealed coating. Since the pores and the rest of the structure was erased by the grinding and polishing, it was impossible to see whether the sealer had penetrated the surface and filled the pores. However, this was seen by polishing the surface of the specimen, rather than the cross section. As the results fails to give any information, they will not be discussed further in the main part of the thesis, but they are found in Appendix B.

5 Discussion

5.1 Effect of alloy and microstructure on current density behavior

Both the TSA specimen from the present experiments and the aluminum plates of alloys AA5082 and AA1050 followed the current density behavior described by Gundersen and Nisancioglu or, at least, had an initial current density peak. The steep increase in the cathodic current density at the beginning indicates that reactions take place on the surfaces, and the following decreasing current is a result of the isolation of cathodic particles. This behavior was expected for the two aluminum alloys AA5082 and AA1050, as they contain cathodic particles. It was also assumed to be the case for the TSA specimen, although it is not possible to see the cathodic particles. The further decrease in current after the initial peak could be explained by precipitation of calcareous deposit. However, calcareous deposit is not found over an extensive area. The EDS analyses showed that the precipitation of calcareous deposit is favored at the particles for the aluminum plates and at certain areas for the TSA. The aluminum alloy Al99.99 did not show this behavior, which was also expected, as Al99.99 should not have any cathodic particles. Hence, the decrease in current density for the Al99.99 would be a result of oxygen polarization, as is the case with steel specimens, with accompanying calcareous deposit. The difference between steel and Al99.99 is, however, the protective aluminum oxide that makes the current requirements ten times smaller for aluminum than for steel. The aluminum plates of the alloys AA5082, AA1050 and Al99.99 confirms that the more alloying elements, the higher current density.

The average current density for the TSA specimens was 80 mA/m^2 after 38 days, which is twice the value found for the TSA specimens from the project work and the long term TSA specimens value after 40 days. There is a clear temperature dependence which will be discussed later. Since findings from literature have reported a temperature between 8 and 12 °C, the current density results from the long term exposure experiment will be more correct to use as comparison. The long term exposed specimen had a current density around 40 mA/m^2 after 40 days while the experiments performed by Gartland and Eggen on an arc sprayed AlMg coating had a current demand around 35 mA/m^2 after one month [17]. However, the potential used in their experiments was slightly lower, at -1030 mV vs Ag/AgCl. After 4 months, the TSA specimen from the present experiment had a current demand at 25 mA/m^2 and was still decreasing. There was also found more Mg at the TSA specimen exposed for 4 months, compared to those from earlier work exposed for only 6 weeks, proving that precipitation does take some time. As the current density found by Gartland and Eggen was just below 20 mA/m^2 after 4 months, the potentiostatic results seem to agree with earlier experiments, and as the current demand found by

Gartland and Eggen was less than 10 mA/m^2 after 16 months (and stable), it is reason to believe that the result would be the same for the present experiments [17].

The current demand for alloy AA5082 is 43 mA/m^2 after 30 days. This is very close to the long term TSA specimen, which also was an AlMg5 alloy. Experiments with both arc sprayed and flame sprayed 99.5% Al alloy was done by Gartland and Eggen, and after one month of exposure to seawater at -1030 mV vs Ag/AgCl, the current demand was respectively 20 mA/m^2 and 15 mA/m^2. The Al plate with 99.5 % Al in the present experiment had a current demand at 21 mA/m^2. This shows that results from aluminum specimens of extruded plates and thermally sprayed coatings are comparable, at least when it comes to current demand.

Comparing the current density behavior shown in this thesis with the current density curves from Barchiche et al will in principal not be adequate as Barchiche et al performed the experiments on steel, and the mechanisms that the current demands are dependent of are different for steel and aluminum. Mainly, the difference is the cathodic sites, which for steel is the entire surface, while for aluminum is at the intermetallic particles. However, assumingly they were comparable; the steep decrease of the current demand for both the TSA specimens and the Al99.99 plates would be considered a typical $CaCO_3$ curve. However, if that was the case, the Mg/Ca ratio would be lower for these specimens.

5.2 Thickness of calcareous deposit

The thickness of the calcareous deposit on the TSA samples or the aluminum alloy samples is not possible to measure, as there is not found any of the typical structure that the calcareous deposit holds on the aluminum surface. In fact, there has not been seen anything that can resemble a calcareous deposit, with the exception of a more rugged and brighter TSA surface. The EDS analyses show something else, however, with detection of Ca and increased content of Mg, O and C. However, this might be expected as cathodic sites on aluminum, i.e. areas favorable for precipitation and growth for calcareous deposit, is not evenly distributed as it is on steel. As a consequence the only clue indicating calcareous deposit is the EDS analysis and bright spots on the surface.

5.3 Mg/Ca ratio for the various specimens

As far as the Mg/Ca ratios reported in this thesis are concerned, there is one essential thing worth mentioning; The Mg/Ca ratios presented in the results are not constant over a whole area, but vary from spot to spot. There has been performed many EDS analyses on several specimens of each type, and all could not be included in this report. The numbers and figures presented in this report are a

representation of the typical results found for each material. The Mg/Ca values are given in [mol/mol].

The SEM images of the TSA specimens show that the surface has changed somewhat from the unexposed surface and it seems like something has precipitated on the surface, although without seeing any specified structure of either aragonite or calcite. In the literature $Mg(OH)_2$ is described as a thin film with a thickness of a few hundred micrometers, difficult to detect in SEM [22]. This may be the reason why the calcareous deposit not was seen in the microscope, although detected by EDS. The EDS analyses confirm that the composition on the TSA surface has changed. Both the Mg and O content has increased given reason to believe that $Mg(OH)_2$ has precipitated. The Mg/Ca ratio is indicating the amount of Mg relative to Ca and used as a measure of the properties of the calcareous deposit, especially the protectiveness. However it does not indicate how much calcareous deposit there is present on the surface. The Mg/Ca ratio for the TSA specimens exposed for 6 weeks will be discussed later, in the view of temperature dependence. However, one result worth noticing for these specimens is the difference between various spots on the surface. The two spots in Figure 4.13 and Figure 4.15 has Mg/Ca ratios at 5.4 and 22.1, respectively. This shows that the calcareous deposit does not precipitate uniformly over the surface, but that certain spots are favorable for the Mg precipitation.

The TSA specimen exposed for 4 months showed an Mg/Ca ratio at 12.3 over an extensive area, after adjusting for initial Mg content, while it was found to be 36.0 at a certain peak in the surface. This high Mg/Ca ratio after 4 months shows that the precipitation of Mg is quite slow, whereas the Ca content is relatively stable from 5 weeks to 4 months. It would be interesting to know the exact composition at these spots before exposure. As the results from the aluminum alloy plates show, however, it is quite possible that there is a higher content of Fe where the Mg/Ca content is the highest.

The values shown here for TSA are, first of all, much higher than what has been reported for steel surfaces and, secondly, show that the calcareous deposit precipitates (more) at certain areas.

For the aluminum plates of alloy AA5082 and AA1050, the intermetallic particles are easy to find, and with that, the emphasis on these surfaces has been on the particles. The EDS analyses have been performed on particles and at points on the matrix, not over an area, as was the case for the TSA specimens. The results from the EDS analyses show that there is a great difference between the composition at the particles and the matrix. Mg was found with increased values at all the particles at specimens of AA5082 and AA1050, and there was more Mg at the particles than at the matrix. Ca was only found at the particles on alloy AA5082 and AA1050, not at the matrix.

5.3 Mg/Ca RATIO FOR THE VARIOUS SPECIMENS

The Mg/Ca ratio for the aluminum plates confirm the theory that the calcareous deposits precipitates at the cathodic intermetallic particles on aluminum alloys. The lack of or lower content of Ca on the matrix and no Mg at the matrix where Mg initially is not present in the alloy, demonstrates this. Secondly, the Mg/Ca ratio at the particles is considerably higher than values found in literature regarding experiments performed on steel specimens [23, 25].

These findings are in accordance with the findings at the TSA specimens in finding more calcareous deposit at certain parts of the surface. For the TSA specimens, the increased amount of calcareous deposit is mostly found at the peaks of the surface, although the amount or the Mg/Ca ratio is not as high at every peak. The Mg/Ca ratio for the TSA specimens were slightly higher than the Mg/Ca ratio found at the AA5082 plates after 6 weeks, however, the difference is small, and there was a difference between the seawater temperatures, so it is probably safe to say that TSA specimens and AlMg5 plates also are comparable when it comes to Mg/Ca ratio. Also, different SEMs were used, which may give different results, as the two microscopes can have a different reference value.

The high Mg/Ca ratios are a consequence of increased Mg content, decreased Ca content or a combination of both. The increase in Mg content have two possible explanations; for one thing, the increase of Mg is due to precipitation of $Mg(OH)_2$ on the surface, ergo, its origin is from the seawater. The second possibility is that it comes from the alloy matrix, since Mg is less noble than Al and, hence, will corrode first. The corrosion products fill the pores between the intermetallic particle and the matrix, increasing the relative amount of Mg at that certain point, hence, the increased Mg content is coming from the metal. However, considering the increased amount of Mg on the aluminum plates of AA1050, where the Mg content initially is close to zero, the most likely origin of Mg is the seawater.

Mg^{2+} is known to inhibit the precipitation of calcite and the growth of aragonite, which may explain why there is detected more Mg than Ca on the surfaces of AlMg5 alloys, including TSA. The question is, however, why there is more Mg than Ca present for alloys not initially containing Mg. As discussed in the theory section, $Mg(OH)_2$ will precipitate at higher pH than $CaCO_3$. pH in seawater is 8.3 and studies have shown the increase of pH near the cathode surface during cathodic protection to the pH needed for $Mg(OH)_2$ to precipitate [11, 31, 32]. pH at the surface was not measured during these experiments, but the pH has must have reached 9.3 at the cathodic sites, as Mg has precipitated. As there is found more Mg at the aluminum surfaces than on steel, the pH at the cathodic site at aluminum might be higher than at the steel surface. In addition, $Mg(OH)_2$ is known to precipitate at low potentials. Low potentials are a contributing factor to increased pH, which again favors the $Mg(OH)_2$ precipitation. The specimens in the present experiments were polarized down to -1050 vs Ag/AgCl, which is lower than what is normally used for steel. However, steel specimens from earlier work, polarized to the same potential, had a much lower Mg/Ca ratio than the aluminum specimen. This seconds the suggestion that the

reactions at the intermetallic particles on aluminum are increasing the pH at aluminum more than at steel surface.

The fact that there were no findings of Mg or Ca at the Al99.99 specimens shows once again that the intermetallic particles do play an important part, regarding the precipitation of calcareous deposit. The current densities at the Al99.99 specimens were probably too low to cause precipitation of calcareous deposit due to low pH.

5.4 Effect of sealer

The cathodic current demand for the sealed TSA specimens was 4 times lower than the long term exposed TSA specimen, reading 10 mA/m^2 after 36 days. The value agrees well with the suggested design current density value at 11mA/m^2 [16]. However, Fischer et al studied flame sprayed Al coating with vinyl sealer at 7-8 °C, polarized between −1030 and −1050 mV vs Ag/AgCl and the current demand was found to be 5 mA/m^2 during the whole period [29]. Gartland and Eggen found in their study in that the cathodic current demand for sealed TSA was less than 1 mA/m^2 during the whole period [17]. Therefore, the slightly higher cathodic current demand in the present experiments may be due to unsatisfying application of the sealer. According to the NORSOK standard, the sealer should be applied soon after application of the TSA to hinder contamination and is to be applied until absorption is complete. There should not be a measurable overlay of sealer on the metallic coating after application [15]. In this experiment, first of all, the sealer was not applied shortly after the TSA coating was applied, and secondly, the sealer was applied using a brush instead of a spraying gun, hence the layer might have become uneven, too thick and not penetrated through the coating. The thickness was not measured, but the sealer was visible on the surface. In addition, sealer was not detected at the surface after grinding and polishing, so the sealer has probably functioned more as an overlay coating than sealing of the pores. The SEM images show the necessity of the sealer, as there are many pores present, up to 20 µm in diameter. A suggestion about the sealer being dissolved by ethanol being used during polishing has been made. However, the sealer was both seen and detected by SEM/EDS on the unpolished surface, and this surface has been rinsed in ethanol as well. So it stands to reason that the sealer has not penetrated through the coating.

In the experiments of Gartland, it took 3-4 months before the current demand for sealed arc sprayed AlMg5 was stable, although the current density had been on the same level almost from the start [16]. The current density for the sealed specimens in the present experiment also had a much more stable progress, compared to the unsealed specimens, only decreasing 20 mA/m^2 during the exposure time. This is probably due to the sealer covering the intermetallic particles and the matrix, hindering the reactions on the surface. The covering of the surface, including the intermetallic particles also seems to have hinder the precipitation of calcareous

deposit, as the small amount of Mg and no detection of Ca on the sealed surface indicate that calcareous deposit has not precipitated on the sealed TSA surface.

5.5 Effect of temperature

The potentiostatic polarization curves show a clear temperature dependence for the TSA specimens. The temperature difference in the seawater for the TSA specimens and the long term exposure TSA specimen was 6-7 °C. That difference led to a difference in current density of 60 mA/m^2 at the most. The resulting higher current density due to temperature increase is expected due to increasing rate of kinetic reactions with increasing temperature. In addition, increased temperature is known to reduce the corrosion resistant of aluminum in alkaline environment, which would increase the current demand [1]. Increase in current density due to increased temperature is confirmed by Fischer. He found that sealed TSA specimens at 70 – 100 °C and -1100 mV vs Ag/AgCl had a current density of 70 mA/m^2 after one month and 30 mA/m^2 after one year [14]. Gartland suggested a design current density for sealed TSA to 17 mA/m^2 at 40 °C [16]. Considering the current density needed for the sealed TSA specimen at 8-10 °C was around 10 mA/m^2 after one month, the design current density seems anything but conservative.

As far as calcareous deposit is concerned, an opposite effect should occur. Both in the studies of Barchiche et al and Deslouis et al, an increase of current density was observed at -1000mV SCE and lower temperatures [30]. The increase was explained by the formation of $Mg(OH)_2$, which is the compound most likely to precipitate in colder water and which is less protective than $CaCO_3$. At lower potentials, e.g. –1200 mV SCE, the temperature dependence on the current demand had a negligible effect, as the solubility of the compounds have less influence on behalf of increased pH at the surface and it was observed an increased deposition of $Mg(OH)_2$ at increasing temperatures.

In the present experiments the TSA surfaces do not seem to have been covered by calcareous deposits, so the effect of temperature is probably not due to a less protective calcareous deposit over a more protective deposit. The temperature difference is probably not big enough either. Comparing the EDS results from the present experiment to the earlier one, however, should give an answer.

The unexposed TSA specimens had an Mg content of 3.4 % and after 6 weeks exposure the Mg/Ca ratio was 9.7, when subtracting the initial Mg content. Analysis from earlier work, where the temperature was 6-7 °C lower, the Mg/Ca ratio at the surface of a TSA specimen exposed for 4 weeks was 4.9, when adjusting for the initial Mg content. According to the literature, the Mg/Ca ratio for the specimens at lower temperature should be higher, than for the higher temperatures, i.e. increased Mg content at lower temperatures. As it is not, the assumption of the temperature difference being too small and/or the amount of calcareous deposit on the surface is

too low, is valid. In addition, as the current decreases after a month, i.e. when the temperature decreased again, the temperature dependence is obvious, and most likely related to the kinetics.

Although the resulting increase in current density was expected as a result of the temperature increase, the temperature increase in itself was not expected. The water flowing through the two tubs came from the same depot and would therefore have the same temperature. The reason for the temperature increase is therefore probably due to hindering of the flow in to the tub, so that the water was not continuously replaced. In that case, considering that the temperature effect is not enough, the effect of flow in the electrolyte also must be considered.

5.6 Effect of flow

If the increase of temperature was due to a stop in circulation of the water, effect of flow, or rather, *no flow* must be considered. First of all, as mentioned in the experimental chapter, the circulation that was supposed to be in the tub was so low that in principle it could be considered as nearly stagnant condition. However, without circulation there is no replacing the electrolyte. For a film forming metal, the need for dissolved oxygen is necessary to form a protective oxide. For aluminum, however, the oxide will deposit by splitting the water molecules, hence the need for dissolved oxygen is not as important as for other metals.

For aluminum, stagnant conditions favor pitting corrosion [1]. However, pitting is easily avoided due to cathodic protection, keeping the potential far below the pitting potential. In addition, AlMg alloys, which the TSA specimens are, are known to be resistant to pitting in chloride environment [1]. It therefore stands to reason that the lack of circulation did not affect the specimens directly; rather indirectly as an increase of temperature was a consequence.

5.7 Potentiodynamic polarization curves

The potentiodynamic polarization curves show first of all the same as the potentiostatic polarization curves; the current decreases with time and the sealed specimens has a much lower current demand than the unsealed.

Besides that, the curves are a measure of corrosion potential. As the current density decreases for each week, so does the corrosion potential. The curves for the unsealed TSA from the first weeks, seem to have a corrosion potential higher than −800 mV vs Ag/AgCl, while after 9 weeks, the corrosion potential seem to be around −900 mV vs Ag/AgCl. The values for the sealed TSA specimens show the same trend.

Calculating the Tafel slope would give an indication on whether the mechanisms were activation controlled or diffusion controlled, and whether the cathodic reaction is oxygen reduction or hydrogen evolution. In this case, however, the anodic and cathodic reactions occur at certain cathodic sites rather than uniformly across the surface. Therefore calculating the Tafel slope will be difficult.

6 Conclusion

Through experiments and literature studies, steel specimens coated with thermally sprayed aluminum exposed to seawater, cathodic protected at -150 mV vs Ag/AgCl have been studied. To validate the mechanisms happening on the surface, extruded plates of three different aluminum alloys was also investigated and exposed to the same conditions as the TSA specimens. The comparisons have proven valid concerning both current demand and Mg/Ca ratio. On the basis of the findings presented, following conclusions can be drawn.

The current density demand for the unsealed TSA specimens polarized to -1050 mV vs Ag/AgCl and 8-12 °C are in the order of 40 mA/m^2 after one month. 4 times lower than for steel specimens. After 4 months the current demand was 25 mA/m^2.

Sealed TSA specimens showed even lower current density demands, at 10 mA/m^2, although the sealer does not seem to have penetrated through the coating.

The potentiostatic curves show an initial peak in current density, indicating cathodic reactions happening on the surface followed by isolation of the cathodic sites. This was shown for both TSA specimens, as well as plates of aluminum alloys AA5082 and AA1050.

Without seeing any typical structure of calcareous deposit, increased Mg, Ca and O was detected with EDS, which confirms that precipitation of calcareous deposit has taken place at the surface.

Precipitation of calcareous deposit was found to be higher at certain areas at the TSA specimens. For the aluminum plates the precipitation was highest at the intermetallic particles.

The Mg/Ca ratios found at the different aluminum specimens are much higher than what has been found at steel surfaces. The reason is not completely understood, but is probably due to a higher pH at the cathodic sites.

Calcareous deposit was not detected on Al99.99.

A temperature increase of 6-7 °C led to an increased current demand of 60 mA/m^2 and is probably due to higher rate of kinetic reactions.

7 Suggestions for further work

This study has emphasized in finding whether calcareous deposit forms on TSA with cathodic protection. Suggestions for further work include:

- Further investigation of the microstructure of TSA coatings, with emphasis on finding possible intermetallic particles

- Finding techniques of measuring pH at the surface during potentiostatic polarization experiments. The main challenge will be to measure the pH at the cathodic sites, not over the whole surface.

- Studying the thermal properties of the TSA coating and calcareous deposit. Will the deposit and/or the aluminum oxide hinder thermal conductivity, like calcareous deposit does on steel surfaces?

- Investigating the temperature dependence. How high will the current demand be using TSA at high temperatures and will that lead to more precipitation of calcareous deposit?

- Finding techniques to “see” the layer of $Mg(OH)_2$.

References

1. Nisancioglu, K., *Corrosion basics and engineering - Lecture Notes for the Course 535233 Korrosjonslære*. 1994, Trondheim: Norges Tekniske Høgskole, Institutt for Teknisk Elektrokjemi.
2. Nisancioglu, K., *Corrosion and potection of alminum alloys in seawater.* Europeam Federation of corrosion publications, 2007. **50**: p. p.145.
3. Shifler, D.A., *Understanding material interactions in marine environments to promote extended structural life.* Corrosion Science, 2004.
4. Mondolfo, L.F., *Aluminum Alloys: Structure and porperties*. 1. ed. 1976, London: Butterworths & Co. 971.
5. Ezuber, H., A. El-Houd, and F. El-Shawesh, *A study on the corrosion behavior of aluminum alloys in seawater.* Materials and Design, 2007. **29**: p. 801-805.
6. Solberg, J.K., *Teknologiske metaller og legeringer*. 2008.
7. The Aluminum Association, *International Alloy Designations and Chemical Composition Limits for Wrought Aluminum and Wrought Aluminum Alloys*. 2009, The aluminum association: Arlington.
8. Bardal, E., *Korrosjon og korrosjonsvern*. 1985, [Trondheim]: Tapir. 293 s.
9. Nisancioglu, K., *Corrosion and protection of aluminum alloys in seawater*, in *Corrosion Behavior and Protection of Coppe and Aluminum Alloys in Seawater*, D. Feron, Editor. 2007, Taylor & Francis Inc.
10. Gundersen, R. and K. Nisancioglu, *Cathodic protection of aluminum in seawater.* Corrosion, 1990. **46**(4): p. 279-285.
11. Hartt, W.H., C.H. Culberson, and S.W. Smith, *Calcareous deposits on metal surfaces in sea water - a critical review*, in *The international corrosion forum*. 1983, NACE: Anaheim, California.
12. Dorfman, M.R., *Thermal spray coatings*, in *Handbook of Environmental Degradation of Materials*, K. Myer, Editor. 2005, William Andrew Publishing: Norwich, NY. p. 405-422.
13. Siegmund, A.J., *Metal alloys; Corrosion protection for the future*, in *NACE international Annual Conference and Exposition*. 1997, NACE international.
14. Fischer, K.P., et al., *Performance History of Thermal-Sprayed Aluminum Coatings in Offshore Service.* Materials Performance, 1995. **34**(4): p. 27-35.

15. NORSOK M-501, *Surface preparation and protective coating*. 2004.
16. Gartland, P.O., *Protective properties of Al-based coatings in seawater*. 1991, SINTEF - the corrosion center (matellurgy).
17. Gartland, P.O. and T.G. Eggen, *Cathodic and anodic properties of thermally sprayed Al- and Zn-based coatings in seawater*, in *NACE international conference and expo*. 1990, NACE international: Las Vegas, Nevada.
18. Eggen, T.G. and J.M. Drugli, *Sea water corrosion of thermal sprayed aluminium*. 1993, SINTEF Metallurgy, Corrosion center: Trondheim. p. 36.
19. Benedetti, A., et al., *Calcareous deposit precipitation on cathodically polarized carbon steel in natural seawater exposed to daylight cycles.* Proc. Int. Offshore Polar Eng. Conf., 2007. **17**(Copyright (C) 2010 American Chemical Society (ACS). All Rights Reserved.): p. 3307-3312.
20. Möller, H., *The influence of Mg^{2+} on the formation of calcareous deposits on a freely corroding low carbon steel in seawater.* Corrosion Science, 2006.
21. Deslouis, C., et al., *Kinetics and Characterisation of Calcareous Deposits under Cathodic Protection in Natural Sea Water.* Materials Science Forum, 1998. **289-292**: p. 1163-1180.
22. Deslouis, C., et al., *Characterization of calcareous deposits in artificial seawater by impedances techniques: 2 -deposit of Mg(OH)2 without CaCO3.* Electrochimica Acta, 2000. **45**: p. 1837-1845.
23. Stangeland, H.W., *Cathodic protection in cold climate - current density requirements and quality of calcareous deposits*, in *Institute of materials science and engineering*. 2008, Norwegian university of science and technology: Trondheim. p. 92.
24. Okstad, T., *Hydrogen evolution by cathodic protection of steel in natural seawater*, in *Institute for material science*. 2005, University of science and technology (NTNU): Trondheim.
25. Egtvedt, S., *Kalkutfelling på termisk sprøytet aluminium under katodisk beskyttelse i sjøvann*, in *Institute for Material Science and Engineering*. 2010, Norwegian University for Science and Technology: Trondheim.
26. Rousseau, C., et al., *Calcareous deposit formed under cathodic protection in the presence of natural marine sediments: A 12 month experiment.* Corros. Sci., 2010. **52**(Copyright (C) 2010 American Chemical Society (ACS). All Rights Reserved.): p. 2206-2218.
27. Ben Amor, Y., et al., *Study of the effect of magnesium concentration on the deposit of allotropic forms of calcium carbonate and related carbon steel interface behavior.* Electrochimica Acta, 2010. **55**(16): p. 4820-4826.

28. Barchiche, C., et al., *Characterization of calcareous deposits in artificial seawater by impedance techniques: 3--Deposit of CaCO3 in the presence of Mg(II).* Electrochimica Acta, 2003. **48**(12): p. 1645-1654.
29. Fischer, K.P., W.H. Thomason, and S. Eliasen, *CP in deep water: the importance of calcareous deposits and the environmental conditions*, in *The NACE Inernational Annual Conference and Exposition*. 1996, NACE International.
30. Barchiche, C., et al., *Characterisation of calcareous deposits by electrochemical methods: role of sulphates, calcium concentration and temperature.* Electrochimica Acta, 2004. **49**(17-18): p. 2833-2839.
31. Salvago, G., et al., *Calcareous deposits, hydrogen evolution and pH on structures under cathodic polarization in seawater.* Proc. Int. Offshore Polar Eng. Conf., 2003. **13**(Copyright (C) 2010 American Chemical Society (ACS). All Rights Reserved.): p. 353-359.
32. Deslouis, C., et al., *Characterization of calcareous deposits in artificial sea water by impedance techniques: 1 - Deposit of CaCO3 without Mg(OH)2.* Electrochimica Acta, 1998. **43**: p. 1891-1901.
33. Kim, K.-J. and W.H. Hartt, *Characteristics of cathodic protection and calcareous deposits for type 316L steel in simulated deep sea conditions*, in *Corrosion NACExpo*. 2006, NACE international.
34. Johnsen, R. and H.W. Stangeland, *Cathodic protection in cold seawater - current density requirements*, in *NACE international corrosion conference & expo*. 2009, NACE international.
35. Astilleros, J.M., L. Fernández-Díaz, and A. Putnis, *The role of magnesium in the growth of calcite: An AFM study.* Chemical Geology, 2010. **271**(1-2): p. 52-58.
36. Deslouis, C., et al., *Influence of clay on calcareous deposit in natural and artificial sea water.* Electrochimica Acta, 2006. **51**(15): p. 3173-3180.
37. Hjelen, J., *Scanning elektron-mikroskopi*. 1989: Metallurgisk institutt, NTH.

Appendix A

Potentiostatic polarization curves

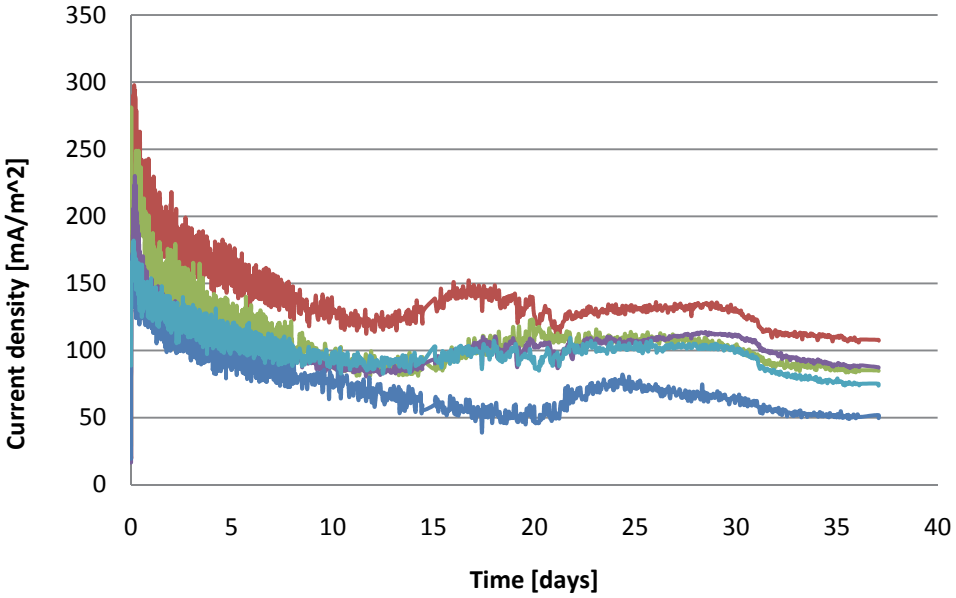

Figure A 1: Current density – time curves for the five TSA samples.

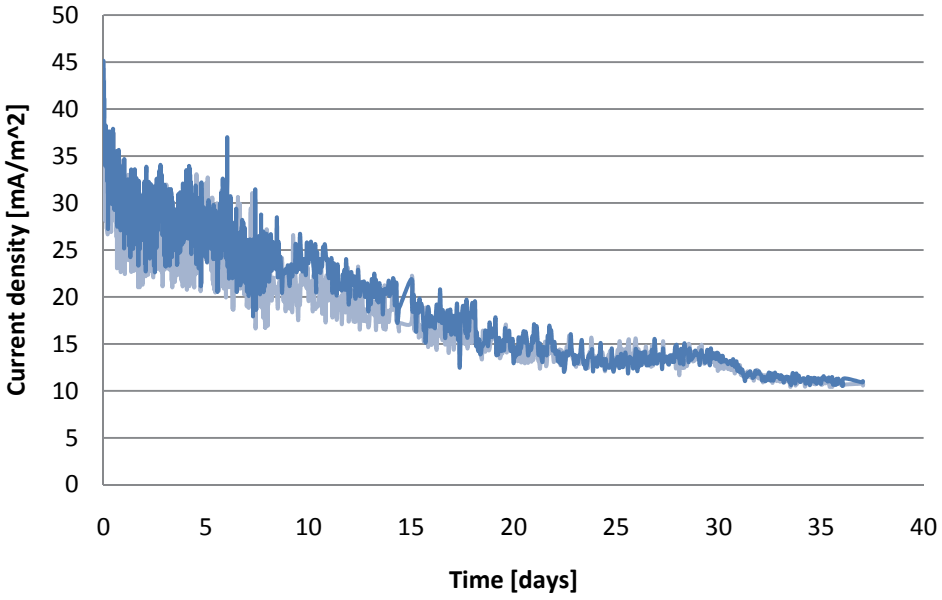

Figure A 2: Current density - time curves for the two TSA specimens that were sealed.

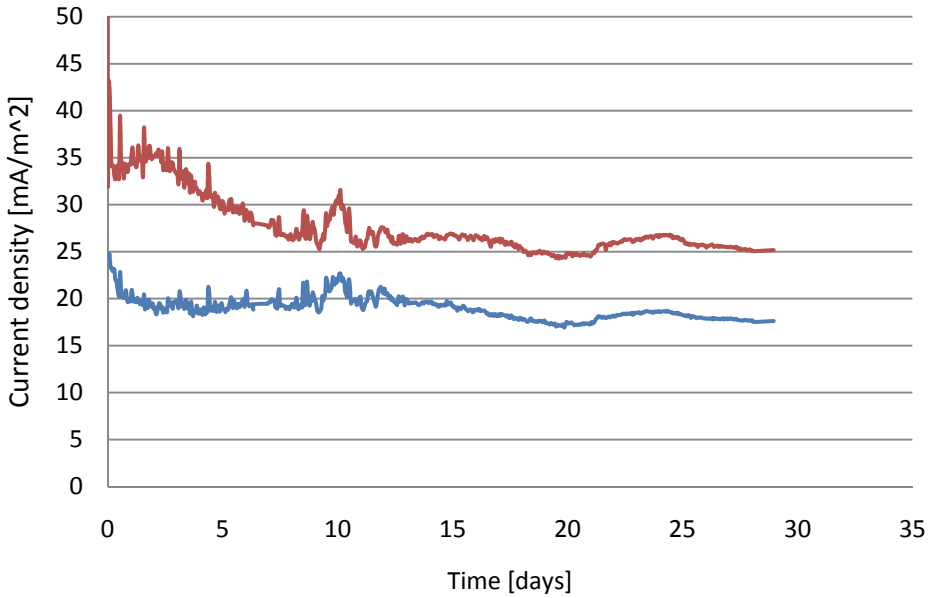

Figure A 3: Current density – time curve for the two specimens of aluminum alloy AA5082.

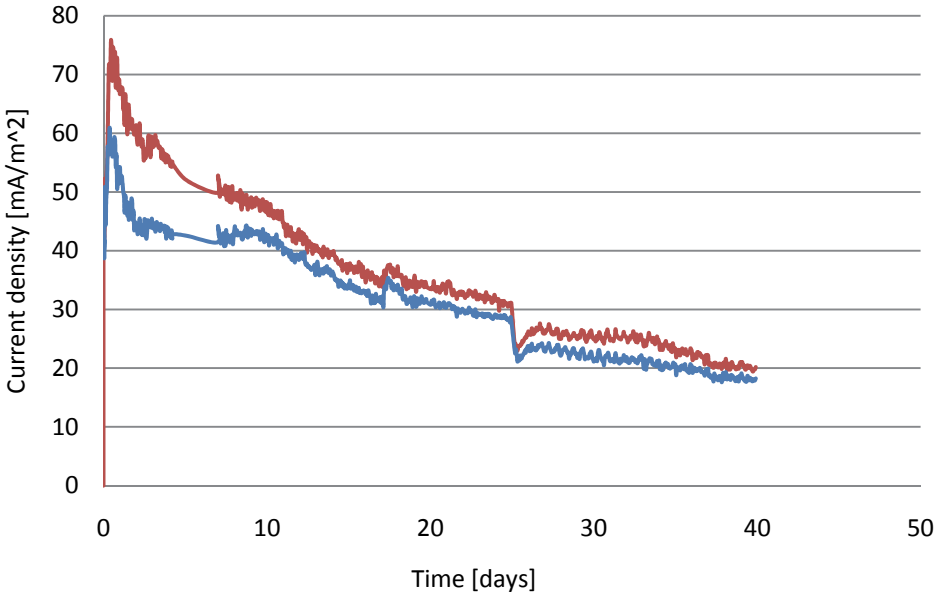

Figure A 4: Potentiostatic polarization curve for the two specimens of aluminum alloy Al1050.

b

Appendix B

Cross section of specimens

The TSA samples were cut in half and the cross section investigated to see if there has been diffusion of oxygen through the surface. The samples investigated were TSA prior to exposure to seawater, for comparison, and TSA exposed to seawater for 6 weeks and 4 months. Sealed TSA specimens exposed to seawater in 6 weeks were investigated to see if the sealer has penetrated the TSA coating and filled the pores.

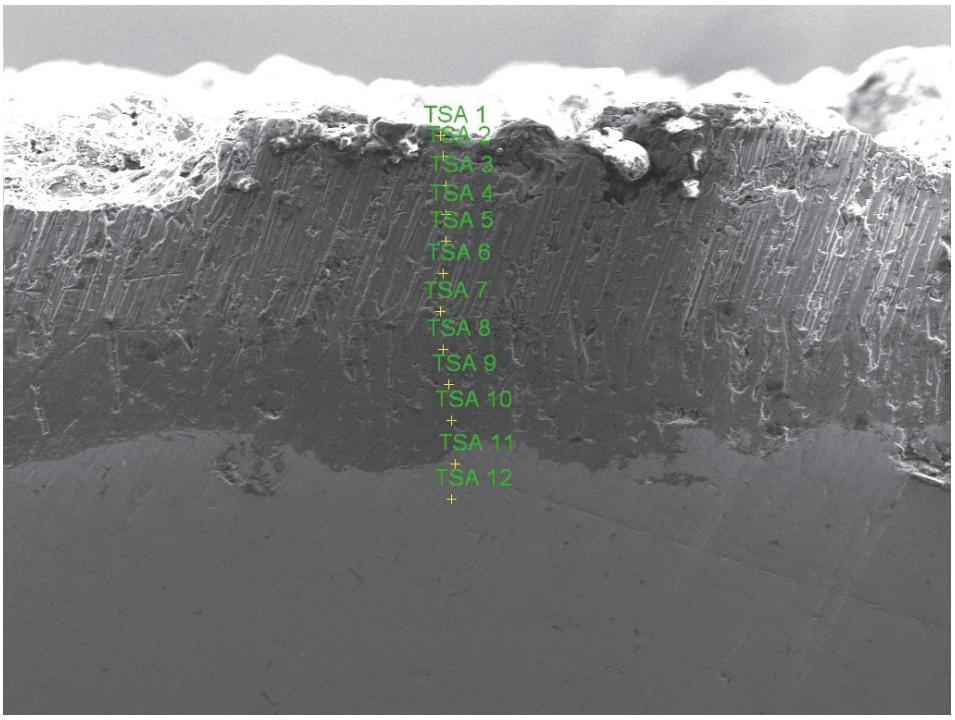

Figure B 1: Cross section of TSA sample, not exposed to seawater.

Table B 1: EDS analysis of the cross section in Figure B 1. The oxygen content is varying through the cross section, with no clear pattern. It can seem as if the oxygen content is higher near the surface, and decreases inwards, but the content increases again closer to the interface between the coating and substrate material, so no well-defined trend is observed.

Spectrum	Mass percent (%)					
	C	O	Mg	Al	Ca	Fe
1	23.0	6.8	0.7	54.7	0.9	
2	30.5	5.9	0.7	45.8	1.0	
3	9.8	5.7	1.0	69.5	0.9	6.4
4	5.7	2.4	0.9	72.4	1.1	8.1
5	6.2	4.3	0.7	70.6	1.0	
6	5.4	2.1	1.3	86.0	0.8	6.9
7	5.3	4.8	1.2	71.2	0.8	6.8
8	10.1	9.7	1.1	65.3	1.0	13.1
9	9.0	15.6	2.9	57.6	1.2	21.7
10	4.1	9.3	4.4	72.6	0.9	7.3
11	3.7	3.3				103.3
12	2.1	1.7				97.0

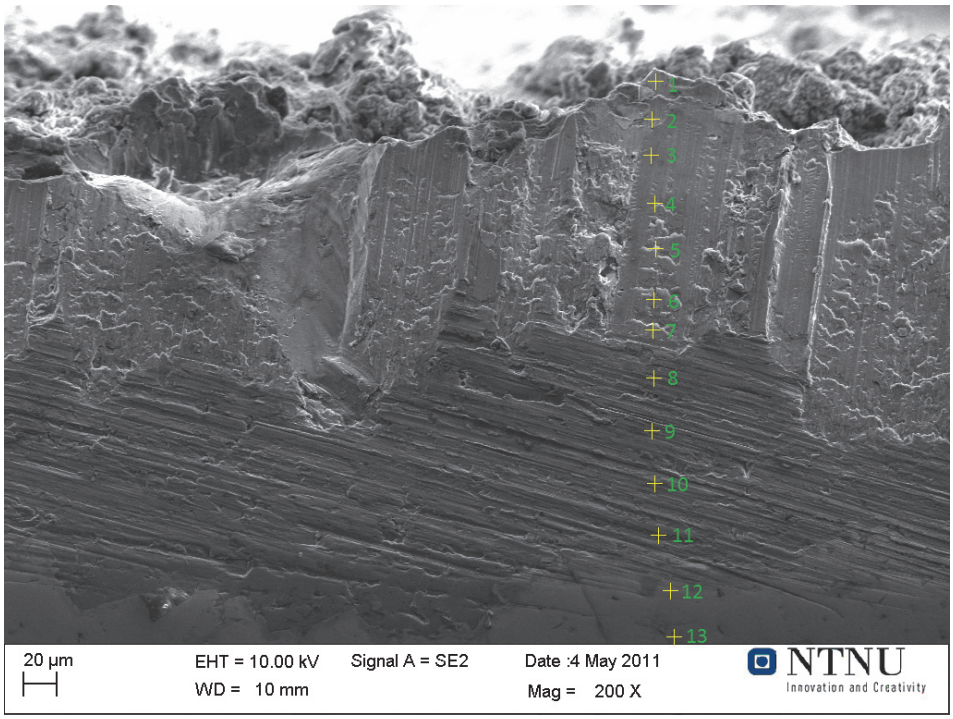

Figure B 2: Cross section of TSA specimen exposed for 6 weeks.

Table B 2: EDS analysis of the cross section in Figure B 2. The oxygen content is more varying at this cross section than the one belonging to the unexposed specimen, but a general view indicates a slightly increase in oxygen content moving towards the substrate material.

Spectrum	Mass percent (%)					
	C	O	Mg	Al	Ca	Fe
1	8.4	2.6	1.0	70.7	1.3	7.3
2	9.2	7.7	0.9	69.8	1.0	7.8
3	10.9	14.4	2.0	59.7	1.1	6.3
4	4.8	5.1	1.5	72.9	0.8	6.2
5	5.3	8.0	1.8	68.4	1.5	6.7
6	9.0	9.0	2.4	89.6	0.8	8.8
7	6.4	10.4	3.2	83.1	1.0	9.5
8	8.5	3.7	0.7	74.5	1.1	5.7
9	5.9	3.2	2.1	72.4	1.4	6.4
10	4.9	17.2	3.0	61.9	1.3	7.3
11	9.1	14.1	2.5	53.4	1.4	8.2
12	3.5	1.1	0.2	0.3	1.4	111.1
13	14.3	7.2	0.3	0.4	0.9	70.3

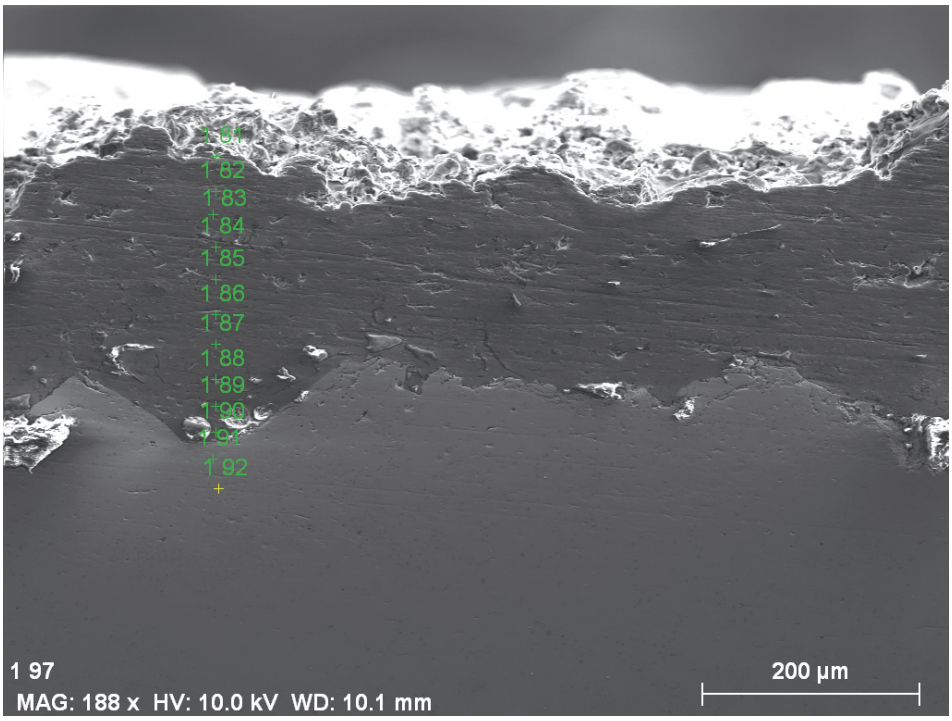

Figure B 3: Cross section of TSA specimen exposed for 4 months.

Table B 3: EDS-analysis for the cross section in Figure B 3. The oxygen content is slightly lower than the previous cross sections. However, as this specimen has had a longer exposure time, a higher oxygen content would be expected.

Spectrum	Mass percent (%)					
	C	O	Mg	Al	Ca	Fe
1 81	3.8	1.9	2.9	73.3	0.4	3.6
1 82	4.0	2.4	2.4	72.1	0.6	3.2
1 83	4.3	2.6	1.5	73.0	0.4	2.8
1 84	3.8	1.9	2.9	73.3	0.4	3.6
1 85	4.0	2.4	2.4	72.1	0.6	3.2
1 86	3.4	9.8	1.2	63.3	0.6	3.2
1 87	3.5	2.4	0.9	74.8	0.5	3.4
1 88	43.2	3.8	1.0	15.8	60.8	0.5
1 89	11.8	6.5	1.0	57.0	12.9	0.4
1 90	3.9	1.7	1.1	79.4	0.4	3.5
1 91	3.9	1.8	1.1	75.9	0.6	3.9
1 92	1.8	0.8	0.2	0.1	0.5	103.0

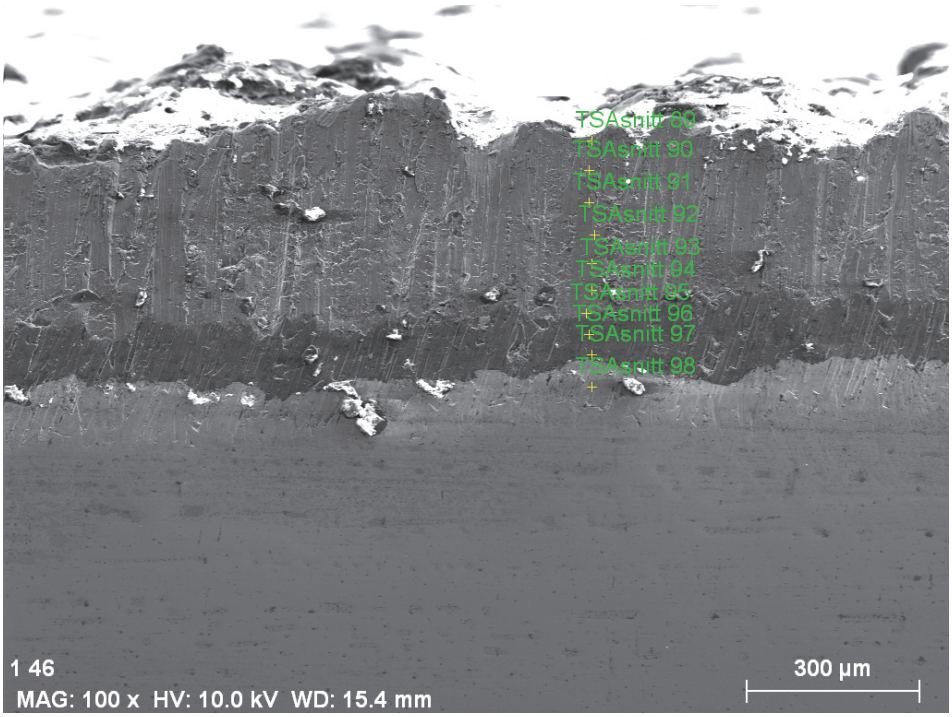

Figure B 4: Cross section of a sealed specimen, exposed for 6 weeks. It is difficult to see whether the sealer has penetrated the coating and filled the pores, because the cutting and polishing has smoothed the surface of the cross section, covering the possible pores.

Table B 4: EDS analysis of the cross section in Figure B 4. The oxygen content for the sealed specimen does not stand out, compared to the other cross sections. I.e. it does not seem to have hindered or made is easier for O to diffuse. No signs of Si below the surface indicate that the sealer has not penetrated through the surface.

Spectrum	Mass percent (%)					
	C	O	Mg	Al	Si	Fe
TSAsnitt 89	18,6	12,4	1,3	59,6	2,0	
TSAsnitt 90		5,2	2,1	66,5		
TSAsnitt 91	7,0	6,2	1,6	66,9		
TSAsnitt 92	10,1	8,7	2,6	76,4		
TSAsnitt 93	6,8	9,2	2,1	60,0		
TSAsnitt 94	7,8	7,6	2,3	62,1		
TSAsnitt 95	7,1	7,6	1,5	67,1		
TSAsnitt 96	7,2	4,4	2,7	69,9		
TSAsnitt 97	6,7	10,2		50,6		
TSAsnitt 98	21,0	6,4				70,4